SATELLITE-TRACKING AND EARTH-DYNAMICS RESEARCH PROGRAMS

Grant Number NGR 09-015-002

Semiannual Progress Report No. 39
Final Report Supplement No. 76

1 July to 31 December 1978

Prepared for

National Aeronautics and Space Administration
Washington, D. C. 20546

May 1979

Smithsonian Institution
Astrophysical Observatory
Cambridge, Massachusetts 02138

The Smithsonian Astrophysical Observatory
and the Harvard College Observatory
are members of the
Center for Astrophysics

The NASA Technical Officer for this grant is Mr. James C. Bavely, Code TN-1, Network Operations, Office of Space Tracking and Data Systems, NASA Headquarters, Washington, D.C. 20546.

SATELLITE-TRACKING AND EARTH-DYNAMICS RESEARCH PROGRAMS

Grant Number NGR 09-015-002

Semiannual Progress Report No. 39
Final Report Supplement No. 76

1 July to 31 December 1978

Prepared for

National Aeronautics and Space Administration
Washington, D. C. 20546

May 1979

Smithsonian Institution
Astrophysical Observatory
Cambridge, Massachusetts 02138

The Smithsonian Astrophysical Observatory
and the Harvard College Observatory
are members of the
Center for Astrophysics

The NASA Technical Officer for this grant is Mr. James C. Bavely, Code TN-1, Network Operations, Office of Space Tracking and Data Systems, NASA Headquarters, Washington, D.C. 20546.

TABLE OF CONTENTS

		Page
1	INTRODUCTION AND SUMMARY	1
2	OPERATING STATUS	4
3	LASER OPERATIONS AT COOPERATING AGENCIES	7
4	SATELLITE OBSERVING CAMPAIGNS	9
5	ENGINEERING	15
	5.1 Pulse-Processing and Detection System	15
	5.2 Minicomputers	15
	5.3 Timing	16
	5.3.1 Status	16
	5.3.2 Omega receivers	17
	5.3.3 Television timing in Natal	19
	5.3.4 NTS receivers	19
	5.3.5 Other timing information	21
6	SYSTEM UPGRADING AND MODIFICATION	22
	6.1 Laser Short-Pulse Modification	22
	6.2 Direct-Connect Computer Control	22
7	COMMUNICATIONS	24
8	DATA SERVICES AND PROGRAMING	25
	8.1 Data Services Group	25
	8.2 Data-Processing Software	26
	8.3 Pulse-Processing and Prediction Software	28
9	ANALYSIS AND SYSTEM PERFORMANCE	29
	9.1 Systematic Errors	29
	9.2 System Noise	40
	9.3 Long-Arc Analysis	40
	9.4 Improvements in Performance	42

TABLE OF CONTENTS (Cont.)

		Page
10	PERSONNEL	44
	10.1 Visitors	44
	10.2 Program Personnel Status	44
	10.3 Travel	44
	APPENDIX A	A-1
	APPENDIX B	B-1

SATELLITE-TRACKING AND EARTH-DYNAMICS RESEARCH PROGRAMS

Semiannual Progress Report No. 39
Final Report Supplement No. 76

1. INTRODUCTION AND SUMMARY

This report describes the activities carried out by the Smithsonian Astrophysical Observatory (SAO) for the National Aeronautics and Space Administration (NASA) under Grant NGR 09-015-002 during the period 1 July to 31 December 1978. The geodesy and geophysics work and the upper atmosphere work are currently funded separately from this grant, although the research is still maintained as part of a total integrated program at the Observatory. Appendices A and B highlight some of the more significant results from those research programs.

All four SAO laser sites were in routine operation during the reporting period; they obtained a 6-month total of 182,529 range observations on 3610 passes. These data have been furnished to the National Space Science Data Center (NSSDC) at Goddard Space Flight Center (GSFC). Routine network participation by cooperating agencies contributed greatly to the success of on-going tracking campaigns. Significant amounts of data were acquired this period from Kootwijk, Netherlands; San Fernando, Spain; Helwan, Egypt; and Wettzell, FRG. Some data were also provided from Borowiec, Poland.

The network performed continuous tracking of several retroreflector satellites. Seasat was tracked at highest priority to support the altimeter experiment and also to develop a refined gravity-field model for orbit determination. Also tracked were Geos 3 for precision orbit determination in support of its altimeter and other on-board experiments, Lageos for geophysical studies

and orbital maintenance, and a complement of others for application in refined determinations of station coordinates and the earth's gravity field and for studies of solid-earth dynamics. The saturation tracking of Seasat, which began in late June, immediately after its launch, was reduced in priority in late September when the spacecraft failed. Routine tracking was maintained until the end of the year.

Laser-system improvement continued as a fundamental part of SAO's tracking program, and progress was made on several fronts during the past 6 months. The first laser pulse chopper, installed and in use at Mt. Hopkins, Arizona, has been operating routinely since July. System ranging accuracy (systematic) to both high and low satellites has been estimated at 10 cm from extended target calibrations, prepass and postpass calibrations, and wavefront measurements. During this reporting period, the chopper was also installed in Arequipa, Peru, and Natal, Brazil. The most impressive part of the chopper program so far has been its success with Lageos, to which we have been able to range routinely at the 1- to 5-photoelectron level. An additional unit is now being prepared by the vendor for installation at Orroral Valley, Australia, in early 1979.

The new NTS receivers have been installed in Arequipa and Natal; a third is slated for Mt. Hopkins. Twin-axis rotator antenna systems have been built for the receivers by SAO to enable the stations to follow both NTS satellites.

Cesium standards and Omega receivers, provided on long-term loan by the Coast Guard for Mt. Hopkins, Natal, and Arequipa, are in use at those stations. With this timekeeping system, the stations should be able to maintain a timing accuracy of 5 to 10 μsec independent of the NTS receivers.

Work continued on the development of software in response to network needs and system improvements. A new production processing system at headquarters, which is intended to meet the 60-day data-turnaround cycle required for Seasat, is completed, and data have been processed through the new format through December 1978.

The recently installed VAX 11/780 computer, which replaces the CDC 6400, has necessitated the development of new programs for generating orbital elements for laser pointing angles and for improving means of treating "difficult" orbits such as NTS II's critical inclination. The quick-look data-processing cycle has also been examined in light of the new computation facility. A preliminary design has been chosen, and many of the programs are in the process of being coded.

2. OPERATING STATUS

The four SAO laser sites — at Mt. Hopkins, Natal, Arequipa, and Orroral Valley — continued routine operations during this reporting period. The stations obtained a 6-month total of 182,529 observations on 3610 passes of Seasat, Geos 1, Geos 3, BE-C, Starlette, Lageos, and NTS II. Validated laser returns for the period have been sent to the NSSDC at GSFC; monthly statistics of the verified points and passes, by station and by satellite, are given in Table 1. For calendar year 1978, the SAO and cooperating stations acquired 332,869 points on 6252 satellite passes.

Ranging tests to NTS II were carried out in September from Arequipa with the newly developed prediction software. The station obtained 11 passes over a period of about 2 weeks. Typical range noise was 1 m.

During the reporting period, SAO continued to maintain the operations reporting procedures requested by NASA. On a monthly basis, SAO provides statistics of tracking success, weather, and maintenance (see Table 2).

Over the past 6 months, the Baker-Nunn camera activities at the laser stations were reduced to a maintenance level. The cameras in São Paulo, Brazil; Maui, Hawaii; and Debre Zeit, Ethiopia, remain in storage. The SAO Baker-Nunn cameras in St. Margaret's, Canada; Naini Tal, India; Dodaira, Japan; and Dionysos, Greece, provided some very low-level coverage in support of orbital maintenance. Procedures to donate the cameras to the cooperating agencies are now in progress.

Table 1. Verified points and passes for the period 1 July through 31 December 1978.

Station	July		August		September		October		November		December		Total	
	Passes	Points	Passes	Points	Passes	Points	Passes	Points	Passes	Points	Passes	Points	Passes	Points
Arequipa	450	29,491	310	21,832	240	14,811	288	14,858	132	6,614	165	6,004	1,585	93,610
Mt. Hopkins	35	887	33	743	152	5,323	191	7,570	128	4,140	90	3,369	629	22,032
Natal	34	1,009	48	1,730	64	2,058	74	2,533	78	2,740	17	475	315	10,545
Orroral Valley	155	10,519	125	9,874	65	5,348	127	9,555	90	7,449	85	5,251	647	47,996
Helwan	41	1,526	18	401	18	468	8	133	—	—	1	7	86	2,535
San Fernando	31	236	3	23	20	160	31	262	13	96	12	105	110	882
Kootwijk	24	336	18	239	17	238	41	540	15	203	27	349	142	1,905
Wettzell	22	919	33	1,312	10	205	30	582	1	6	—	—	96	3,024
Total	792	44,923	588	36,154	586	28,611	790	36,033	457	21,248	397	15,560	3,610	182,529
Satellite														
BE-C	133	4,893	81	3,697	98	3,645	120	4,426	64	2,403	80	2,706	576	21,770
Geos 1	159	8,764	83	5,015	70	2,735	154	7,061	106	6,532	66	3,304	638	33,411
Starlette	144	6,246	132	4,564	103	4,292	146	5,802	67	2,041	79	2,536	671	25,481
Geos 3	162	6,513	151	6,435	145	5,275	167	5,941	107	3,683	108	3,735	840	31,582
Lageos	97	14,570	89	14,506	82	10,205	98	9,602	56	4,954	51	2,972	473	56,809
NTS II	—	—	—	—	11	268	—	—	—	—	—	—	11	268
Seasat	97	3,937	52	1,937	77	2,191	105	3,201	57	1,635	13	307	401	13,208
Total	792	44,923	588	36,154	586	28,611	790	36,033	457	21,248	397	15,560	3,610	182,529

Table 2. Laser operations summary, July through December 1978.

Station	Passes scheduled	Passes supported	Data obtained*	Passes canceled owing to		
				Weather†	System down	Other
Mt. Hopkins	2901 (100%)	1065 (37%)	794 (59%)	1545 (53%)	237 (8%)	54 (2%)
Natal	2338 (100%)	777 (33%)	348 (30%)	1194 (51%)	305 (13%)	62 (3%)
Arequipa	2831 (100%)	2166 (76%)	1715 (75%)	557 (20%)	81 (3%)	27 (1%)
Orroral Valley	2518 (100%)	937 (37%)	681 (67%)	1502 (60%)	69 (2%)	10 (1%)

*Number of passes and percent of total scheduled minus passes canceled because of weather.

†Not included are passes attempted but unsuccessful because of poor weather.

3. LASER OPERATIONS AT COOPERATING AGENCIES

SAO continues to maintain its close working relationship with a number of organizations around the world that provide cooperation in tracking programs.

During the past 6 months, SAO actively supported the Centre National d'Etudes Spatiales (CNES) Starlette program with routine laser tracking, providing CNES with orbital elements to sustain its tracking operation. Under a joint cooperative arrangement among SAO, CNES, and the Instituto y Observatorio de Marina, a CNES laser is in routine operation at the SAO camera site in San Fernando. The laser tracked several retroreflector satellites, including Seasat, Geos 3, and Starlette, and regularly furnished SAO with quick-look data throughout the reporting period. SAO also provided communications and timing support to the laser operation.

The Institut für Angewandte Geodäsie's (IFAG) satellite-ranging system in Wettzell routinely tracked Lageos, Seasat, Geos 3, and other laser retroreflector satellites through November. The new system, which began operations last April, has a ranging accuracy of a few centimeters. SAO provided IFAG with orbital elements for laser pointing predictions and assisted in screening and validating IFAG data.

The Technische Hogeschool Delft, Netherlands, has an operating laser system in Kootwijk, which regularly obtained tracking data on retroreflector satellites during the past 6 months. SAO supplied orbital elements for laser predictions and provided routine processing of quick-look data.

A cooperative laser tracking program with the Soviet Academy of Science, the Technical University in Prague, Czechoslovakia, the Helwan Observatory in Egypt, and SAO has been in operation at Helwan for more than a year. For this program, the Soviet Union and the Czechoslovakians provide and maintain a laser tracking system at Helwan, the Helwan Observatory furnishes personnel

to operate the system, and SAO supplies technical consultation, a station clock, and partial operating support from PL 480 (Excess Currency) funds. The data are routinely screened and validated by SAO. The station has been supplying significant amounts of range data. During the reporting period, the equipment was upgraded with a short-pulse laser and some new electronics. With these improvements, the system appears to be operating at an accuracy of 20 to 30 cm. Additional upgrading is planned for next summer.

The first data from the laser site in Borowiec, Poland, were received in August; they were taken on Geos 3 and Seasat. Several more passes were obtained in October. This station is also being operated under partial support from the Excess Currency program.

The station in Dionysos, which is in the process of being upgraded for improved ranging capability, continued to suffer many hardware problems and was unable to participate in the program during the reporting period. The laser is operated by the National Technical University.

Very few data were provided by the Dodaira station during the past 6 months. Efforts are under way to have the station operational by early 1979.

In all, 8346 quick-look observations were submitted to SAO from the cooperating agencies between July and December 1978. From Helwan, 2535 points on 86 passes of final data for the same period were received by SAO and forwarded to GSFC. Final data from Wettzell, San Fernando, and Kootwijk are being sent directly to Goddard.

4. SATELLITE OBSERVING CAMPAIGNS

Tracking of Seasat, Lageos, and Geos 3 continued at high priority throughout the past 6 months; these three satellites are yielding valuable data for oceanographic, geodetic, and earth-dynamics investigations.

Seasat, which was launched on 27 June 1978, was a dedicated oceanographic satellite carrying an array of ocean-sensing equipment for measuring the oceans' surface conditions and dynamical properties. Of particular interest to SAO and many other investigators was the satellite-to-sea-surface radar altimeter, which was being used to map ocean-surface topography for investigations in both solid-earth and ocean physics. With its 10-cm accuracy, Seasat's altimeter had a considerably improved performance over that of Geos 3. This 10-cm capability was to be used to develop comprehensive maps of ocean currents and general circulation, to monitor the mesoscale eddy field and the ocean tides for oceanographic requirements, and to determine a detailed ocean geoid for use in studying the underlying solid earth. For this program, the SAO network laser systems provided saturation tracking of Seasat. Since the altimeter was operational nearly full time, all Seasat passes at each station were high priority, and schedules were adjusted to provide maximum coverage. In addition to the tracking support, SAO also served as interface for NASA with all the overseas tracking participants. In this role, SAO furnished orbital elements for predictions, quick-look data screening and status reports, and quick-look data catalogs, plus coordination, scheduling, and other support.

On 10 October, Seasat experienced a catastrophic failure, and all systems ceased functioning. In the 3 months of operation, the satellite acquired approximately 2000 passes of altimeter data, a much smaller set of data than anticipated yet an extremely valuable one. SAO continued routine tracking of Seasat into November, when satellite stability precluded routine ranging. Tracking was in support of gravity-field model development for altimeter data reduction.

During the Seasat tracking campaign, between launch and the cessation of tracking, the four SAO lasers acquired 412 passes on Seasat. A breakdown of the data yield is shown in Table 3.

The network also provided continuous tracking coverage on Lageos. After the failure on Seasat, Lageos became top priority. Launched in May 1976, Lageos remains a fundamental tool for the study of solid-earth geophysics. At its 5900-km altitude, this retroreflector satellite serves as a stable reference platform in space, against which small motions of the earth's surface can be measured. It is being used for the precise measurement of plate and fault motion, polar motion, earth rotation, and other related phenomena. Data from Lageos are being used at SAO and GSFC to develop new analytical techniques for improved baseline measurements and earth-dynamics investigations. SAO's laser network has provided continuous tracking data on Lageos for routine orbital maintenance and for orbital and geophysical analysis since launch. These data, and those to be taken in the future, will form a significant part of the data set to be made available to investigators under NASA's Lageos Announcement of Opportunity. A summary of the network's tracking activity on Lageos from July through December 1978 is included in Table 4.

SAO continued to track Geos 3 as one of the complex of retroreflector satellites for gravity-field and geophysical studies. With the demise of Seasat, Geos 3 suddenly took on far greater importance, and tracking priority was raised in order to support the altimeter experiment fully. The altimeter on board Geos 3 had been operating at an estimated accuracy of better than 50 cm since its launch in 1975, providing precision tracking and orbit determination for ocean-surface topography and gravity-field analysis. Although Seasat had a more accurate altimeter, there were strong indications that Geos 3 operation would be continued in order to enhance coverage, increase the data yield, and support some two-satellite experiments. Proper interpretation of the altimeter data required precision tracking and orbit determination, and the SAO laser systems have been tracking Geos 3 in support of this. Long-term tracking has also been performed for gravity-field analysis.

Table 3. Seasat passes and points, 1 July through 31 December 1978.

Station	July		August		September		October		November		December		Total	
	Passes	Points	Passes	Points	Passes	Points	Passes	Points	Passes	Points	Passes	Points	Passes	Points
Mt. Hopkins	3	51	—	—	25	576	30	871	15	300	1	6	74	1804
Orroral Valley	21	692	7	168	8	265	20	598	15	495	3	58	74	2276
Natal	5	116	2	47	6	141	7	160	4	66	2	61	26	591
Arequipa	58	2833	28	1170	33	1149	41	1478	19	720	7	182	186	7532
Borowiec*	—	—	2	17	—	—	—	—	—	—	—	—	2	17
San Fernando*	—	—	7	70	2	18	—	—	—	—	—	—	9	88
Kootwijk	5	70	2	28	4	53	7	94	4	54	—	—	22	299
Helwan	2	20	8	224	—	—	—	—	—	—	—	—	10	244
Wettzell	3	155	5	300	1	7	—	—	—	—	—	—	9	462
Total	97	3937	61	2024	79	2209	105	3201	57	1635	13	307	412	13,313

*Quick-look data.

Table 4. Quick-look Lageos passes, 1 July through 31 December 1978.

Station	July	August	September	October	November	December	Total
Mt. Hopkins	10	2	11	16	9	11	59
Orroral Valley	33	29	19	36	27	18	162
Natal	2	5	6	13	7	2	35
Arequipa	45	43	41	25	13	17	184
Borowiec	—	—	—	—	—	—	—
San Fernando	—	—	—	—	—	—	—
Kootwijk	3	1	3	5	—	3	15
Helwan	—	—	—	—	—	—	—
Wettzell	4	9	2	3	—	—	18
Total	97	89	82	98	56	51	473

In the fall of 1978, however, the Geos 3 altimeter began to have difficulties with the high-intensity mode. With some nursing, the system was able to acquire data for short periods, but by November, operation became impractical and was discontinued. The altimeter continues to function in the global mode, which is now being used to measure wind speed and to study ice regions.

SAO also continued to provide orbital elements and scheduling for Geos 3 for the overseas cooperating laser stations. Geos 3 pass statistics for the past 6 months are given in Table 5.

Besides the above three satellites, the SAO network lasers have been tracking Starlette since its launch in 1975 in support of gravity-field development and orbital analysis at SAO, CNES, and GSFC. SAO also provided the tracking community with precision orbital elements for Starlette during the reporting period. A low-orbiting satellite, Starlette is used to supply data for the refinement of the intermediate- and long-wavelength terms in the earth's geopotential model and the development of solid-earth and ocean tidal models. This information is fundamental to an understanding of the dynamics and structure of the earth; it is being incorporated in the specific gravity-field model development that is being used in the analysis of Seasat and

Table 5. Geos 3 passes for the period 1 July through 31 December 1978.

Station	July	August	September	October	November	December	Total
Mt. Hopkins	1	11	34	42	22	15	125
Orroral Valley	32	25	8	17	17	21	120
Natal	10	18	26	19	28	8	109
Arequipa	89	78	59	61	32	50	369
Borowiec*	—	9	—	2	—	—	11
San Fernando	3	2	7	1	1	2	16
Kootwijk	14	10	4	15	7	12	62
Helwan	9	—	5	3	—	—	17
Wettzell	4	7	2	9	—	—	22
Total	162	160	145	169	107	108	851

*Quick-look data.

Geos 3 altimeter data. Moreover, the satellite's compact design and high mass-to-area ratio make it very useful for investigations of the earth's surface motions; indeed, the design and orbit of Starlette were chosen explicitly to support geophysical and geodetic research. In addition, Starlette has a retroreflector-array geometry that permits laser ranging at very low elevation angles (10 to 15°). This enables the ground systems to acquire very long data tracks, thereby significantly enhancing the orbital coverage and its influence on geodetic model development.

The SAO lasers have also been supplying data for GSFC's San Andreas Fault Experiment, a program to measure regional fault motions and determine the position of the earth's pole by means of laser ranging techniques. In support of this project, SAO has been furnishing laser data to assist in global orbit determinations. Of particular interest in the experiment are tracking data from Mt. Hopkins. This station, which is on the North American plate yet removed from the local motions within the fault area, serves as a fiducial reference point.

A major criterion in selecting satellites for tracking is for the total complement to represent a good distribution of orbital parameters in order to support the development of gravity-field models. Thus, Geos 1 and BE-C, which are also laser retroreflector satellites, were also tracked during the past 6 months for improving station coordinates and the gravity-field model in support of Seasat, Lageos, and Geos 3 projects. Because Geos 1 is less subject to variable atmospheric drag than are other satellites, its vertical stabilization and compact geometric shape result in stable orbits, which make the predictions more accurate. This factor, together with its high orbital inclination, consistently produces more observations. Further, both drag and photon pressure can be more accurately modeled for this satellite than for some of the other satellites equipped with laser retroreflectors. The superior data coverage and more stable orbits will improve the determination of polar motion. BE-C, though a little less favorable dynamically, has a very good orbit for geophysical investigations and an extremely compact retroreflector array capable of yielding range measurements to decimeter accuracies.

The laser network also provided some range data to NTS II for verification of the retroreflector-array integrity.

5. ENGINEERING

5.1 Pulse-Processing and Detection System

All the pulse-processing systems continued to work well, providing a dramatic improvement in data quality and system performance. No major failures were experienced during the reporting period. A malfunctioning 10-db amplifier had to be replaced because of a pulse-distortion problem.

Measurements made at Mt. Hopkins last spring, in preparation for installation of the pulse chopper, showed that the pulse-processor electronics could be operated with a single configuration for both the long and the chopped laser-pulse modes, thus enabling the operational mode to be changed with a minimum of adjustment. Another modification permits the oscillator output to be monitored continuously, preventing the laser from overdriving in the chopper mode. This change, which requires a new circuit card in the start-channel electronics, was done first at Mt. Hopkins and subsequently at Arequipa and Natal in the fall, before pulse-chopper installation. This modification will be carried out at Orroral Valley in early 1979.

During the engineer's visit to Peru, station grounding was reviewed and a complete new ground bed was constructed, with extensive wiring changes. In Brazil, the grounding connections between the equipment racks were rearranged.

5.2 Minicomputers

The minicomputers in the field continued to perform data collection and processing satisfactorily, although minor difficulties were encountered. A malfunctioning memory board and central-processing unit were repaired in Cambridge and returned to Orroral Valley. The system in Brazil experienced fatal run-time errors, which were finally traced to a defective Data General memory module. A substitute, dispatched from Cambridge and installed in

October, seems to have resolved the difficulty. Meanwhile, the weak memory drivers on the original module are being replaced. Substitution of another +5-volt regulator in the Linc tape power supply in Brazil solved a Linc tape drive problem.

Several minor difficulties with minicomputer hardware were experienced at headquarters during the reporting period. Some disk hardware and operating problems were resolved by substituting modules and discarding old versions of some of the utility programs. One failure was traced to a faulty test loop in the Y write circuitry of an older 4K memory board; the system is now operational. Another system failed to bootstrap properly for initial program loading; the problem was isolated to the read/write head, and tests are under way to find a suitable replacement head. A problem with the computer-based field-data system simulator and prototype direct-connect interface was also corrected. Cambridge experienced a failure in a lexiscope interface board. A spare one was pressed into service, but it, too, developed problems. The latter, still under warranty, has been returned to the vendor for a second time. The original one was repaired in-house and is back in use.

As a result of the more stringent requirements imposed by the direct-connect system, SAO has been cycling all Linc tape units through the vendor for refurbishing and upgrading to improve reliability and reduce the data error rate. All the field units have now been processed, along with all but one of the headquarters' systems. New disk packs have been received from an independent vendor. They are being formated and tested in Cambridge before being used for new program development and as backup units.

5.3 Timing

5.3.1 Status

The SAO timekeeping performance improved considerably during the last half of 1978. The main station clocks were converted to low-drift cesium standards, Omega VLF receivers tracked highly stable Coast Guard transmissions

for a good frequency reference, time-interval meters replaced oscilloscopes for making measurements, and NTS receivers were installed at SAO's South American sites for daily epoch checks. All contributed to a more trouble-free operation and improved accuracy. The South American stations experienced a three-fold improvement in timing accuracy.

During the past 6 months, the SAO laser stations, utilizing a combination of cesium and rubidium oscillators, VLF reception, and routine epoch checks with portable clocks, NTS satellite data, and Loran, have been maintaining time traceable to UTC/United States Naval Observatory (USNO) with an accuracy of better than ±10 μsec, except for Egypt, which maintained time to ±50 μsec.

Portable-clock epoch checks made during this period are listed in Table 6. A portable cesium clock set time at Natal and Arequipa to better than 0.5 μsec of USNO in July. A clock trip during November between Mt. Hopkins and the National Bureau of Standards (NBS) showed a shift of only 1 μsec from a clock comparison made a year earlier.

5.3.2 Omega receivers

As part of a program to monitor Omega broadcast quality and transmission variations, the U.S. Coast Guard has made cesium clocks available to SAO on a long-term loan for the stations in Arequipa, Natal, and Mt. Hopkins; one was already available at Orroral Valley. The units will provide the Coast Guard with data on received signal strength and phase variations. The cesium clocks, which have replaced the rubidium oscillators in the main channel of the timing system, are now operational at all four SAO stations.

The Coast Guard has also furnished microprocessor-controlled Omega receivers to Arequipa and Natal as part of the monitoring program. The receivers are being used by SAO to provide an additional VLF phase reference. The receivers at SAO sites in Natal and Arequipa and at the Observatorio Nacional in Rio de Janeiro were checked out and made operational. The best antenna sites were selected, cesium oscillators were connected to the receivers,

Table 6. Clock comparisons performed between 1 July and 31 December 1978.

Station	Type of comparison	Month	Comparison agency	Set uncertainty of comparison (μsec)
Orroral Valley, Australia	rubidium clock	July	NASA Minitrack/Australia	±1
	rubidium clock	July	NASA Minitrack/Australia	±1
	cesium clock	August	National Mapping/Australia	±1
	cesium clock	September	National Mapping/Australia	±1
Natal, Brazil	cesium clock	July	USNO/Washington, D.C.	±1
	rubidium clock	October	Observatorio National/Rio	±3
Mt. Hopkins, Arizona	crystal clock	November	NBS/Boulder, Colorado	±3
Arequipa, Peru	cesium clock	July	USNO/Washington, D.C.	±1

and the units were integrated into the Natal and Arequipa timing systems. The Rio receiving system was sent to Natal to correct a cassette recording problem, where it is being held until replacement parts arrive.

5.3.3 Television timing in Natal

Line 10 television timekeeping equipment was repaired at Natal for daily time comparisons with the Rio Observatory. The data appear satisfactory and are being reduced at Rio. With this system operational, one timing facility will check the other should time ambiguities occur in the future.

5.3.4 NTS receivers

In December 1977, GSFC agreed to supply three NTS receivers for use at the laser stations, in anticipation of achieving a timing accuracy of 1 μsec with the combination of NTS receivers and cesium clocks. The first unit, received in December 1977, was intstalled in Arequipa with a temporary antenna mount last reporting period.

Because of a transmitter failure aboard NTS II, making its data unreliable, NTS I has been used instead. However, whereas the geocentrically stable orbit of NTS II gives reproducible satellite tracks twice daily, the NTS I orbit precesses relative to the earth, requiring daily adjustments to the antenna position. Hence, SAO has built steerable antenna mounts to enable the orbital precession of NTS I to be tracked. The assembly consists of commercially available twin-axis rotator mounts capable of pointing in both altitude and azimuth to an accuracy of 5°. The first unit was installed in Arequipa in August, replacing the temporary antenna mount.

The operational procedure for the new NTS receiver entails recording the data on cassette, editing the data in the minicomputer, and transmitting a five-level tape to the Naval Research Laboratory (NRL). Early results from Arequipa, reduced by the NRL, indicated an accuracy of about ±1 μsec. However, in August, a 500-μsec jump had occurred in the NTS data, followed by a 50-μsec

discrepancy at the end of the reporting period. This discrepancy still exists between the station-reduced epoch time and the NRL-reduced data; the problem appears to be in the NTS receiver. A clock trip is planned from Arequipa to the NASA site in Santiago, Chile, in early 1979 to verify that the receiver is at fault.

The second NTS receiver was installed in Natal in October, along with a new antenna rotator system. Reduced data from that unit are supported by station timekeeping data to within 4 μsec.

Mt. Hopkins will be the site of the third receiver and antenna. This equipment has undergone extensive testing in Cambridge over the past several months. The receiver data have been verified with a clock trip. The dual rotator assembly is being constructed in Cambridge, but a defective motor had to be returned to the manufacturer. It still failed to operate properly on return to Cambridge; another replacement unit will be furnished by the manufacturer. When the assembly has been readied, the unit will be shipped to Mt. Hopkins for installation.

The NTS I satellite operated sporadically throughout the reporting period owing to overheating. Its transmitter was shut down during all of December until the satellite cooled. Day-to-day epoch measurements could not be relied on owing to the transmission irregularities.

Checkout and calibration of the NTS receivers require a special calibrator, one that simulates the operation of the satellite at P band frequencies. SAO had planned to build these from an existing NRL design. Drawings for the calibrator have been completed and reviewed, preliminary parts lists formulated, and some parts acquired. As other agencies showed interest in the calibrator, preliminary specifications were sent to GSFC, NBS, and IFAG. Owing to the failure of the NTS II satellite transmitter and the overheating problem of the NTS I version, however, we have decided not to construct the calibrator at this time.

5.3.5 Other timing information

The only hardware problems encountered with the timing equipment during this reporting period involved faulty rubidium standards from Arequipa and Mt. Hopkins; the latter was repaired in Cambridge.

Work is under way on a computer program to aid in time reduction.

6. SYSTEM UPGRADING AND MODIFICATION

6.1 Laser Short-Pulse Modification

The first pulse chopper, installed at Mt. Hopkins last reporting period, has been operating without difficulty since July. The chopper, which uses a krytron-triggered Blumlein circuit to activate a Pockels cell, produces a 0.7- to 1.0-joule pulse with a width of 6 nsec. Extensive calibrations show the system accuracy to be about 10 cm (see Section 9); satellite range noise is between 10 and 30 cm, depending on the return signal strength.

Following successful installation of the preproduction model, three additional units were ordered from the vendor, Lasermetrics, Inc. The first of these was acceptance-tested at the factory in October and hand-carried by an SAO engineer to Peru; by November, installation was completed. The second unit was accepted and installed in Natal in December. Construction of the chopper for Orroral Valley is nearly complete; it will be shipped to Cambridge in January for a final check before being sent to Australia.

Construction and calibration of eight high-voltage attenuators for use with the pulse chopper are nearly completed. These units will be used as test equipment for the high-voltage circuit in the pulse chopper.

A method has been devised to enable either single Q-switch or pulse-chopping operation to be done without physically removing the pulse chopper from the laser transmitter. A facility has been incorporated into the electronics to put a DC level on the Pockels cell to pass the full laser pulse when desired. This "pass" operation may be required during routine ranging to the more distant satellites, such as NTS II.

6.2 Direct-Connect Computer Control

The direct-connect computer-control facility between the minicomputer and the laser system has now been operational at all four field stations for over

a year. The facility permits the pointing predictions generated by the minicomputer and stored on Linc (directly accessible) magnetic tape to be fed directly to the laser system when required. Raw data from the pulse processor can be fed back to the minicomputer and partially processed in real time. The new system provides a control framework for much of the processing at the stations and eliminates most of the requirements for punched paper-tape equipment. The facility also provides an on-line CRT, replacing many of the operator functions on the teletype.

No major problems have been experienced with the system since initial installation. The savings in paper-tape handling and electromechanical hardware problems have been a great relief to station personnel.

7. COMMUNICATIONS

Radio-teletype communications to Arequipa and Natal continued to work satisfactorily during most of the reporting period, although, toward the end of November, teletype traffic was more garbled than usual. After realigning the HAL-ST6 demodulator and tone keyer, the situation improved.

The periodic transmission difficulties with the FTS teletype circuit between Cambridge and Mt. Hopkins seem to have been resolved, and operations continued routinely.

In an attempt to speed up communications with the field stations from the present rate of 10 words per minute, we have been experimenting with thermal printers as terminals. The teletype link between Mt. Hopkins and Cambridge has been operating for several months at 30 words per minute over the FTS telephone line with the Miniterm terminals. We have also been able to use the terminals with the radio link, but this has been limited to 10 to 15 words per minute because of limitations in the radio's frequency-shift converters. This limitation is being examined.

With the closeout of the CDC 6400 computer (see Section 8.2), a Data General Nova 1200 used within the computer system will be made available to the tracking program. Plans are being made now to utilize the minicomputer for message preparation, editing, and archiving and as an interface with some of the communications equipment. Software now in use for data and text editing in the Data Services Group has already been used for several months by the Communications Center for message handling. An on-site facility will permit considerably greater flexibility. Currently, we plan to have the Nova with Linc tape drives, paper-tape equipment, and a lexiscope display set up in a dedicated manner for use by late spring.

8. DATA SERVICES AND PROGRAMING

8.1 Data Services Group

The Data Services Group maintains the operational and prediction cycle necessary for the efficient flow of data to and from the stations. In particular, the Group screens and validates all incoming data, generates orbital elements for all satellites being tracked by the SAO network, supplies orbital elements to SAO laser stations and other agencies, and furnishes SAO laser data to GSFC. The Group has been able to accommodate, without serious impact, the large increase in data yield over the past several years resulting from the implementation of minicomputers at the four SAO laser stations. Pointing predictions are developed in the field from orbital elements furnished weekly by Data Services. Then the field stations send their quick-look data, a small subset of the acquired data, through communications channels to Cambridge; these form the basis on which new orbital elements are generated for predictions. The full data sets are mailed from the field on Linc tape for detailed processing and analysis.

An orbit for Seasat, computed early in July from Baker-Nunn camera data, was used to generate ephemerides for laser acquisition. By 7 July, Arequipa had successfully recorded the satellite, and other network lasers soon followed. Tracking ceased from 15 to 26 August following an orbital maneuver and resumed on 30 August from an orbit determined from GSFC elements and quick-look laser data. In September, a month's worth of uninterrupted data was achieved. On 10 October, Seasat's on-board electronics failed, but laser tracking data were obtained and processed through 21 December. The format for the laser data had previously been modified to include additional error-source information and to be compatible with the requirements of the Seasat program; data from 1 January 1978 were processed through the new format for uniformity. By the end of December, final data on all satellites tracked through 1978 had been transmitted to the NASA Data Bank.

8.2 Data-Processing Software

SAO has purchased a DEC VAX 11/780 computer to replace the CDC 6400, in order to improve machine capability and reliability. The new computer is now fully operational. Efforts have been directed toward developing a software package on the VAX to predict orbits for use in generating laser pointing angles for satellite tracking.

The quick-look laser data-processing cycle was examined in view of the new computation facility. A new design was chosen, with major criteria being to exploit the interactive capabilities of the VAX and to localize and minimize the number of points requiring manual intervention. Elements of the new design include: 1) the precise analytical satellite orbit-determination program, 2) the data preprocessor, 3) an elements manager, 4) an interface program for orbit determination, and 5) an elements transmitter. By December, the preprocessor (see Figure 1) had been fully converted to process SAO laser data, and formating to handle NASA teletype quick-look data was in progress. The orbit-determination program is currently being debugged; all the other programs have been designed and are in the process of being coded.

A major consideration in designing the new quick-look package was whether to retain the production orbit program (DOI) or to use the precise analytical orbit-determination program (GRIPE). A compatibility study comparing DOI and GRIPE, each used with the field laser-pointing package (FLPPS), was begun. In order to do this, a modification to FLPPS was necessary to make the treatment of long-period zonal-harmonics perturbations compatible with that of GRIPE. Long-period perturbations due to the zonal harmonics of the earth's gravitational field are now expressed in nonsingular variable ($\xi = e \cos \omega$, $\eta = e \sin \omega$, $\lambda = m + \omega$, Ω, and i) rather than in Keplerian elements (ω, Ω, i, e, and m). This modification had been completed by December, and tests were begun. The tests will include a comparison of the pointing angles produced by the present DOI and FLPPS programs with those from GRIPE and the revised prediction program. Very preliminary results suggest no serious problem with compatibility.

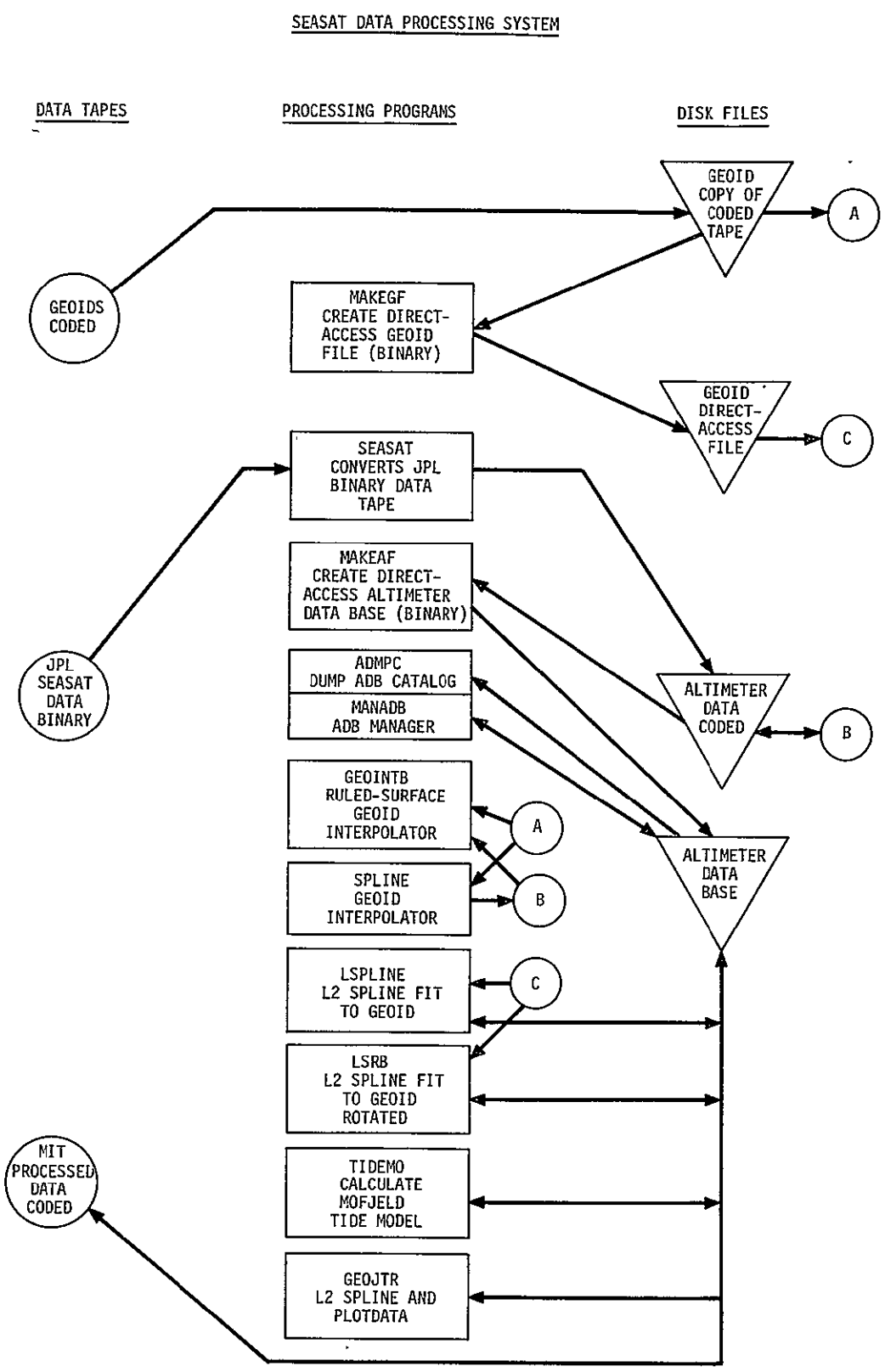

Figure 1. SAO quick-look data-processing system.

8.3 Pulse-Processing and Prediction Software

With the tracking of satellites now controlled by the computer control system, all the detailed information is available on the CRT and much of the printout from the prediction system is not needed. The laser prediction software, FLPPS, has undergone several modifications to produce a much briefer summary of those pass characteristics that are of interest to the operator; this task is completed, and the programs are being tested before being sent to the field. One recent modification enables only a summary output of the time-delineated portions of passes to be predicted, rather than the whole horizon-to-horizon passes predicted formerly. This capability will be used to schedule nonconflicting arc segments with the NTS II satellite, which orbits above the horizon for several hours, enabling field stations to fit short periods of NTS data acquisition into their operating schedules. Another change enables users to input a satellite delay time, thus adjusting and updating the mean-anomaly term, in order to correct for the early or late arrival of a satellite as a result of atmospheric drag; final testing of this facility has been completed.

During the past 6 months, changes were made in the direct-connect computer control software to accommodate the addition of the pulse chopper. The software now uses the laser output pulse for return-signal processing (centroid correction). The program also provides many operations and system diagnostics in real time on the CRT. A capability to apply predetermined corrections to the azimuth and altitude settings of the mount has also been incorporated into the direct-connect system to account for reproducible errors in the mechanical system.

Other modifications were made to the start and target-calibration programs and to the format of the heading of the intercoupler. A correction was made in the calculation of pulse width, and another change facilitates the reprocessing of raw data files. With the addition of the chopper, the output of the oscillator becomes more critical; changes in the software are being made to include the digitized area of the oscillator in the display.

9. ANALYSIS AND SYSTEM PERFORMANCE

During this reporting period, the pulse chopper was installed in the SAO laser systems at Mt. Hopkins, Arequipa, and Natal; installation is scheduled for Orroral Valley in early 1979. The choppers, coupled with the pulse processing, have improved the system accuracy considerably; several other small items, short of major upgrading, would improve the performance further.

9.1 Systematic Errors

The systematic errors of the laser ranging system can be divided into three categories: spatial, temporal, and signal-strength variations. Spatial variations refer to differences in time of flight depending on the position of the target within the laser beam. Temporal variations relate to system drift between prepass calibration, satellite ranging, and postpass calibration. Variations in range due to changes in signal strength from pulse to pulse are a function of receiver characteristics and digitizer baseline interval.

Spatial variations. The spatial variations, or wavefront error, have been measured at Mt. Hopkins several times. Figure 2 and Table 7 give the results before and after installation of the pulse chopper. The two wavefront measurements performed with the chopper show a maximum deviation of ±0.3 nsec (4.5 cm) from the mean value across the wavefront. The standard deviation of the excursions is about 0.2 nsec (3 cm).

Temporal variations. The temporal variations are estimated by the difference between prepass and postpass calibration measurements. These differences represent an upper bound, since other statistical errors are also included. The results of recent calibration differences at Mt. Hopkins and Arequipa are shown in Figures 3 and 4; they average 0.3 nsec (4.5 cm) for Arequipa and 0.4 nsec (6 cm) for Mt. Hopkins.

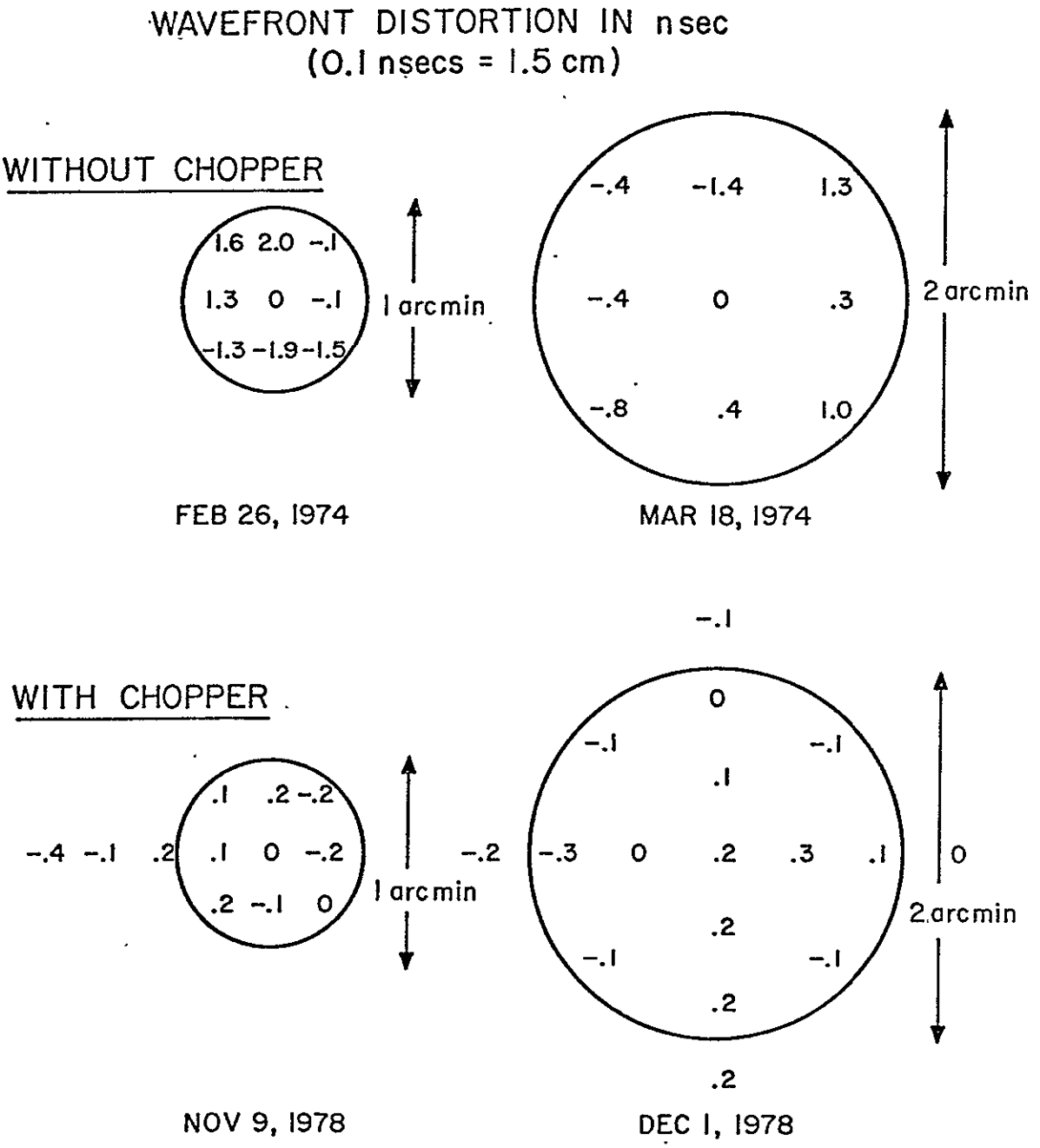
WAVEFRONT DISTORTION IN nsec
(0.1 nsecs = 1.5 cm)
WITHOUT CHOPPER
1.6 2.0 -.1
1.3 0 -.1
-1.3 -1.9 -1.5
1 arcmin
-.4 -1.4 1.3
-.4 0 .3
-.8 .4 1.0
2 arcmin
FEB 26, 1974
MAR 18, 1974
WITH CHOPPER
-.1
.1 .2 -.2
-.4 -.1 .2 .1 0 -.2 -.2
.2 -.1 0
1 arcmin
0
-.1 -.1
.1
-.3 0 .2 .3 .1
.2
-.1 -.1
.2
.2
0
2 arcmin
NOV 9, 1978
DEC 1, 1978

Figure 2.

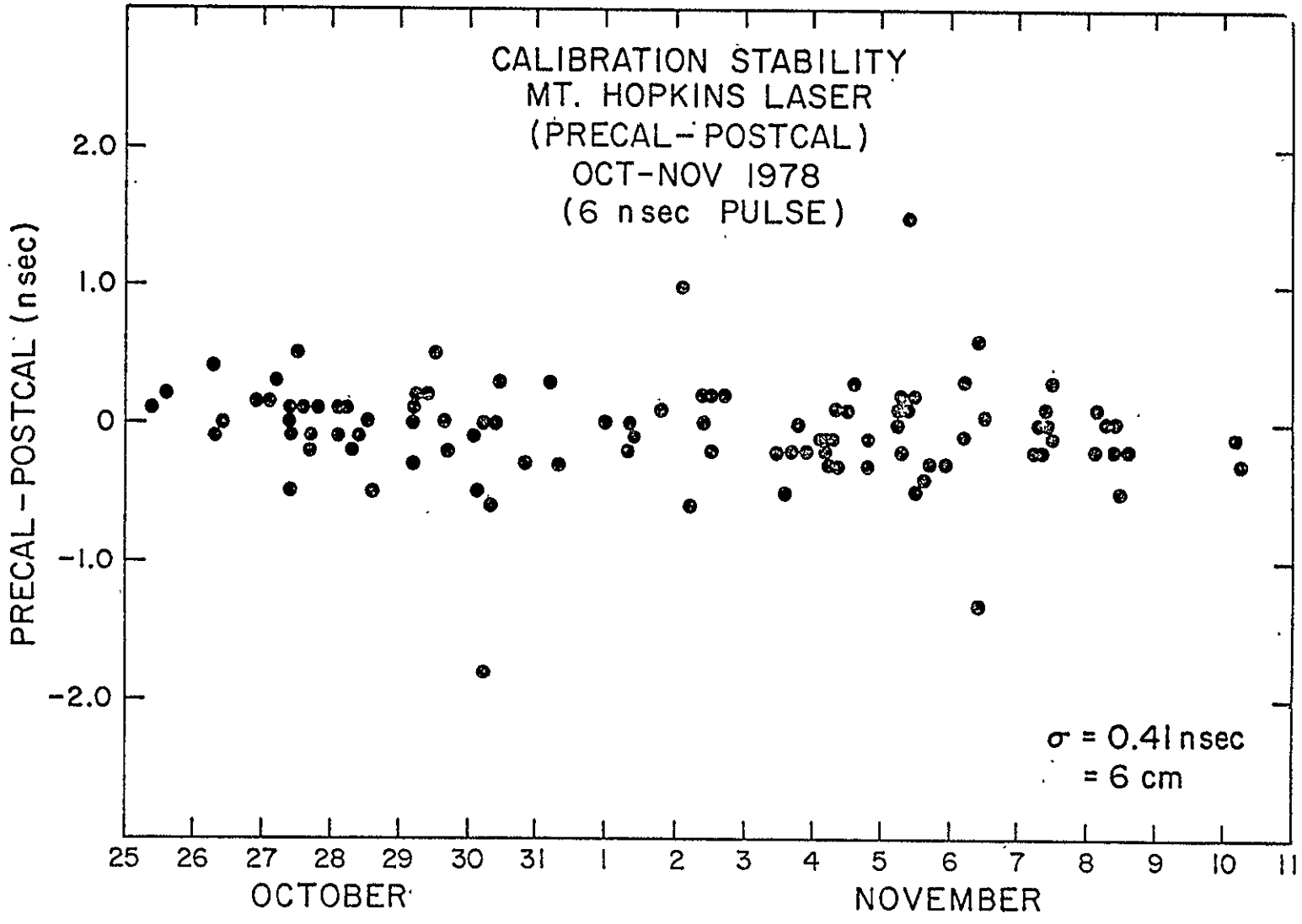
CALIBRATION STABILITY
MT. HOPKINS LASER
(PRECAL-POSTCAL)
OCT-NOV 1978
(6 n sec PULSE)
PRECAL-POSTCAL (n sec)
2.0
1.0
0
-1.0
-2.0
σ = 0.41 n sec
= 6 cm
25 26 27 28 29 30 31 1 2 3 4 5 6 7 8 9 10 11
OCTOBER
NOVEMBER

Figure 3.

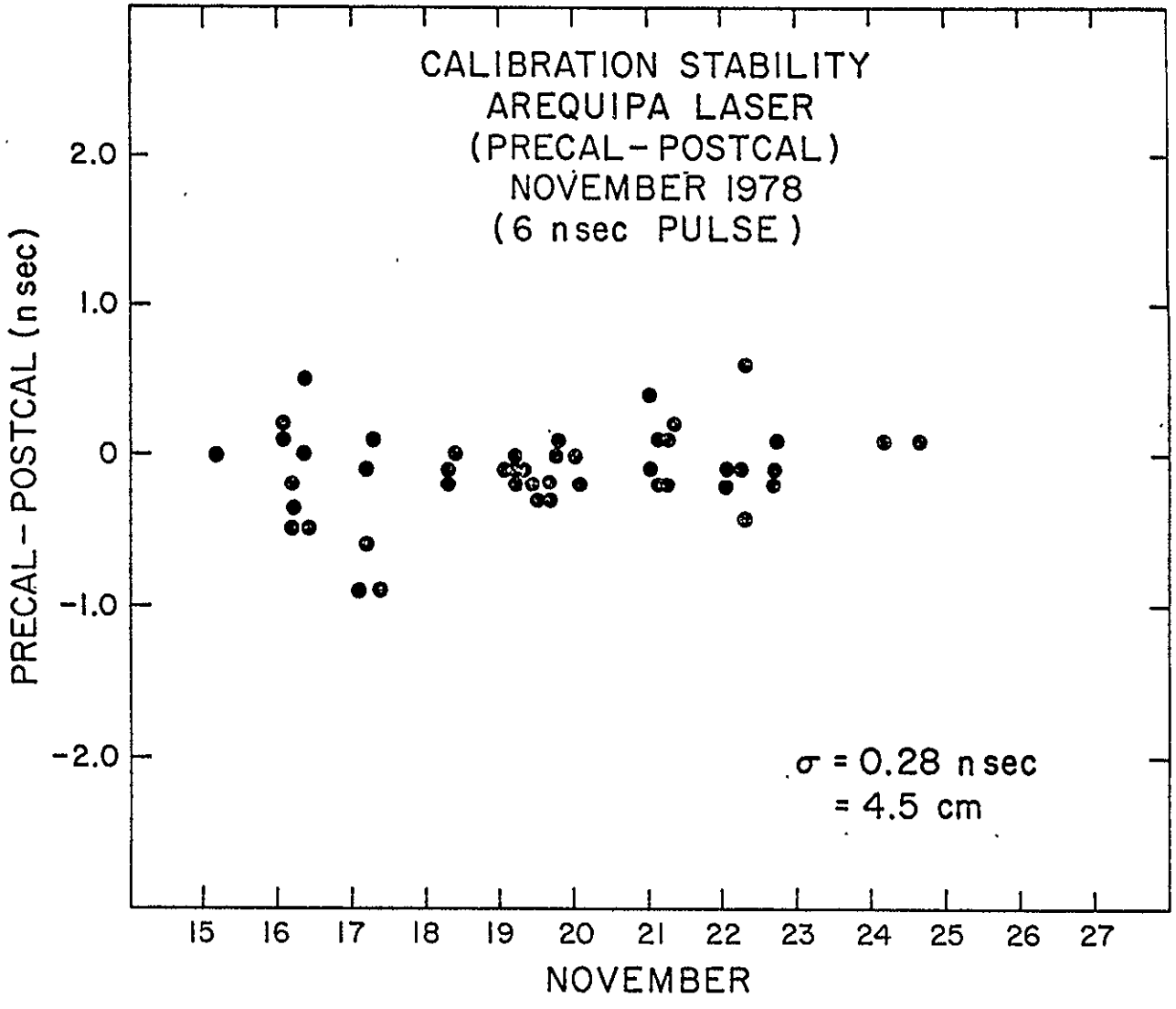
CALIBRATION STABILITY
AREQUIPA LASER
(PRECAL-POSTCAL)
NOVEMBER 1978
(6 nsec PULSE)
PRECAL-POSTCAL (n sec)
2.0
1.0
0
-1.0
-2.0
σ = 0.28 n sec
= 4.5 cm
15
16
17
18
19
20
21
22
23
24
25
26
27
NOVEMBER

Figure 4.

Table 7. Wavefront distortion.

Date of measurement	Spacing between points (arcmin)	Average number of photoelectrons received	rms wavefront distortion (nsec)	Maximum excursion (nsec)
26 February 1974	0.3	88	1.4	3.9
18 March 1974	0.6	56	0.8	2.7
9 November 1978	0.3	56	0.19	0.6
1 December 1978	0.42	87	0.17	0.6

Signal-strength variations. Variations in apparent range with signal strength have been examined with extended target calibrations over the dynamic range of the laser instrument. Calibration curves are obtained separately for high and low satellites. With low satellites, return signal strengths are typically 10 to 500 photoelectrons and the waveform digitizer is operated with a 50-nsec baseline (2.5-nsec sampling). On high satellites, the chopper is operated right down to the single-photoelectron level and the digitizer functions with a 20-nsec baseline (1-nsec sampling).

The extended target calibration data taken in the low-satellite mode (see Figures 5 and 6) show a flat response in the 5- to 500-photoelectron region to ±0.3 nsec (4.5 cm) or better. The deviation at very low signal strengths is due to poor digitizer sampling of the narrow single-photoelectron events.

In the high-satellite configuration, the extended target calibrations show a flat response in the 1- to 50-photoelectron region to ±0.4 nsec (6 cm) or better (see Figures 7 through 10). The deviation at higher signal strengths is due to saturation of the photomultiplier tube (PMT) in this mode.

Error budget. Using systematic error values of 4.5, 6, and 4.5 cm for the spatial, temporal, and signal-strength variations for low satellites and assuming that these errors are independent, the root-sum-square (rss) error due to systematic sources is about 9 cm (see Table 8). For the higher satellites, the errors are typically 4.5, 6, and 6 cm, respectively, giving

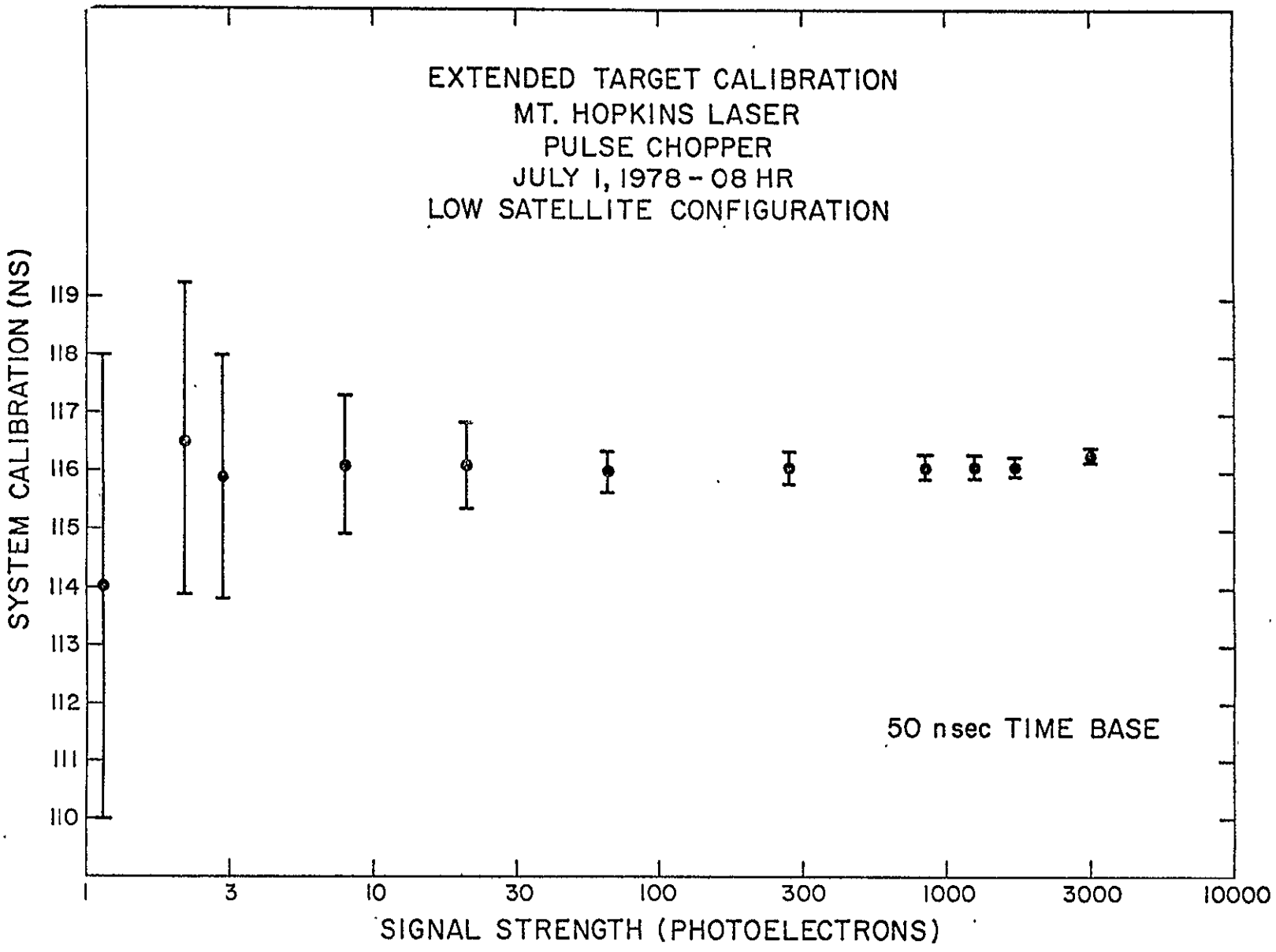
EXTENDED TARGET CALIBRATION
MT. HOPKINS LASER
PULSE CHOPPER
JULY 1, 1978 - 08 HR
LOW SATELLITE CONFIGURATION
SYSTEM CALIBRATION (NS)
119
118
117
116
115
114
113
112
111
110
50 nsec TIME BASE
1
3
10
30
100
300
1000
3000
10000
SIGNAL STRENGTH (PHOTOELECTRONS)

Figure 5.

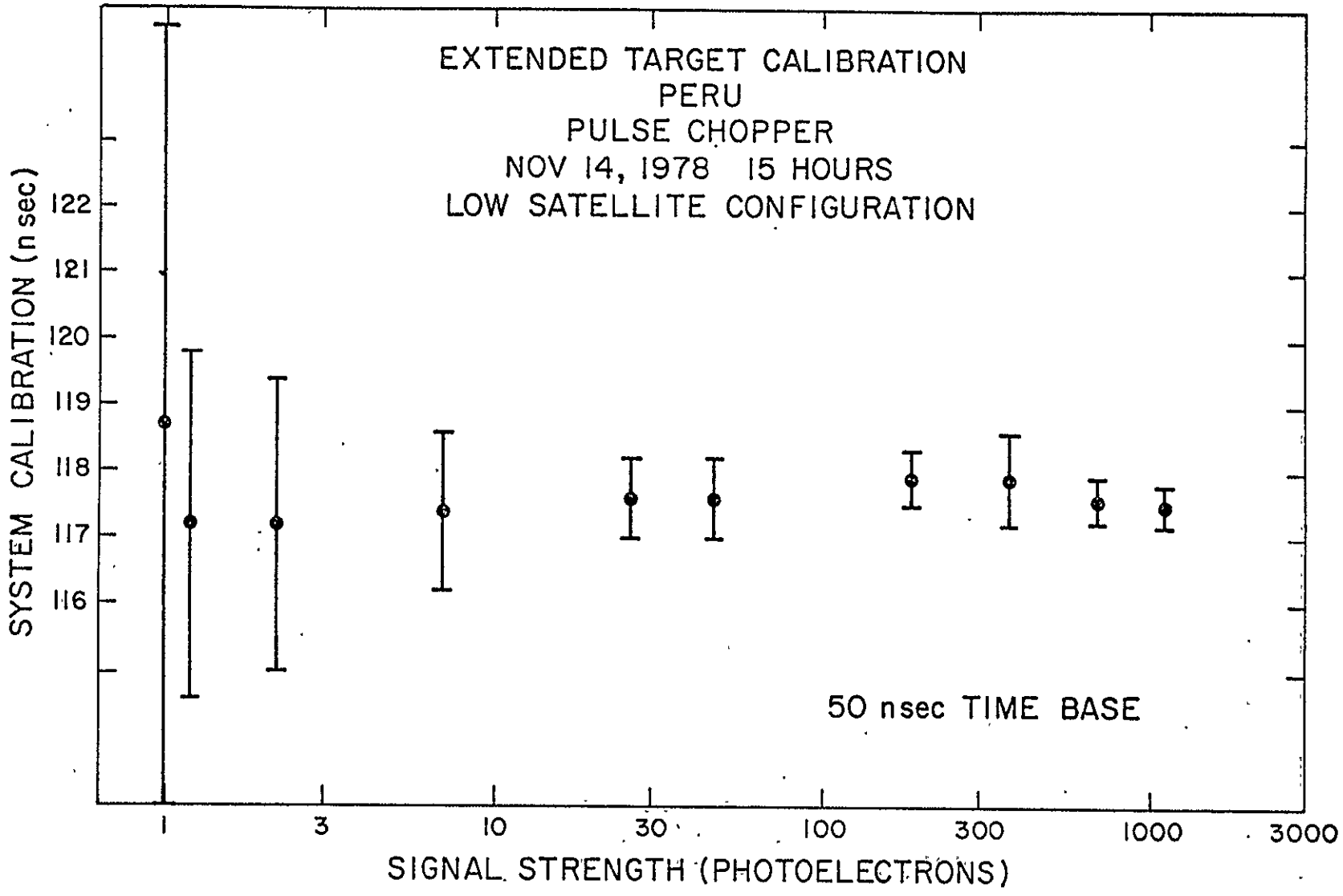
EXTENDED TARGET CALIBRATION
PERU
PULSE CHOPPER
NOV 14, 1978 15 HOURS
LOW SATELLITE CONFIGURATION
SYSTEM CALIBRATION (n sec)
122
121
120
119
118
117
116
50 nsec TIME BASE
1
3
10
30
100
300
1000
3000
SIGNAL STRENGTH (PHOTOELECTRONS)

Figure 6.

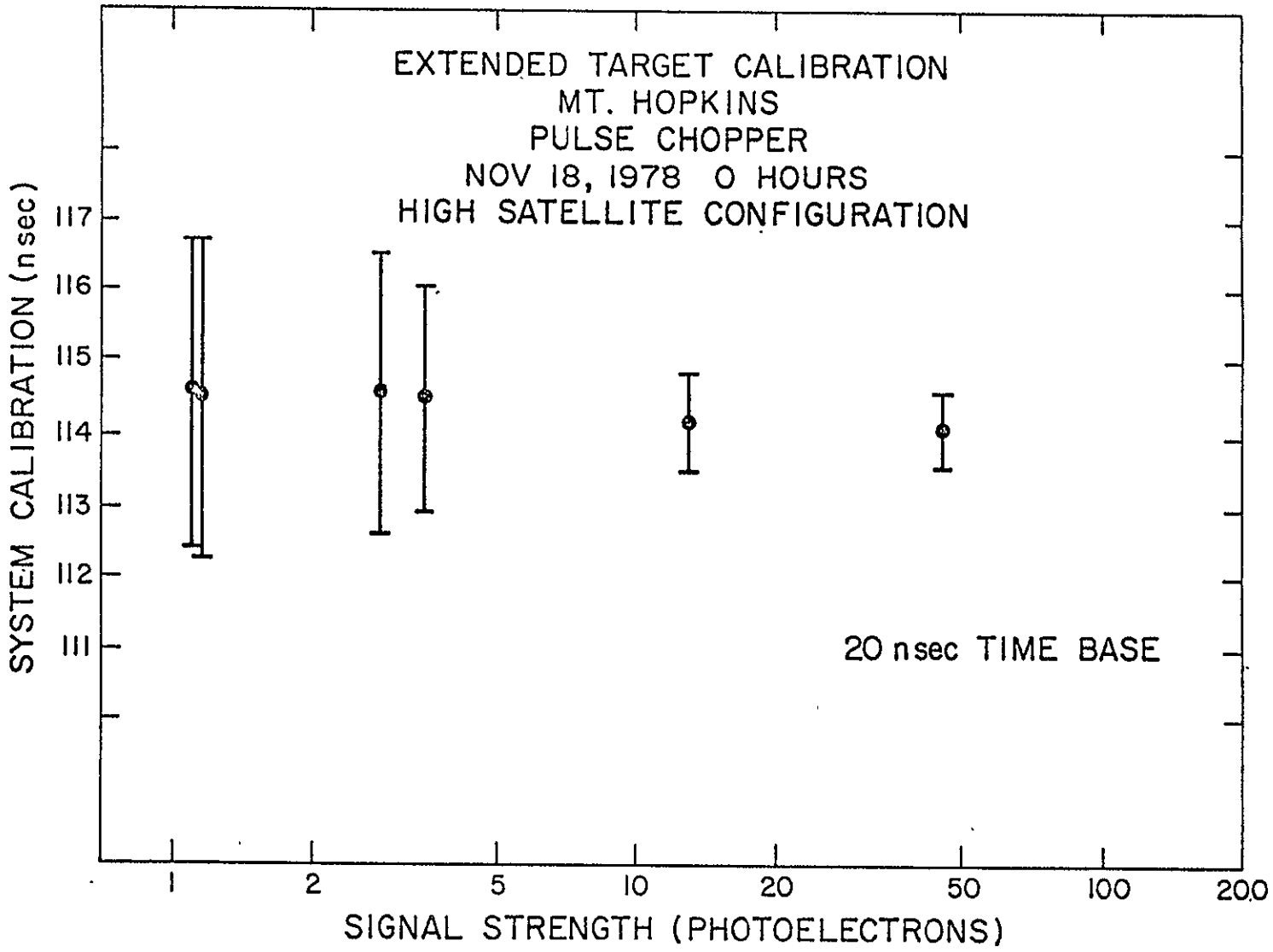
EXTENDED TARGET CALIBRATION
MT. HOPKINS
PULSE CHOPPER
NOV 18, 1978 0 HOURS
HIGH SATELLITE CONFIGURATION
SYSTEM CALIBRATION (nsec)
117
116
115
114
113
112
111
20 nsec TIME BASE
1
2
5
10
20
50
100
200
SIGNAL STRENGTH (PHOTOELECTRONS)

Figure 7.

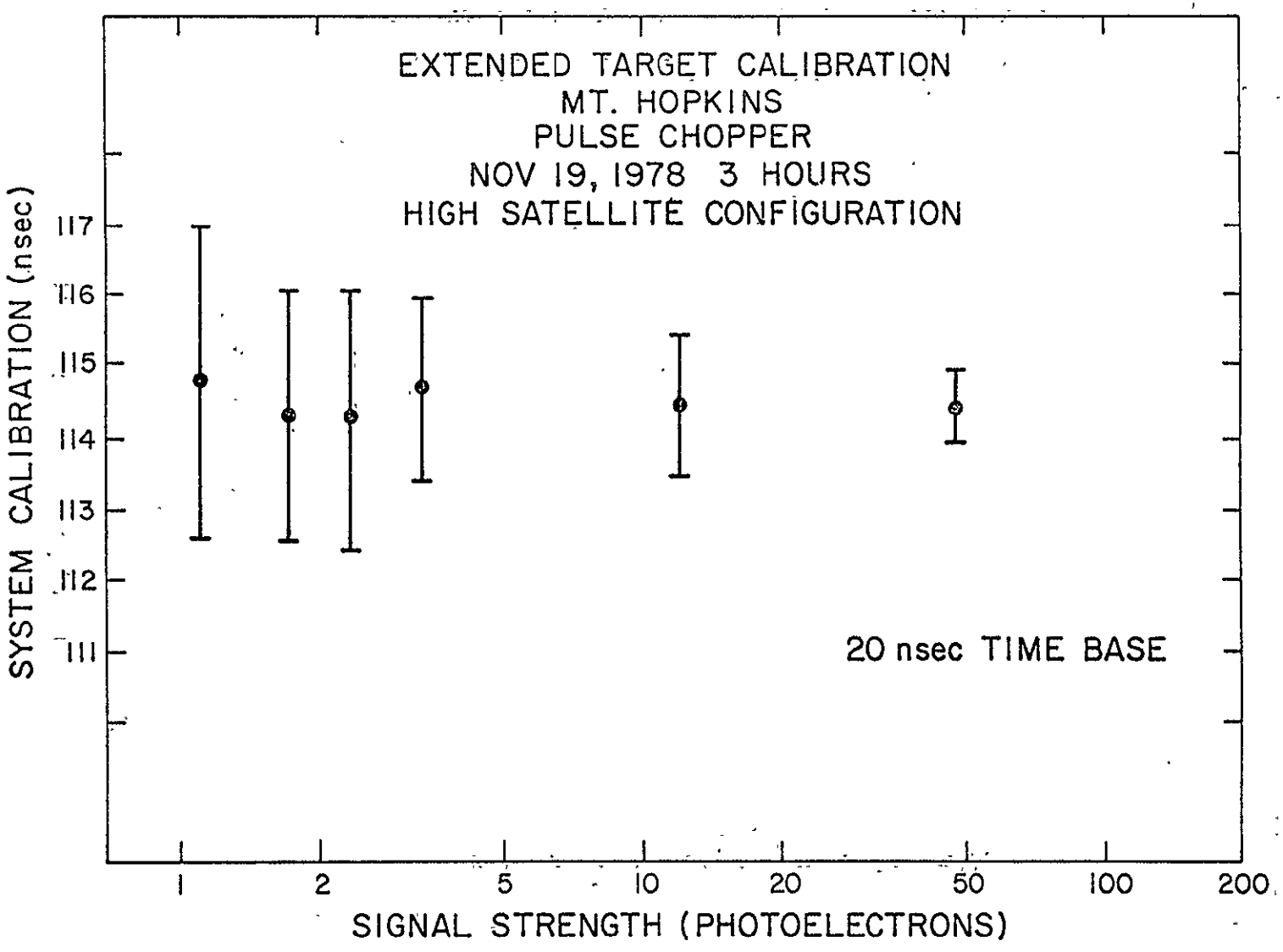
EXTENDED TARGET CALIBRATION
MT. HOPKINS
PULSE CHOPPER
NOV 19, 1978 3 HOURS
HIGH SATELLITE CONFIGURATION
20 nsec TIME BASE
SYSTEM CALIBRATION (nsec)
117
116
115
114
113
112
111
1
2
5
10
20
50
100
200
SIGNAL STRENGTH (PHOTOELECTRONS)

Figure 8.

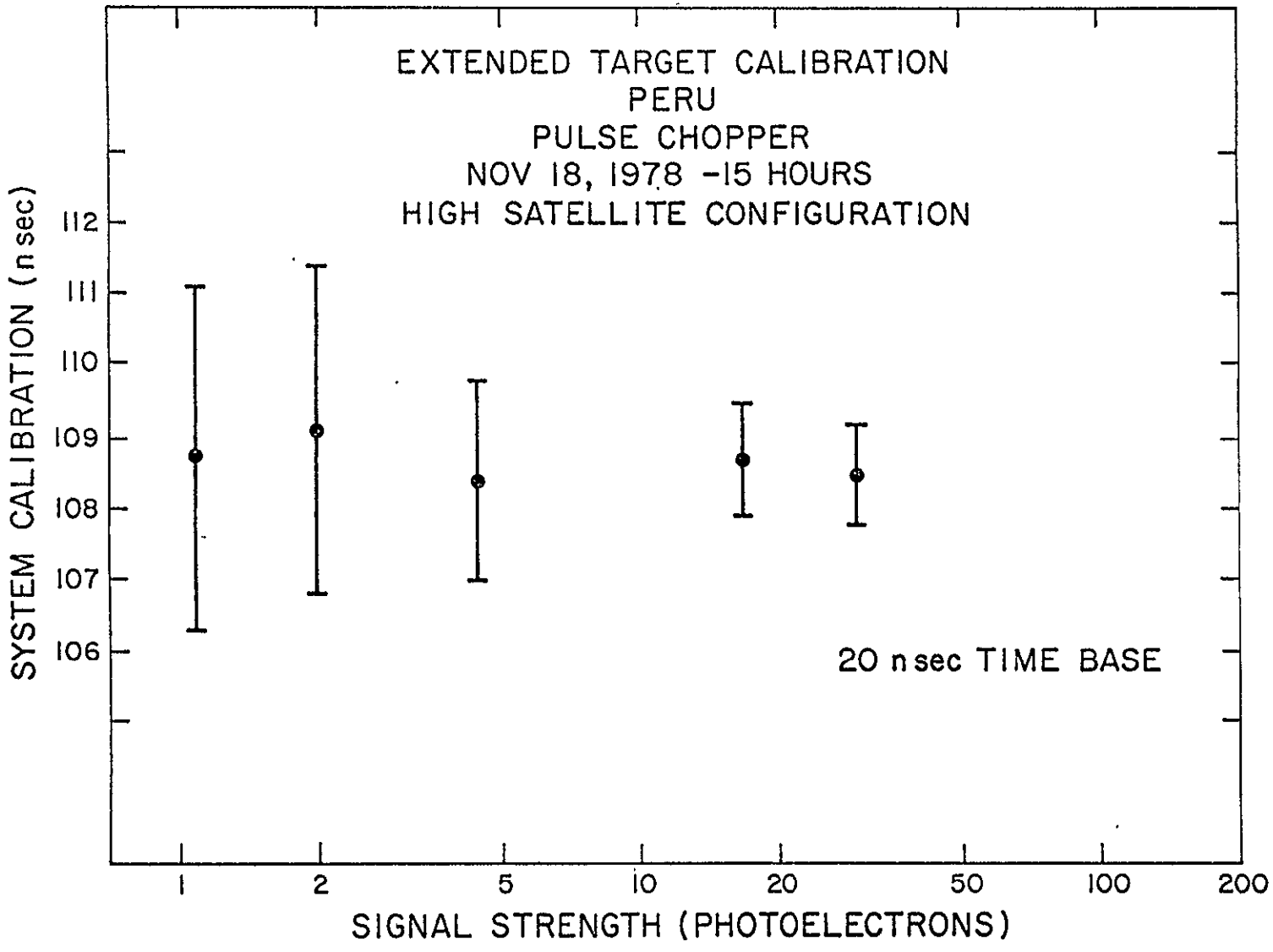
EXTENDED TARGET CALIBRATION
PERU
PULSE CHOPPER
NOV 18, 1978 -15 HOURS
HIGH SATELLITE CONFIGURATION
SYSTEM CALIBRATION (n sec)
112
111
110
109
108
107
106
20 n sec TIME BASE
1
2
5
10
20
50
100
200
SIGNAL STRENGTH (PHOTOELECTRONS)

Figure 9.

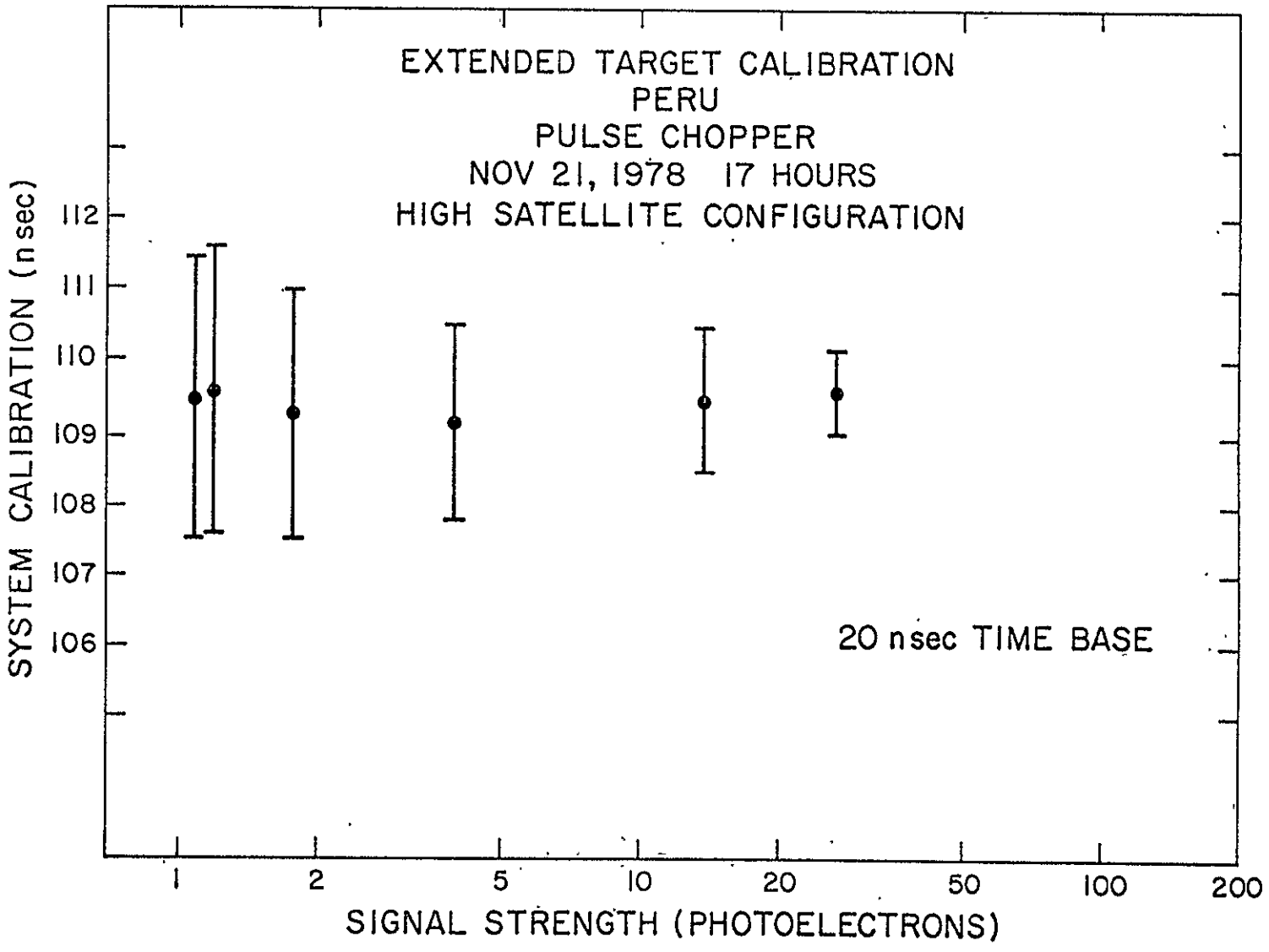
EXTENDED TARGET CALIBRATION
PERU
PULSE CHOPPER
NOV 21, 1978 17 HOURS
HIGH SATELLITE CONFIGURATION
SYSTEM CALIBRATION (n sec)
112
111
110
109
108
107
106
20 n sec TIME BASE
1
2
5
10
20
50
100
200
SIGNAL STRENGTH (PHOTOELECTRONS)

Figure 10.

Table 8. Summary of systematic errors.

Source	Low satellites (cm)	High satellites (cm)
Wavefront distortion (spatial)	4.5	4.5
System drift (temporal)	6.0	6.0
Calibration (signal strength)	4.5	6.0
rss	8.7	9.5

an rss of 9.5 cm. These, then, are the systematic errors that we would expect for data averaged over a pass. In addition, errors in timing, refraction, and spacecraft center-of-mass corrections need to be applied to the data; these errors are basically the same as those in the NASA systems, since essentially the same equipment and models are used.

9.2 System Noise

The range noise in the SAO lasers is determined in large part by return signal strength. Table 9 shows a recent history of passes taken at Mt. Hopkins and Arequipa on Geos 3 and Seasat. Noise figures in the 10- to 15-cm range are common. Passes with larger noise figures are the result of very low signal strengths (poor weather or tracking) or operator error (some operators are still learning to track with a chopped pulse).

With Lageos, at signal strengths of 1 to 2 photoelectrons, we get noise figures several times larger (see Table 10). It should be noted that the theoretical random statistics from photoquantization with the 6-nsec chopped pulse are about 30 to 40 cm.

9.3 Long-Arc Analysis

A long-arc analysis has been performed on 24 days of Lageos data taken in May 1978. Sixty-five passes from the stations at Mt. Hopkins, Arequipa,

Table 9. Recent history of pulse-chopper low-satellite passes.

Date	Station	Satellite	Pass stability	rms (m)	Number of points
1 November	Arizona	Seasat	-0.249	0.478	14
7 November	Arizona	Geos 3	-0.25	0.110	32
7 November	Arizona	Geos 3	-0.19	0.157	30
7 November	Arizona	Seasat	0.09	0.169	43
8 November	Arizona	Geos 3	-0.19	0.157	30
8 November	Arizona	Seasat	-0.03	0.219	31
8 November	Arizona	Seasat	-0.19	0.219	36
13 November	Arizona	Geos 3	-0.51	0.169	17
15 November	Peru	Geos 3	0.02	0.108	57
15 November	Peru	Geos 3	-0.06	0.129	29
16 November	Peru	Geos 3	0.03	0.097	55
16 November	Peru	Geos 3	-0.15	0.137	51
16 November	Peru	Seasat	0.46	0.119	71
17 November	Peru	Geos 3	-0.95	0.153	35
17 November	Peru	Geos 3	-0.07	0.077	76
17 November	Peru	Seasat	0.18	0.122	25
17 November	Arizona	Geos 3	-0.68	0.146	62
17 November	Arizona	Geos 3	-0.13	0.157	11
18 November	Peru	Seasat	-0.21	0.121	46
18 November	Peru	Seasat	-0.16	0.262	45
18 November	Arizona	Geos 3	0.20	0.079	62
19 November	Peru	Geos 3	-0.18	0.065	79
19 November	Peru	Seasat	-0.12	0.386	48
19 November	Arizona	Geos 3	-0.22	0.095	18
19 November	Peru	Geos 3	-0.22	0.115	13
21 November	Peru	Geos 3	0.11	0.057	49
21 November	Peru	Seasat	0.06	0.316	32
22 November	Peru	Geos 3	0.57	0.131	21
22 November	Peru	Seasat	-0.17	0.941	22
22 November	Peru	Geos 3	-0.22	0.117	42
24 November	Peru	Geos 3	0.12	0.102	35
24 November	Peru	Geos 3	0.18	0.098	11
27 November	Arizona	Geos 3	-0.17	0.941	22
27 November	Arizona	Seasat	0.06	0.580	23

Table 10. Lageos passes with pulse chopper and 20-nsec time base.

Date	Station	Pass stability (m)	rms (m)	Number of points
9 November	Arizona	0.51	0.277	25
15 November	Peru	0.00	0.420	35
16 November	Peru	0.45	0.342	38
19 November	Peru	0.04	0.396	32
19 November	Peru	0.22	0.279	68
22 November	Peru	0.11	0.412	61

and Natal, all before installation of the pulse chopper, gave root-mean-square (rms) fits comparable to the noise in the data (see Table 11). With the Q-switch mode of operation, range noise on Lageos was typically 1.2 to 1.5 m from short-arc analysis. With system noise now reduced by a factor of 3 to 4 because of the pulse chopper, we anticipate a commensurate improvement in orbital fit. This will be tried as soon as the data are available in final form.

Table 11. Long-arc analysis on Lageos (24 days) before installation of the chopper.

Station	Observations	rms (m)
Mt. Hopkins	1533	1.13
Arequipa	671	1.35
Natal	489	1.37

9.4 Improvements in Performance

Several relatively simple steps should be taken to improve performance further. A narrower interference filter (2 to 4 Å) would improve the daytime signal-to-noise ratio by a factor of 2 to 3. The installation of a shutter

in front of the PMT would greatly enhance sensitivity (generation efficiency) to low satellites, thereby reducing range noise. In addition, the noise introduced by the electronics is a little higher than we would expect; this should be examined more closely.

10: PERSONNEL

10.1 Visitors

Donald Patterson, an observer formerly at Mt. Hopkins, visited headquarters in July en route to a new assignment in Natal. The following month found Stephen Criswell, from Mt. Hopkins, D. Kirk Gilmore, from Natal, and David Hallenback, from Arequipa, in Cambridge for a week of administrative and technical discussions.

10.2 Program Personnel Status

Rita Filipowicz joined the staff in Cambridge, replacing Joan Fitzpatrick as department secretary. Ilo Gene Campbell resigned as senior programer/analyst to accept another position at the Observatory. Recruitment is under way for a replacement. Senior observer Dana Seaman transferred from duty in Natal to Arequipa in October.

On 17 October, William Johnson died while working on laser electronic equipment at the observing station in Dionysos. A field engineer, Johnson had been with the tracking network since 1973, with assignments in South Africa, South America, and Greece. In the years that he was part of our satellite-tracking network, he earned our respect and friendship as a loyal, capable member of our field staff.

10.3 Travel

Technical adjustments to the timing equipment at the South American stations were made by Edward Imbier in July. Imbier also attended the Precise Time and Time Interval Applications and Planning Meeting in Washington in November.

Jacob Wohn and James Maddox traveled to Teaneck, New Jersey, in October to complete factory-acceptance tests of the new pulse choppers at Lasermetrics, Inc.

After completing tests of the prototype pulse chopper at Mt. Hopkins, Noel Lanham visited the two South American stations for installation of the electronic equipment and for technical discussions in anticipation of pulse-chopper installation. Before Lanham returned in October, Wohn joined him in Arequipa to oversee installation; Wohn then went on to Natal for similar duty.

Both Michael R. Pearlman and Margaret A. Warner traveled to Washington in July, Pearlman for a meeting on tether applications at NASA headquarters and Warner for administrative and technical discussions at Smithsonian Institution. Pearlman also held administrative and technical discussions with personnel from NASA headquarters and the Defense Mapping Agency in Washington in December.

Pearlman, accompanied by John Gregory and James Maddox, attended William Johnson's funeral in Flint, Michigan. Pearlman also represented SAO in Athens during the official investigation of Johnson's death; he met with embassy and local officials and station personnel. A report on the findings of the circumstances surrounding the death will be forthcoming.

APPENDIX A

LAGEOS ORBITAL ANALYSIS IN SUPPORT OF VALIDATION

Grant NSG 5261

Final Report

For the period 1 April to 30 November 1978

Principal Investigator: Dr. E. M. Gaposchkin

Prepared for
National Aeronautics and Space Administration
Goddard Space Flight Center
Greenbelt, Maryland 20771

April 1979

Smithsonian Institution
Astrophysical Observatory
Cambridge, Massachusetts 02138

TABLE OF CONTENTS

		Page
	ABSTRACT	v
1	INTRODUCTION	1
2	LAGEOS: PHYSICAL DESCRIPTION	3
3	LAGEOS: ORBITAL DESCRIPTION	6
4	DISTRIBUTION OF THE LASER TRACKING DATA	7
5	DATA REDUCTION	12
6	COMPUTATION OF MEAN ELEMENTS	13
7	DISCUSSION OF MEAN ELEMENTS	36
	7.1 Variation in the Semimajor Axis	36
	7.2 Variations in the Inclination and the Right Ascension of the Ascending Node	47
	7.3 Orbital Accuracy	55
8	CONCLUSIONS	65
9	ACKNOWLEDGMENTS	66
10	REFERENCES	67
	APPENDIX A: DEFINITIVE MEAN ELEMENTS	A-1

ABSTRACT

The Laser Geodynamic Satellite (Lageos) was launched on May 4, 1976, with an objective to make highly accurate measurements of the geocentric coordinates on the earth's surface, tectonic plate motion, polar motion, and earth tides, by using precision laser range data. One method of data analysis involves computing a precision ephemeris and then using the satellite as a stable reference point in space. Analysis of the first 2 years of data is complete. The results indicate that the design goals of the satellite can be met with continued model development. The present accuracy for short-period orbital variations is limited by geopotential-model errors, station-coordinate errors, and, to some extent, data accuracy. The accuracy for long-term predictions is limited by tidal models and, to a lesser extent, the zonal harmonics of the geopotential. At present, the orbital accuracy is approximately 50 cm for short-period ($\leq$1 day) effects and about 10 m for long-period effects involving orbital geometry. An unmodeled secular acceleration in the mean anomaly has yet to be explained.

LAGEOS ORBITAL ANALYSIS IN SUPPORT OF VALIDATION

Final Report

1. INTRODUCTION

The Laser Geodynamic Satellite (Lageos) was designed to be used as a stable reference for the study of solid-earth geophysics. The concept for such a satellite grew out of the Williamstown study (Kaula, 1970), one of whose principal recommendations was to develop techniques for satellite ranging to an accuracy of ±2 cm. A preliminary design by Weiffenbach and Hoffman (1970), then nicknamed Cannonball, evolved into the Lageos satellite, which was launched on May 4, 1976. The design of the satellite was carefully selected to satisfy a number of considerations: The physical geometry should allow definition of the satellite's center of mass with an error of less than 1 cm; the laser radar cross section should allow ranging with existing ground equipment; the satellite should be bright enough for acquisition with satellite-tracking cameras; the orbital geometry should allow global coverage, as well as simultaneous observations by ground stations separated by continental distances; and the satellite design and orbit configuration should facilitate precise orbit determination and ephemeris calculation. It is this last point that is the object of the study reported here.

One of the major considerations in designing the Lageos satellite was to be able to determine a precise ephemeris for it, since that would enable the satellite to be used as a reference in space for subsequent measurements of station positions, tectonic plate motions, polar motion, and earth rotation. Determining an ephemeris depends on three factors: 1) the accuracy of the observations, 2) the adequacy of the model describing the satellite's motion, and 3) the accuracy of the numerical parameters that enter the computation. In the analysis presented here, each of these

factors is discussed and an overall accuracy assessment is made. From the study, it is apparent that the design objectives have been met and that further refinement of geodetic and tidal parameters will shortly lead to the use of Lageos for geodynamic measurements.

2. LAGEOS: PHYSICAL DESCRIPTION

The Lageos satellite is a sphere 60 cm in diameter with 426 retro-reflectors distributed over the surface (Figure 1). Four of the cube corners are made of germanium for use at infrared wavelengths, and the other 422, of fused silica for use at visible wavelengths. The sphere consists of two hemispheres bolted together. The physical characteristics of Lageos are summarized in Table 1, and a schematic assembly is shown in Figure 2. For further details on the mechanical construction of the satellite, see Arnold (1978), Fitzmaurice et al. (1977), and the National Aeronautics and Space Administration (1975).

Table 1. Physical characteristics of Lageos.

Parameter	Value
Diameter	60 cm
Mass	4.1095×10^5 g
Core material	brass
Surface material	aluminum 6061 T6
Surface finish	diffuse (chemically cleaned)
Surface-area aluminum	57%
A/m	0.00689 $cm^2\ g^{-1}$

Of particular interest for this study is Lageos' area-to-mass ratio (A/m), which enters into calculations of drag, radiation pressure, and albedo pressure; the percentage of the surface area that would have a diffuse reflectivity, also necessary for the calculation of radiation pressure; and the amount of the satellite made of brass and of aluminum, for the spin-down calculation.

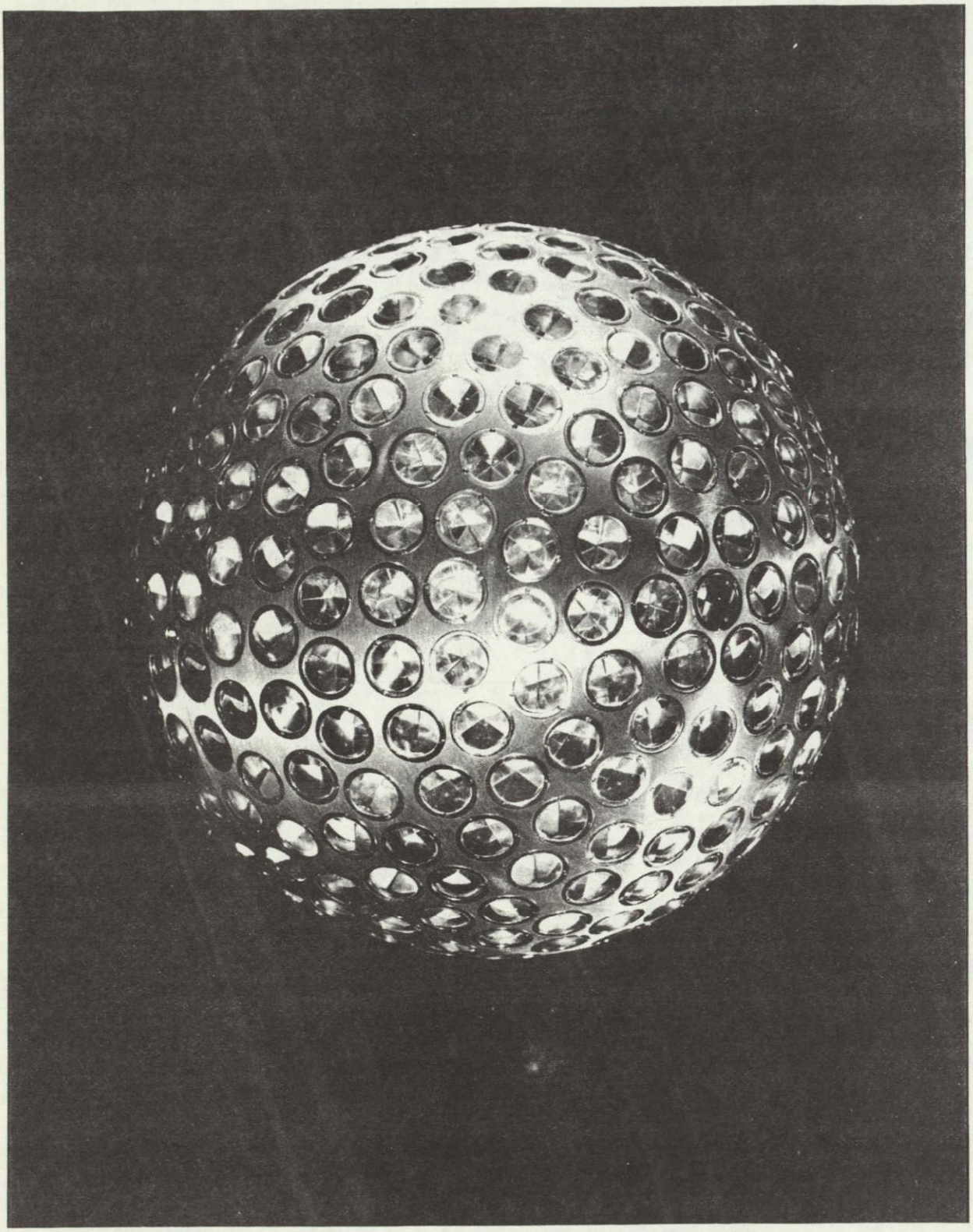

Figure 1. The Lageos satellite.

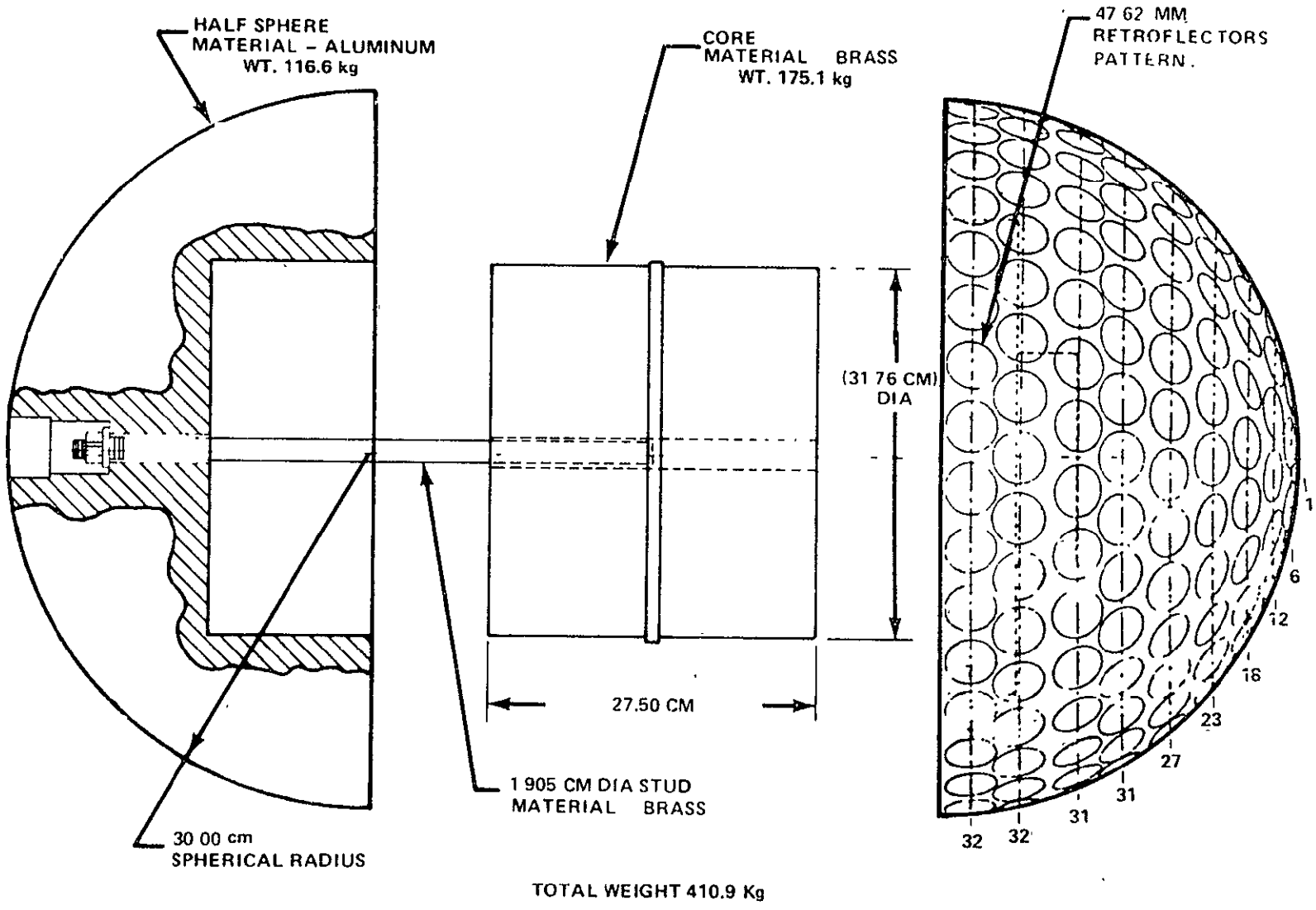

Figure 2. Schematic assembly of Lageos.

3. LAGEOS: ORBITAL DESCRIPTION

The nominal orbital characteristics of Lageos are listed in Table 2. Its nearly polar orbit, at a height of almost 5800 km, was selected so as to optimize global coverage, allow simultaneous observations from stations on separate continents, and reduce the effects of the earth's anomalous gravity field.

In addition, the mean motion of Lageos was chosen to minimize possible resonances with the tesseral harmonics of the earth's gravity field.

Table 2. Nominal orbital characteristics for Lageos.

Orbital element	Nominal value
a	12.2700 Mm
e	0.00444
I	109°.864
n	6.38664 rev day^{-1}
$\dot{\omega}$	-0°.21326 day^{-1}
$\dot{\Omega}$	0°.34266 day^{-1}

4. DISTRIBUTION OF THE LASER TRACKING DATA

During the first 2 years of Lageos' lifetime, eight laser tracking stations obtained sufficient data to be useful in calculating definitive orbits. Four of the stations are operated by the Smithsonian Astrophysical Observatory (SAO) and four by the National Aeronautics and Space Administration/Goddard Space Flight Center (NASA/GSFC). Table 3 gives the station locations, the coordinates used in this analysis, and a rough estimate of the accuracy and noise of the tracking data for Lageos. The tracking accuracy is better for lower satellites, with their more favorable signal strength.

The distribution of the tracking stations, shown in Figure 3, is not excellent for precision orbit computation, since four of the sites are clustered in the Western United States. However, as will be seen in the actual data distribution, the four SAO sites provided most of the tracking data and those sites are reasonably well distributed in longitude, plus provided fair latitude coverage as well.

The station distribution directs the type of analysis possible. Since the stations are more or less near the equator and the satellite has a high inclination, none of the stations can observe Lageos at its maximum or minimum latitude and thus its inclination (I) is difficult to determine. Conversely, because of the good distribution in longitude, the right ascension of the ascending node (Ω) can be determined very well. We are therefore led to examine the satellite's node for possible geophysical phenomena of interest, such as tides and variations in UT1.

The distribution of the data is illustrated in Figure 4, where, for each day, the number of satellite passes obtained on Lageos and the number of stations contributing data are depicted. The figure was obtained from

Table 3. Geocentric station coordinates used for tracking Lageos.

Station number	X (Mm)	Y (Mm)	Z (Mm)	Station location	Accuracy (cm)	Agency
7061	-2.4288306	-4.7997531	3.4172747	San Diego, California	10	NASA
7063	1.1307118	-4.8313719	3.9940900	GSFC, Maryland	10	NASA
7080	-2.5168977	-4.1988464	4.0764145	Quincy, California	10	NASA
7082	-1.7360010	-4.4250506	4.2414331	Bear Lake, Utah	10	NASA
7907	1.9427877	-5.8040801	-1.7969196	Arequipa, Peru	150	SAO
7921	-1.9367636	-5.0777058	3.3319226	Mt. Hopkins, Arizona	150	SAO
7929	5.1864655	-3.6538602	-0.6543223	Natal, Brazil	150	SAO
7943	-4.4475480	2.6771379	-3.6949976	Orroral Valley, Australia	150	SAO

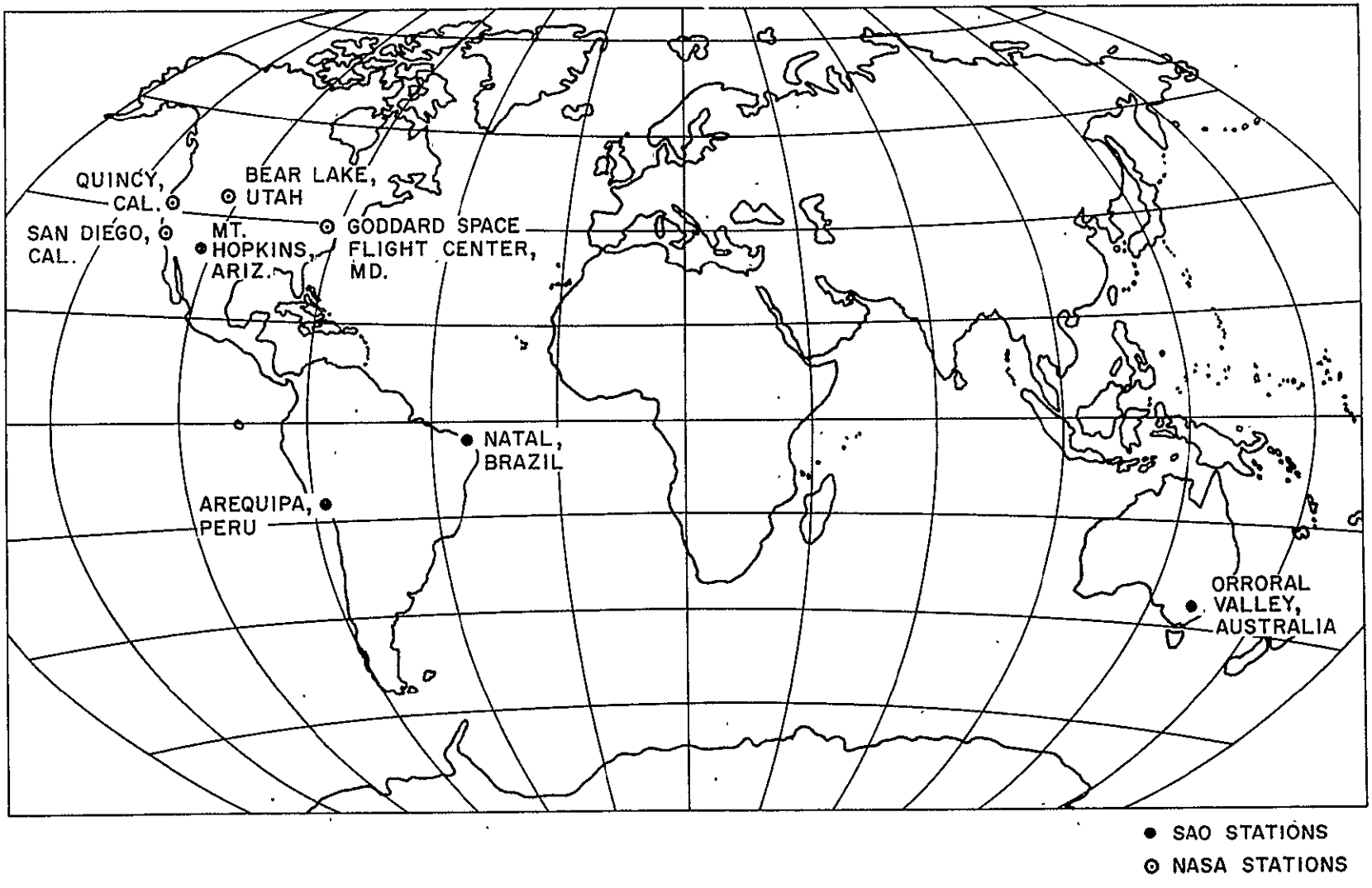

Figure 3. Locations of the laser stations observing Lageos.

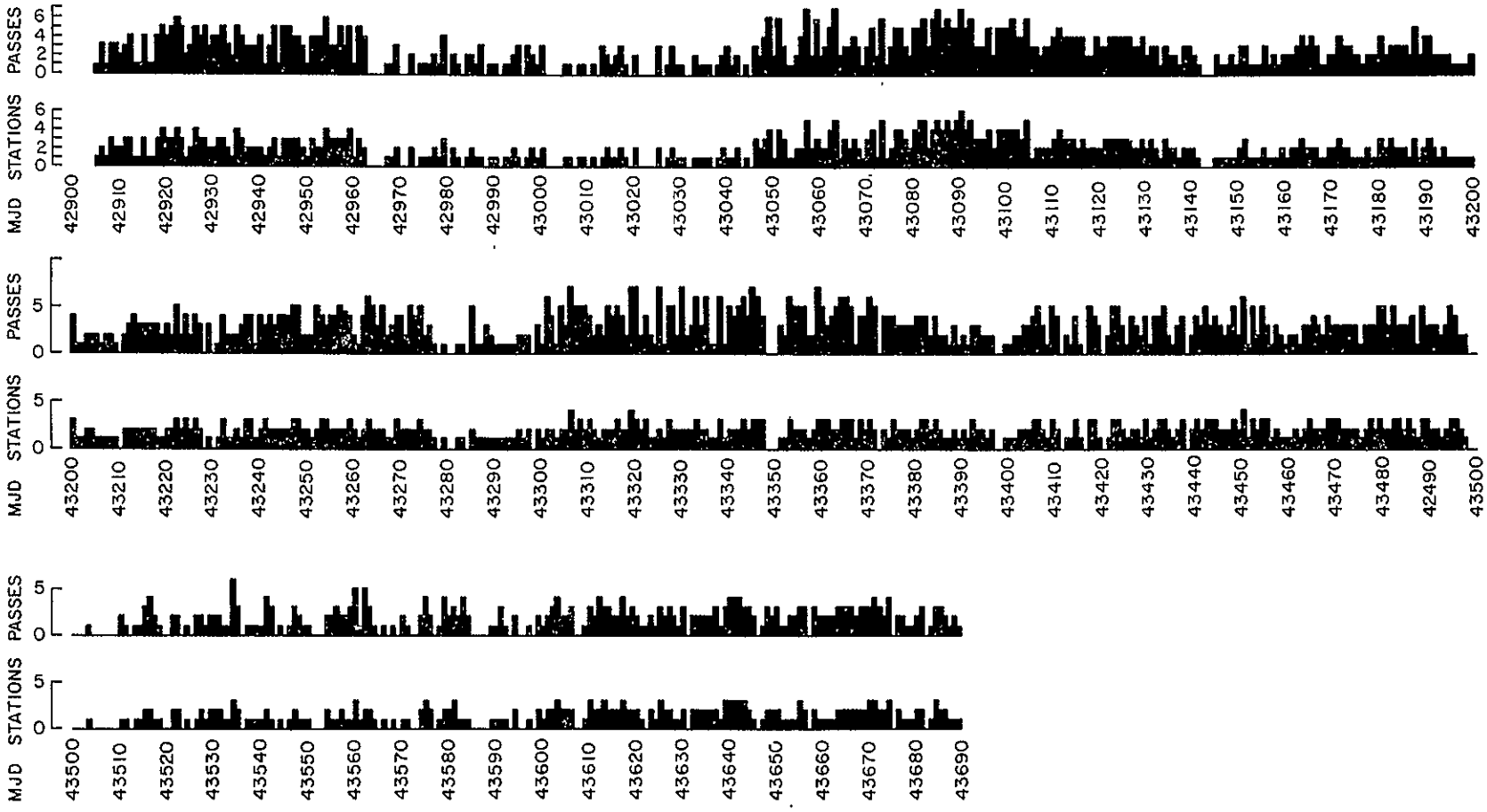

Figure 4. Distribution of laser data, passes per day and stations observing per day.

the data archives after the data had been screened but before they had been used in a definitive orbit computation. Therefore, some of these passes may be rejected in the precision orbit computation.

The tracking-station coordinates given in Table 3 were obtained by David Smith of Goddard Space Flight Center by analyzing Lageos tracking data. They were used for all the orbit computation reported here, and they constitute the definition of the reference system used. We have also estimated the relation between this Lageos reference system and the FK4 system, by using the coordinates from Gaposchkin (1973a, 1974) for those seven stations that are also in the FK4 system. The relation between the two systems defines the transformation T:

$$T(\varepsilon_x, \varepsilon_y, \varepsilon_z)\ \overline{X}_{FK4} = \overline{X}_{Lageos} \quad ,$$

with the parameters given in Table 4. The two coordinate systems also have a translation and a scale difference, but these are not important for discussion of the orientation between the two reference systems.

Table 4. Transformation from the FK4 reference system to the Lageos reference system.

ε_x (arcsec)	ε_y (arcsec)	ε_z (arcsec)
0.1417	-0.0897	0.9675

5. DATA REDUCTION

In preparation for orbital analysis, it is necessary to transform the measured light travel time of a laser pulse into the observed metric range. The definition of scale is essentially imposed by the adopted value of the speed of light c in vacuum, which is taken to be that recommended by the International Astronomical Union and the International Union of Geodesy and Geophysics (Melchior, 1975):

$$c = 2.99792458 \times 10^{10} \text{ cm sec}^{-1}$$

When a path of light passes through the atmosphere, a slowing of the light speed results. The lengthening of the apparent distance is generally called refraction. The observed range is corrected for refraction by using the observed pressure and temperature at the observing station with the algorithm of Marini and Murray (1973).

The Lageos satellite having finite dimensions, laser range measurements refer to some point other than the satellite's center of mass. A detailed calculation (Arnold, 1978) gives the following correction:

$$\Delta r = 24.3 \pm 0.5 \text{ cm} \quad ,$$

the range to the center of mass being longer than the observed range by this amount.

6. COMPUTATION OF MEAN ELEMENTS

Computation of a satellite's mean elements is based on an analytical and semianalytical theory of a close-earth satellite. For a review of the present status of this theory, see Gaposchkin (1978); a brief summary follows.

A third-order solution to the main problem — i.e., for the motion of a satellite in the geopotential containing only J_2, J_3, and J_4 terms — has been obtained by Kinoshita (1977). Third-order periodic perturbations with fourth-order secular perturbations are derived by the method due to Hori (1966). All quantities are expanded into power series in the eccentricity, but the solution is closed with respect to inclination. A comparison with results obtained by numerical integration of the equations of motion indicates that the solution can predict the position of a close-earth satellite with an accuracy of better than 1 cm over a period of 1 month. For this check, a special-purpose Taylor-type integrator is adopted, in which the positions and velocities are expanded into a power series of time and the coefficients of the series are determined by recurrence formulas (Rabe, 1961; Deprit and Zahar, 1966).

Periodic perturbations due to tesseral harmonics are calculated from a first-order linear theory based on integration of the Lagrange planetary equations as developed by Kaula (1966). The theory also includes the interaction with J_2 and second-order interactions with the mean motion through Kepler's third law. Although the theory is essentially that of Kaula, the details of the calculation have been considerably revised by using the inclination function as described by Gaposchkin (1973b) or Kinoshita (1977) and the eccentricity function calculated as Hansen coefficients.

Lunisolar perturbations in satellite motion are calculated semi-analytically (Kozai, 1973), where the disturbing function is expressed by the orbital elements of the satellite and the geocentric polar coordinates of the moon and the sun. The geocentric coordinates are obtained by using the larger terms in Brown's theory (United States Naval Observatory, 1954): 26 terms in longitude, 14 in latitude, and 12 in the parallax. The secular and long-period perturbations are derived by numerical integration, and the short-period perturbations are obtained in analytical form. Perturbations due to the solid-body tide are included in the same way.

The orbital elements of a close-earth satellite have perturbations caused by the motion of the equatorial plane of the earth due to precession and nutation. Kozai and Kinoshita (1973) derived exact differential equations for the perturbations of satellite orbital elements due to the motion of the earth's equatorial plane and solved them to second order in precession. This theory, in fact, defines the reference system used for satellite motion, in which the inclination and the argument of perigee are referred to the equator of date and the longitude of the ascending node is measured from a fixed point along a fixed plane and then along the equator of date.

The perturbations of a spherical satellite due to direct solar radiation are computed according to a semianalytical algorithm developed by Aksnes (1976), which is based on expressions derived by Kozai (1961). Through some simple modifications, the algorithm also holds when $e = 0$ and $i = 0$. The perturbations are obtained by summing over the sunlit segment of the satellite's orbit during each revolution or partial revolution; the end points of the segment are evaluated numerically once per revolution. The algorithm is tested by means of numerical integration of the equations of motion and through comparisons with observations of the balloon satellite 1963 30D during a 200-day interval.

Perturbations due to solar radiation diffusely reflected from the earth have been treated by Lautman (1977a), who used a semianalytical method based on the assumptions that the satellite is spherically symmetric and that solar radiation is reflected from the earth according to Lambert's law with uniform albedo. Expressions for the radiation-pressure force are developed into series in true anomaly. The perturbations within a given revolution are obtained analytically by integrating with respect to the true anomaly, while holding all slowly varying quantities constant. The long-term perturbations are then obtained by summing the net perturbations at the end of each revolution. This theory has been extended (Lautman, 1977b) to account for the increasing reflectivity of the earth toward the poles; the earth's albedo α is assumed to have a latitude ϕ dependence given by

$$\alpha = \alpha_0 + \alpha_2 \sin^2 \phi \quad ,$$

where α_0 and α_2 are constants.

The periodic perturbations due to ocean tides are taken from Gaposchkin (1973b, 1978). They are based on a Fourier description of the lunisolar gravitational potential given by Doodson (1921). The theory casts the perturbations for each Fourier component separately — including the interaction with J_2, which can be larger than the direct effect — and integrates the Lagrange planetary equations as a forced harmonic oscillator.

The analytical theory employs a value of GM to establish an orbit scale; the value adopted for this analysis is

$$GM = 3.986005 \times 10^{20} \text{ cm}^3 \text{ sec}^{-2}$$

The terrestrial scale is obtained from the coordinates of the station locations (see Table 3). Station positions, of course, are not invariant, since the earth undergoes regular periodic deformations known as earth tides.

For the purposes of this calculation, the deformation of the earth — i.e., the change in station coordinates — is computed by using the Love numbers h and ℓ, for which we adopt global values of

$$h = 0.58 \quad ,$$

$$\ell = 0.05 \quad .$$

The expressions are developed so that the mean value of the deformation for each station is zero. Therefore, the coordinates given in Table 3 can be viewed as the average earth model.

The geopotential model for the orbit computation is Lerch et al.'s (1977) GEM-10 solution, with the exception that the values of $\bar{C}_{2,1}$ and $\bar{S}_{2,1}$ used are those caused by the dynamical pole of the earth as described by Gaposchkin (1973b). The dynamical pole is caused by the polar motion of the earth, which has two components: The first is due to the motion of the axis of figure, and the second is the elastic deformation of the earth as a result of polar motion. Therefore, we have assumed that the GEM-10 solution refers to the terrestrial system defined by the axis of figure, although no effort was made by Lerch et al. to achieve that system.

The elastic deformation of the earth, which causes a change in the external potential, is modeled by using global values for the Love number k and a phase lag ε. For this calculation, the Love number for the lunar and solar deformations and the associated phase angles are taken to be the same for all frequencies of the disturbing potential. They are given for the second-degree disturbing potential as

$$k_2^{moon} = 0.29 \quad , \qquad \varepsilon_2^{moon} = 0.0 \quad ,$$

$$k_2^{sun} = 0.29 \quad , \qquad \varepsilon_2^{sun} = 0.0 \quad .$$

The ocean-tide perturbation required revision in the course of this investigation, and the initial values were substantially improved. The final values used to report the results are given in terms of a complex ocean-tide amplitude (Table 5).

Table 5. Ocean-tide parameters.

Tide		Perturbation period	Amplitude
Darwin	Doodson	(days)	(cm)
P1	163555	221	-1.140 + 1.720 i
K1M + K1S	165555	1050	1.711 + 0.931 i
S2	273555	280	2.740 + 1.420 i

For the radiation-pressure calculation, the nominal area-to-mass ratio of the satellite (from Table 1) is adopted:

$$A/m = 0.00689 \text{ cm}^2 \text{ g}^{-1}$$

For the earth-reflected pressure, a variable albedo model is used to account for the increasing reflectivity of the earth toward the poles. The earth's albedo is assumed to have a latitude dependence given by

$$\alpha = 0.219 + 0.410 \sin^2 \phi$$

Since the principal objective of this analysis is to study the long-term variation of the orbit, the arc length was chosen to be 8 days. That is, each set of orbital elements was computed using 8 days of data, every 4 days, with the epoch of the mean elements in the center of the period. This 8-day period is longer than the principal resonant period of 2.66 days. In the analysis, no evidence arose that this weak resonance is not adequately modeled with the GEM-10 gravity field. For a balanced distribution of data, each pass of laser data was edited to obtain approximately 50 data points, uniformly distributed in the pass.

The reference system defining the mean elements is obtained from the adopted values of polar motion and UT1 as published by the Bureau International de l'Heure. The orbital system is assumed to be the equator of date and the equinox of 1950.0.

Mean elements were computed from MJD 42911 (just after launch) until MJD 43684; they are listed in detail in Appendix A. The first computation of the mean elements resulted in the variations in a, I, and Ω shown in Figures 5a, 5b, and 5c. The main finding is that Lageos has a very stable orbit, even for an initial set of orbits. A well-established secular decrease in the semimajor axis of approximately 1 mm day^{-1} is seen; as will be discussed more fully later, this surprising decrease is as yet unexplained. As expected, the inclination of Lageos is reasonably constant; on the other hand, because of the essentially equatorial distribution of stations, the inclination is not determined very well. Another surprise in the first run of data is the large variation in the argument of the node. The internal consistency of the orbital elements is excellent, however.

As described by Gaposchkin (1978), several ocean-tide parameters cause a large perturbation on Lageos. These perturbations, obtained from analysis of observations, are given in Table 6. Also analyzed are possible effects of M2 and O1 tides, although they are too small to be seen in data of this accuracy. We have taken the ocean-tide values adopted by Gaposchkin (1978) for a second calculation of mean elements. These ocean-tide parameters were obtained from an analysis of the variations in the inclination of Geos 1 and Geos 2, and thus their use with Lageos can be viewed as a test.

The revised ocean-tide parameters and some software improvements described in Gaposchkin (1978) were used to recompute the set of mean elements. Each 8-day arc is given in Appendix A. Figures 6a-e show the mean elements, and Figures 7a-h are the calculated perturbations in a, e, and I due to radiation pressure, albedo pressure, and the sun and moon. Several factors in Figure 6 need to be noted: The secular decrease persists; the variation

in inclination is reduced, although some unmodeled effects are still obvious; and the variation in the right ascension of the node is significantly reduced. The inclination and the node data can be used to obtain geophysical information, but the decrease in semimajor axis still defies explanation. These final orbital elements are discussed in Section 7.

Table 6. Harmonic analysis for Lageos ($t = T_{MJD} - 43237$).

						Tide
$\Delta\omega$ =	-0.29×10^{-2} ±12	cos $(2\pi t/221)$	+	0.02×10^{-2} ±8	sin $(2\pi t/221)$	P1
	$+0.64 \times 10^{-2}$ ±31	cos $(2\pi t/280)$	+	0.12×10^{-2} ±21	sin $(2\pi t/280)$	S2
	$+0.13 \times 10^{-3}$ ±21	cos $(2\pi t/13.84)$	+	0.31×10^{-3} ±21	sin $(2\pi t/13.84)$	O1
	-0.13×10^{-3} ±21	cos $(2\pi t/14.03)$	+	0.07×10^{-3} ±20	sin $(2\pi t/14.03)$	M2
$\Delta\Omega$ =	0.26×10^{-4} ±12	cos $(2\pi t/221)$	+	0.10×10^{-4} ±8	sin $(2\pi t/221)$	P1
	-0.98×10^{-4} ±33	cos $(2\pi t/280)$	-	0.16×10^{-4} ±21	sin $(2\pi t/280)$	S2
	-0.10×10^{-5} ±21	cos $(2\pi t/13.84)$	+	0.08×10^{-5} ±21	sin $(2\pi t/13.84)$	O1
	-0.03×10^{-5} ±21	cos $(2\pi t/14.03)$	+	0.18×10^{-5} ±20	sin $(2\pi t/14.03)$	M2
ΔI =	-0.12×10^{-4} ±3	cos $(2\pi t/221)$	+	0.13×10^{-4} ±3	sin $(2\pi t/221)$	P1
	$+0.24 \times 10^{-4}$ ±56	cos $(2\pi t/280)$	+	0.24×10^{-4} ±20	sin $(2\pi t/280)$	S2
	$+0.27 \times 10^{-5}$ ±32	cos $(2\pi t/13.84)$	+	0.26×10^{-5} ±32	sin $(2\pi t/13.84)$	O1
	-0.26×10^{-5} ±32	cos $(2\pi t/14.03)$	-	0.03×10^{-5} ±31	sin $(2\pi t/14.03)$	M2

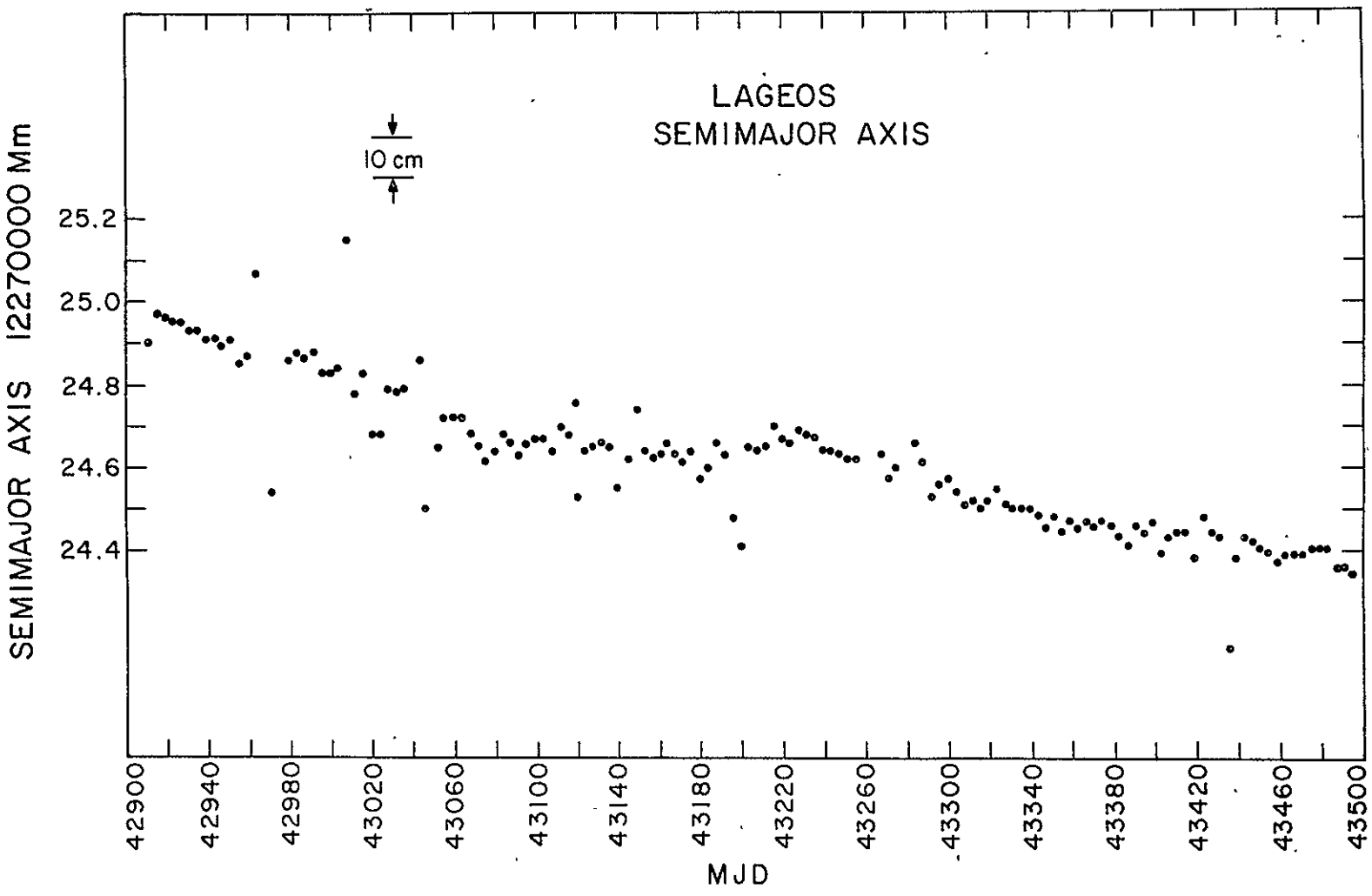

Figure 5a. First calculation of the semimajor axis of Lageos.

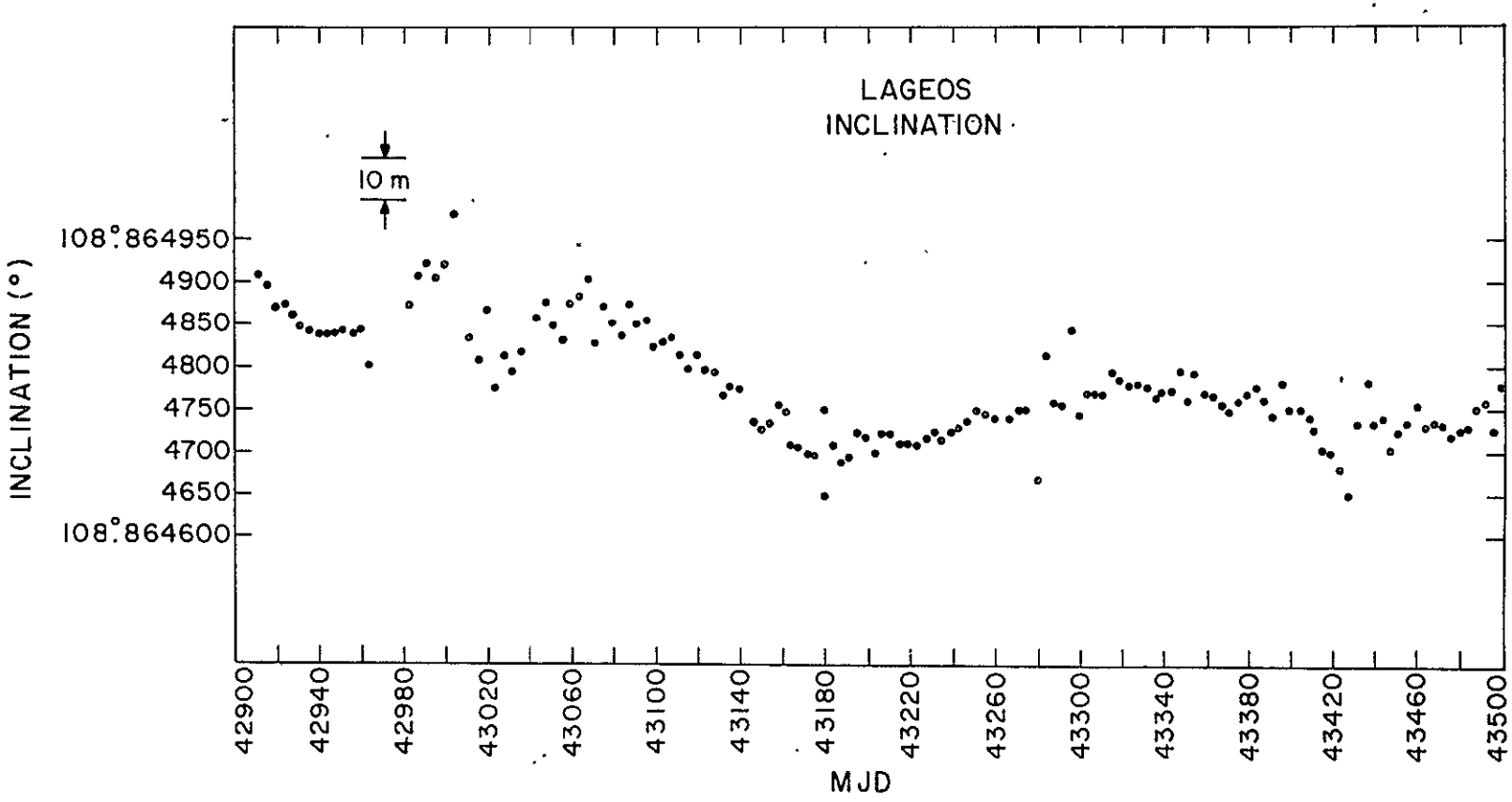

Figure 5b. First calculation of the inclination of Lageos.

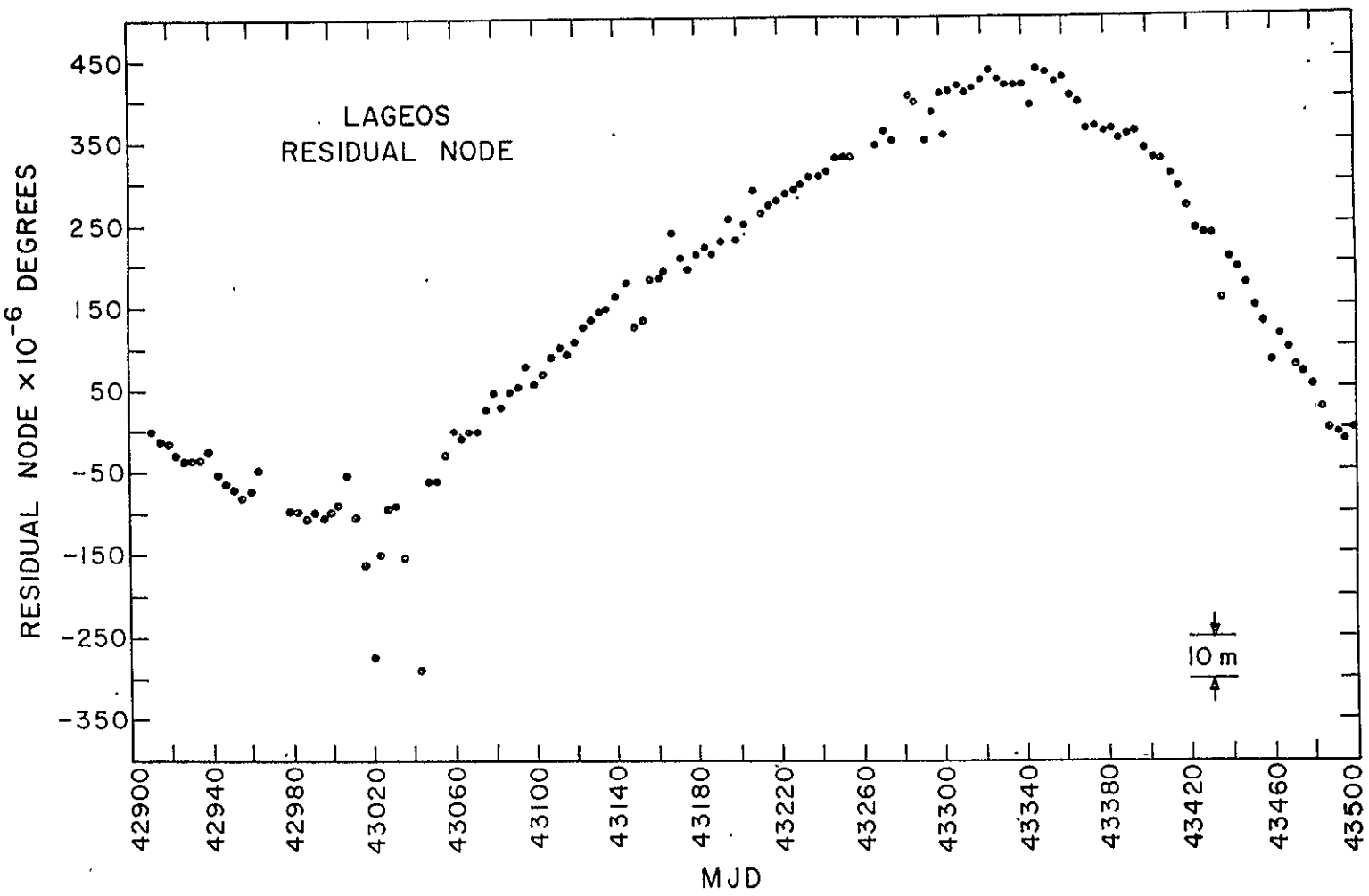

Figure 5c. First calculation of the right ascension of the ascending node of Lageos.

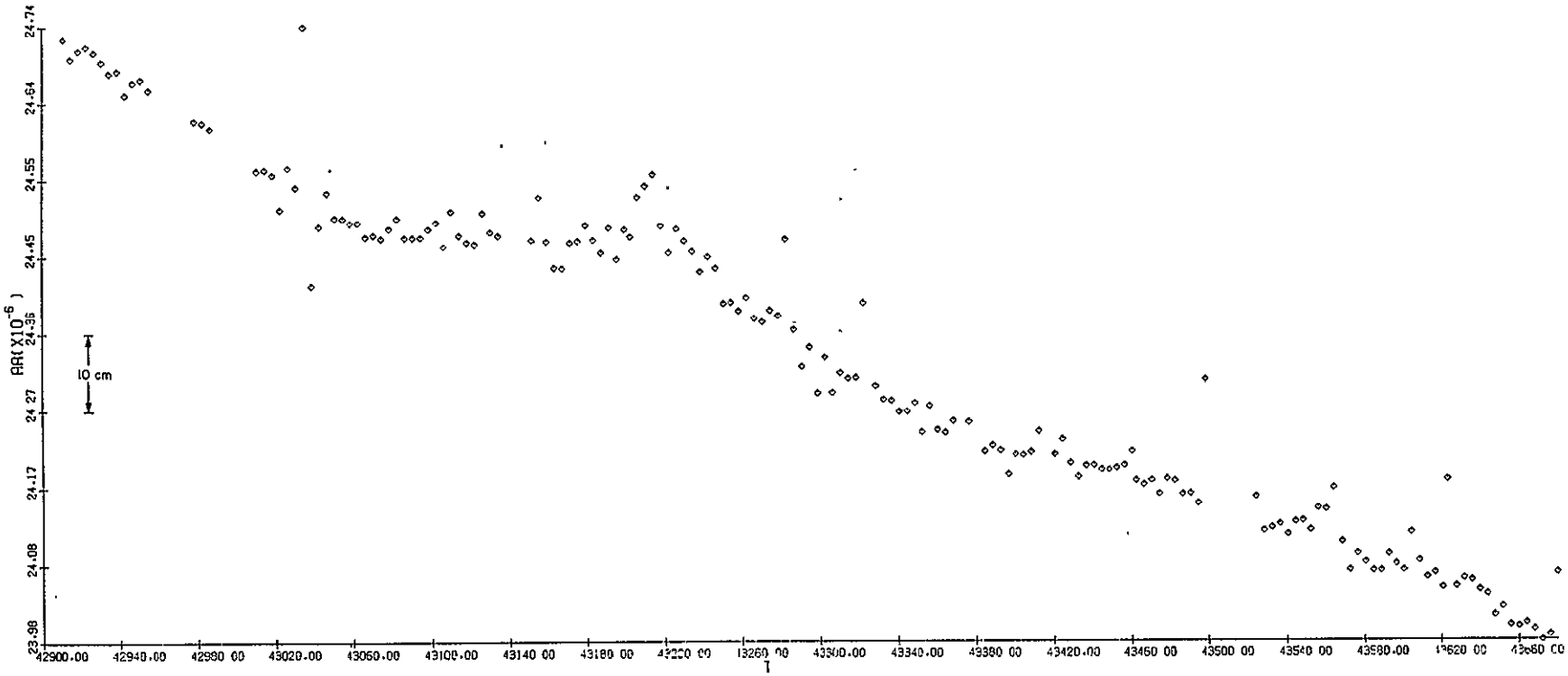

Figure 6a. Semimajor axis of Lageos.

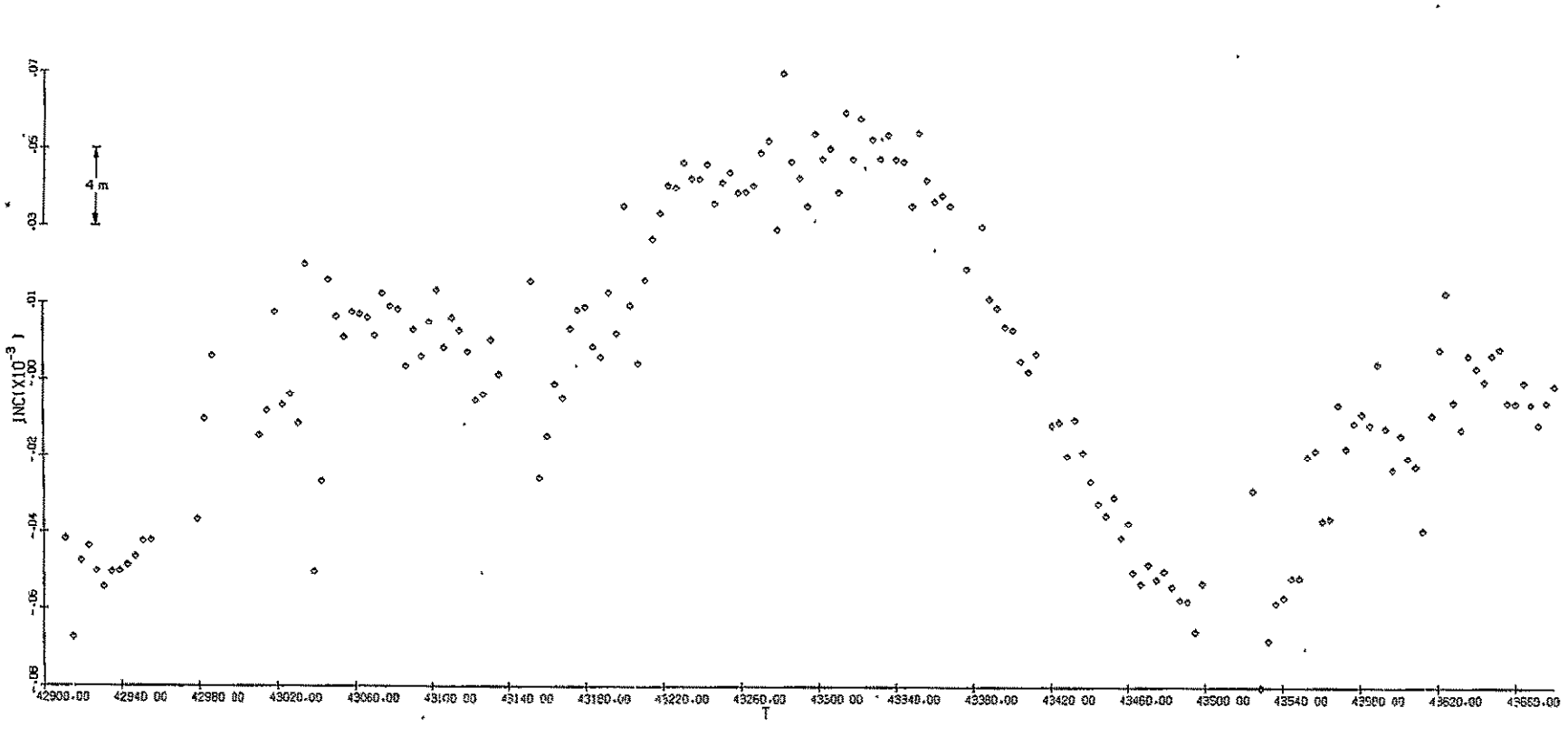

Figure 6b. Inclination of Lageos.

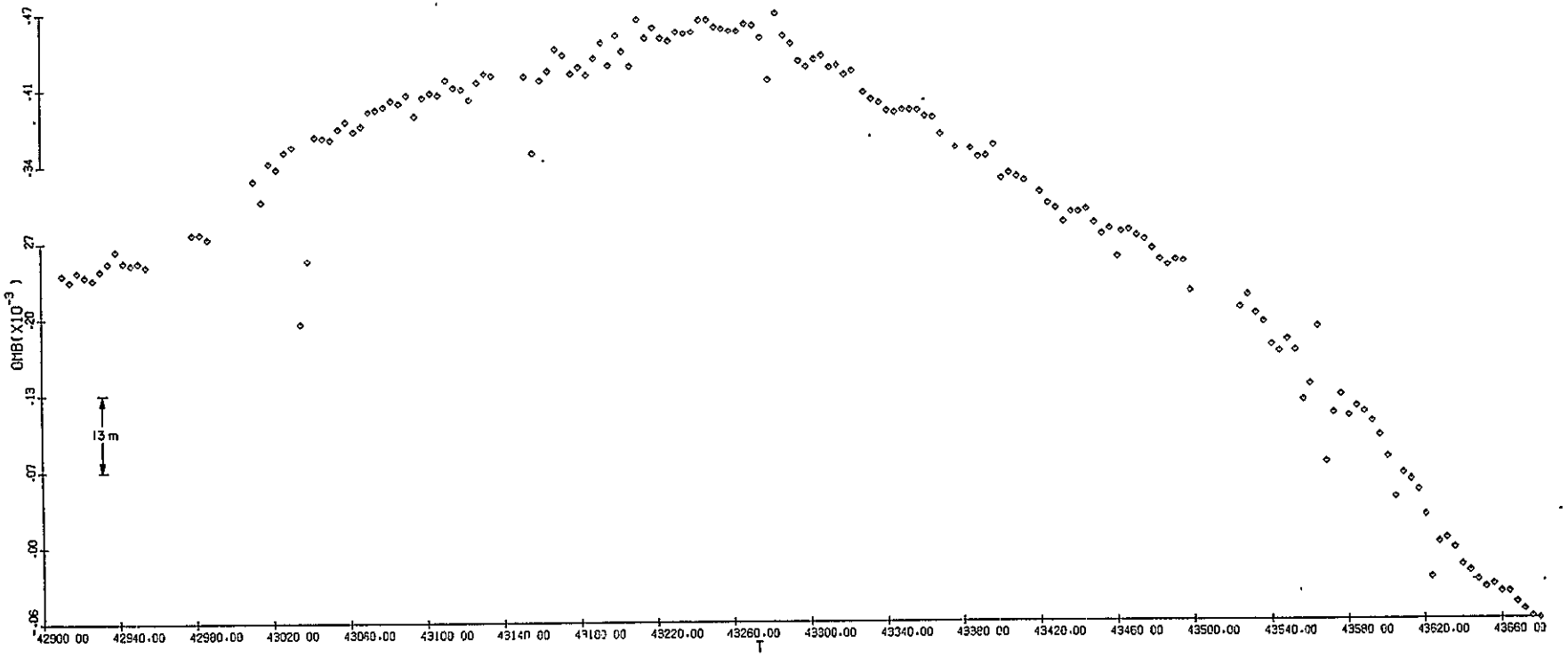

Figure 6c. Right ascension of the ascending node of Lageos (residual).

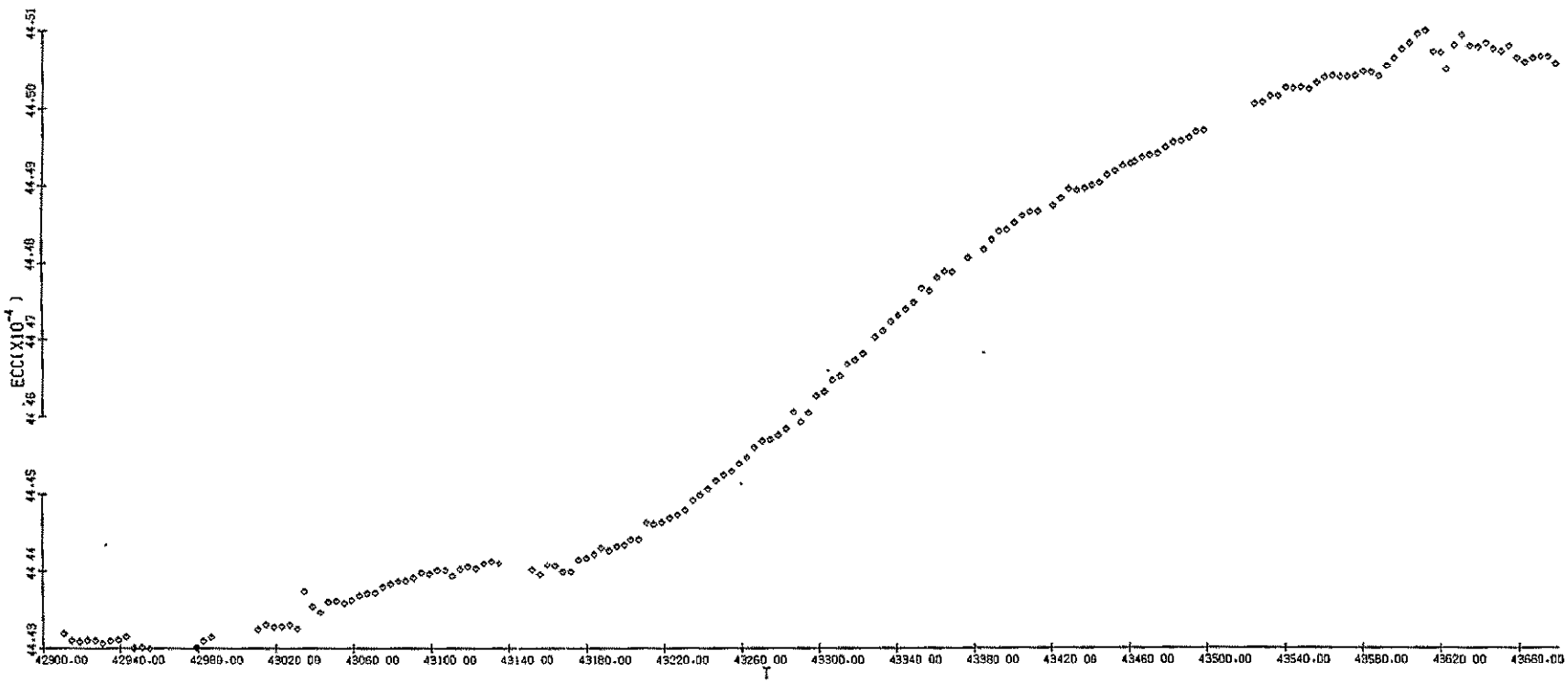

Figure 6d. Eccentricity of Lageos.

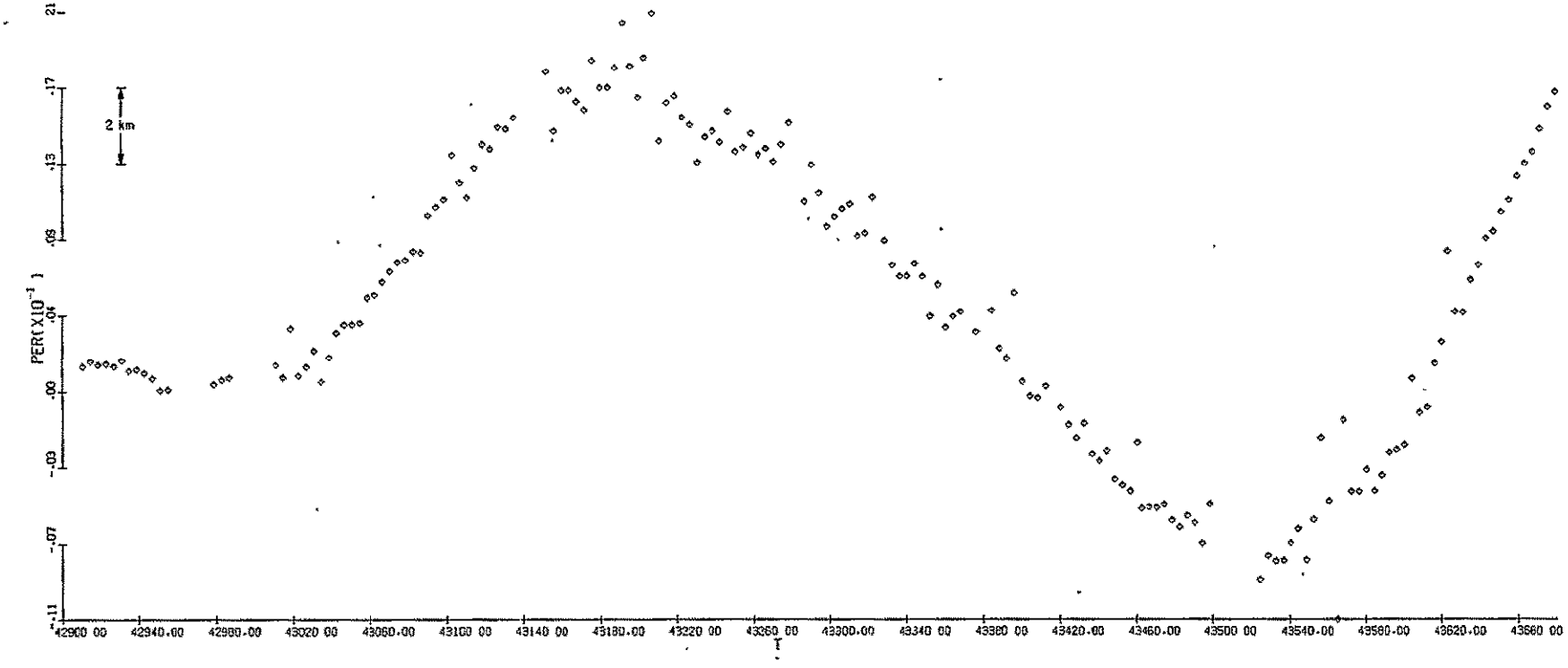

Figure 6e. Argument of perigee of Lageos (residual).

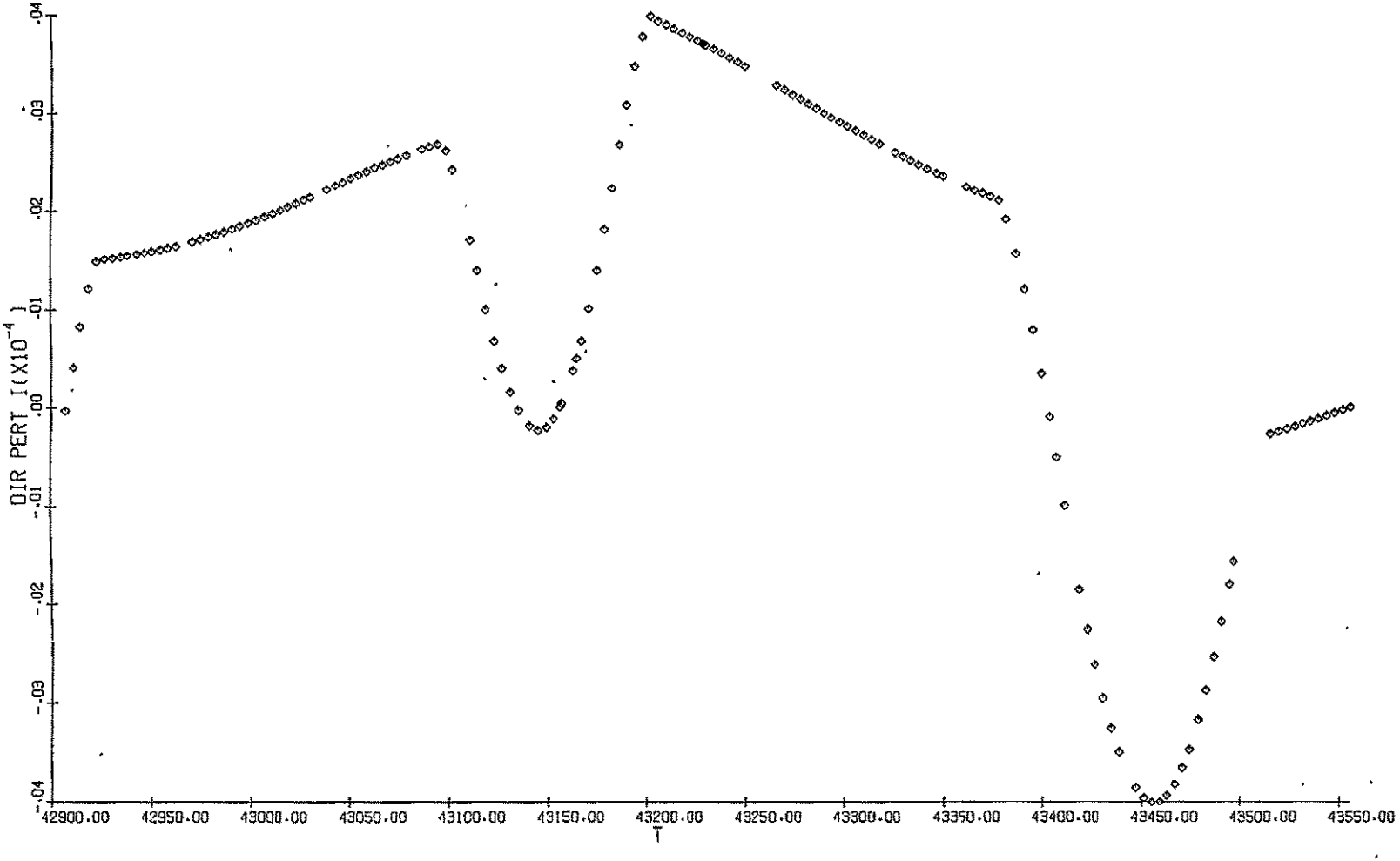

Figure 7a. Direct radiation-pressure perturbation on the inclination of Lageos.

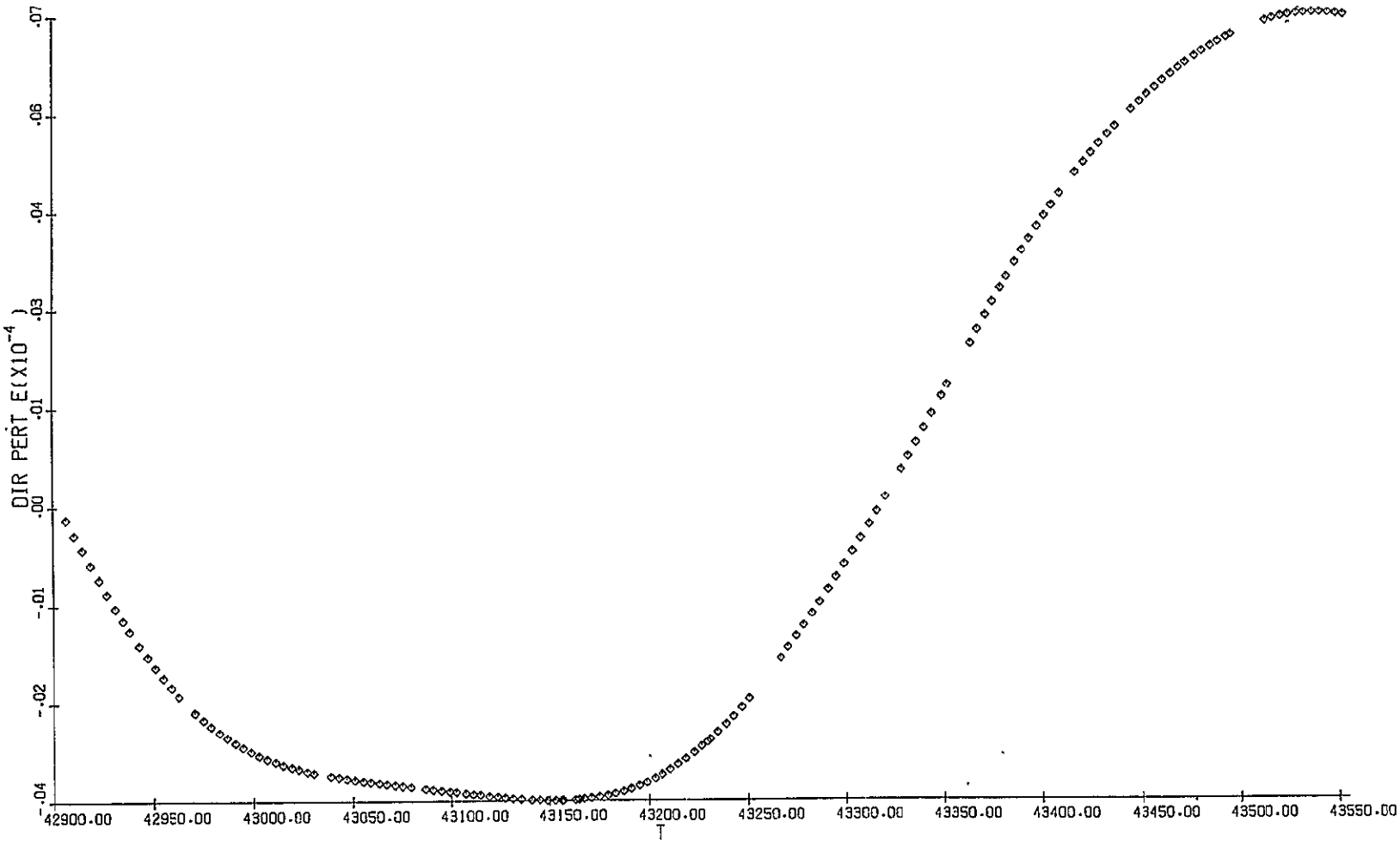

Figure 7b. Direct radiation-pressure perturbation on the eccentricity of Lageos.

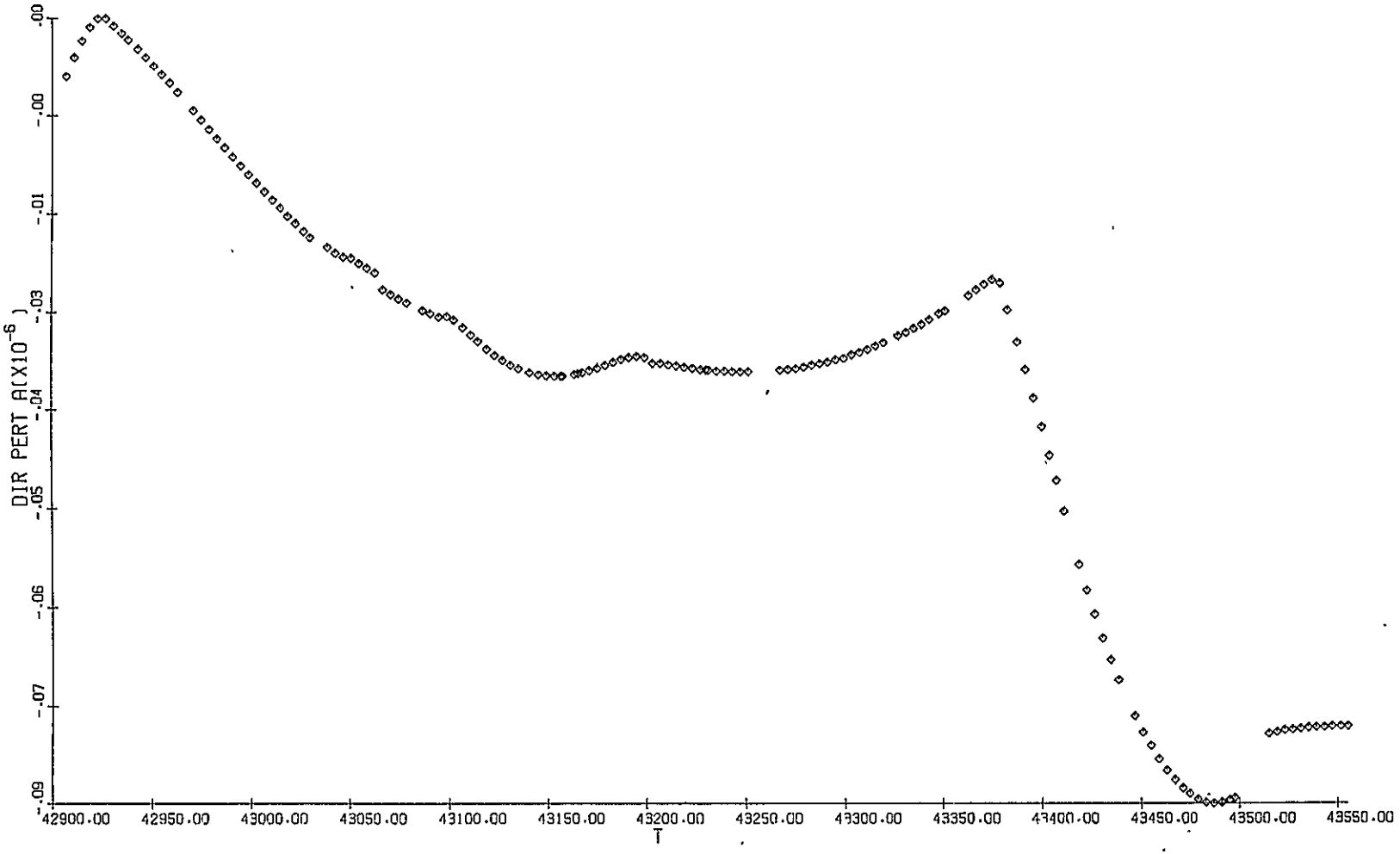

Figure 7c. Direct radiation-pressure perturbation on the semimajor axis of Lageos.

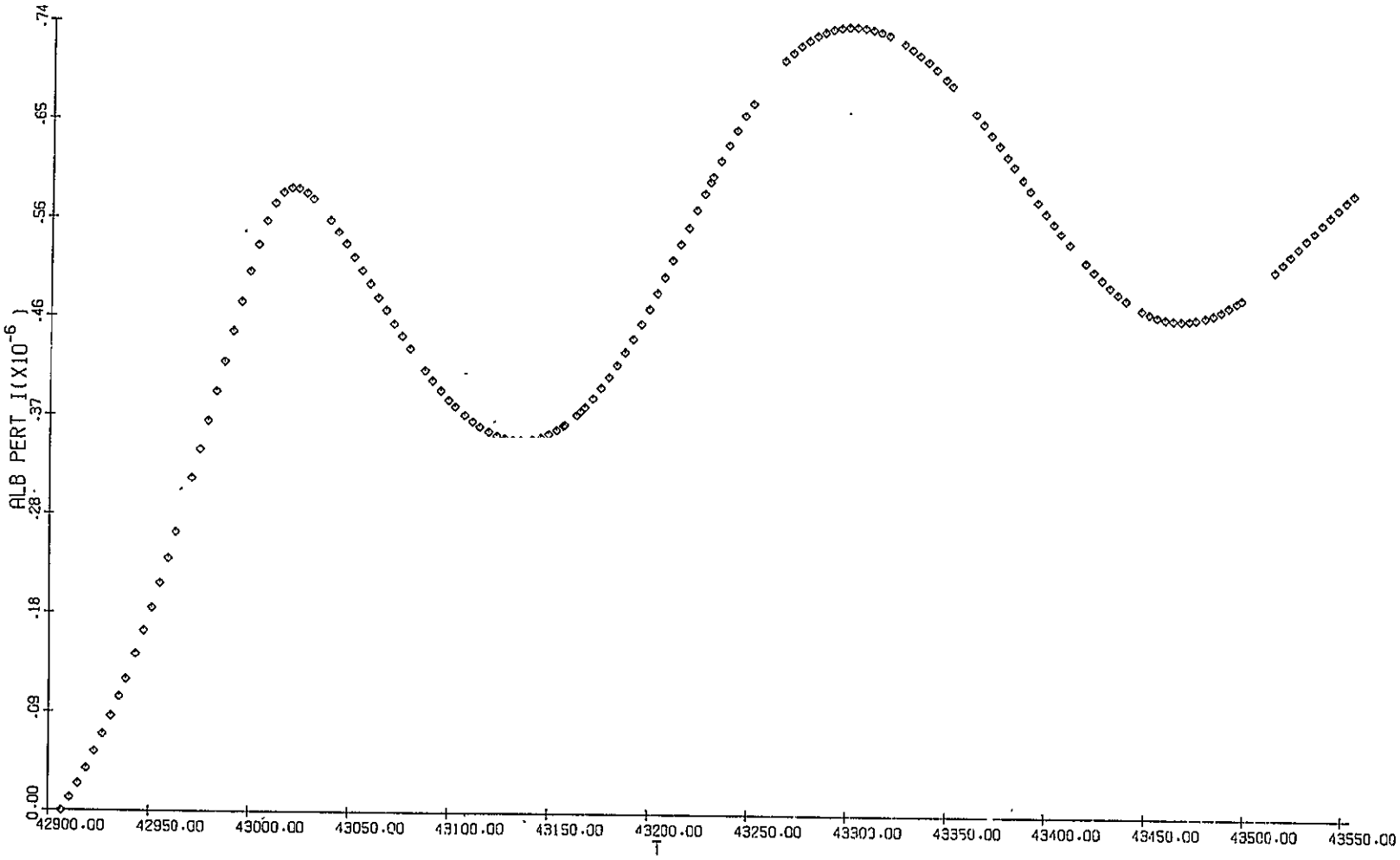

Figure 7d. Albedo radiation-pressure perturbation on the inclination of Lageos.

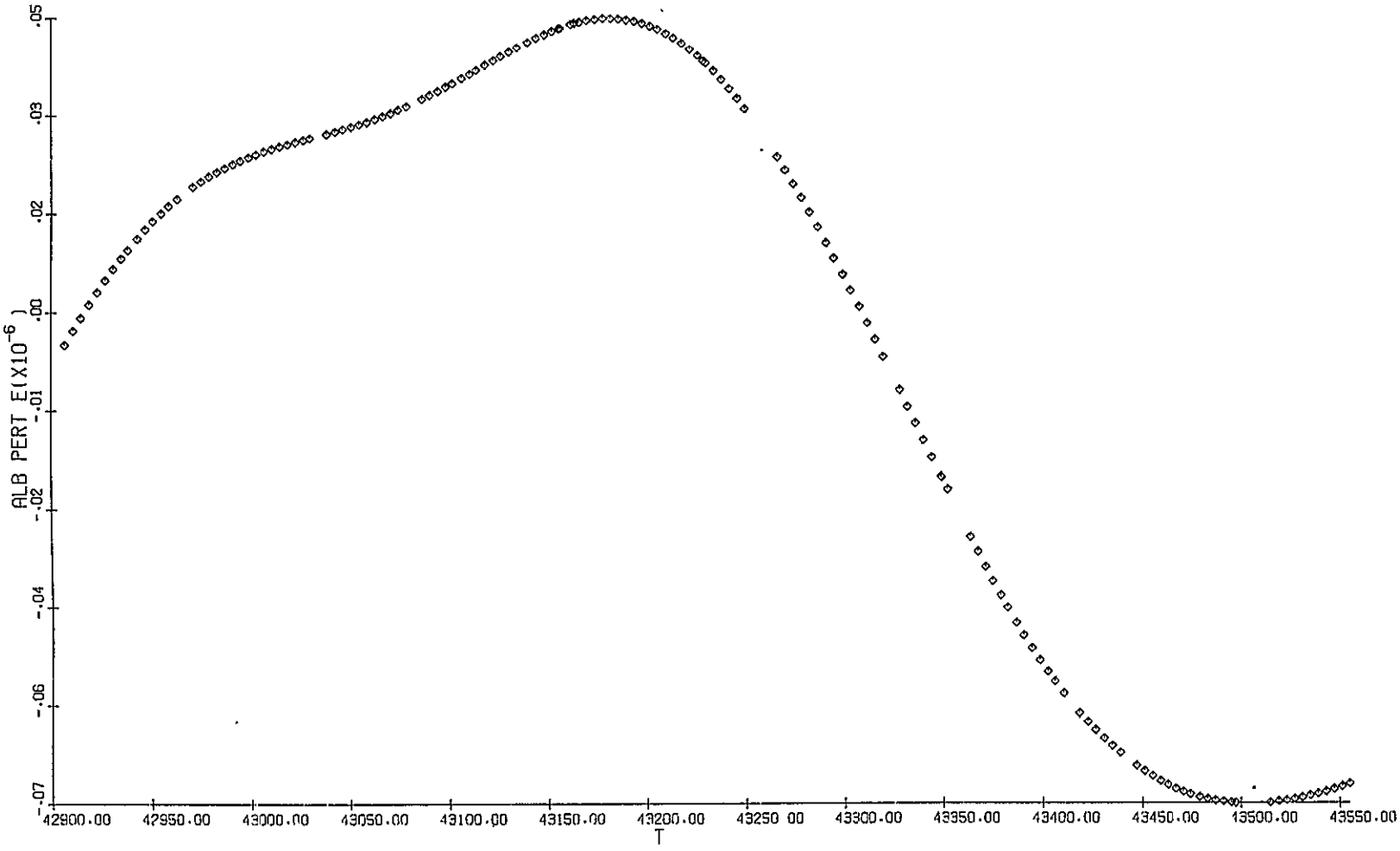

Figure 7e. Albedo radiation-pressure perturbation on the eccentricity of Lageos.

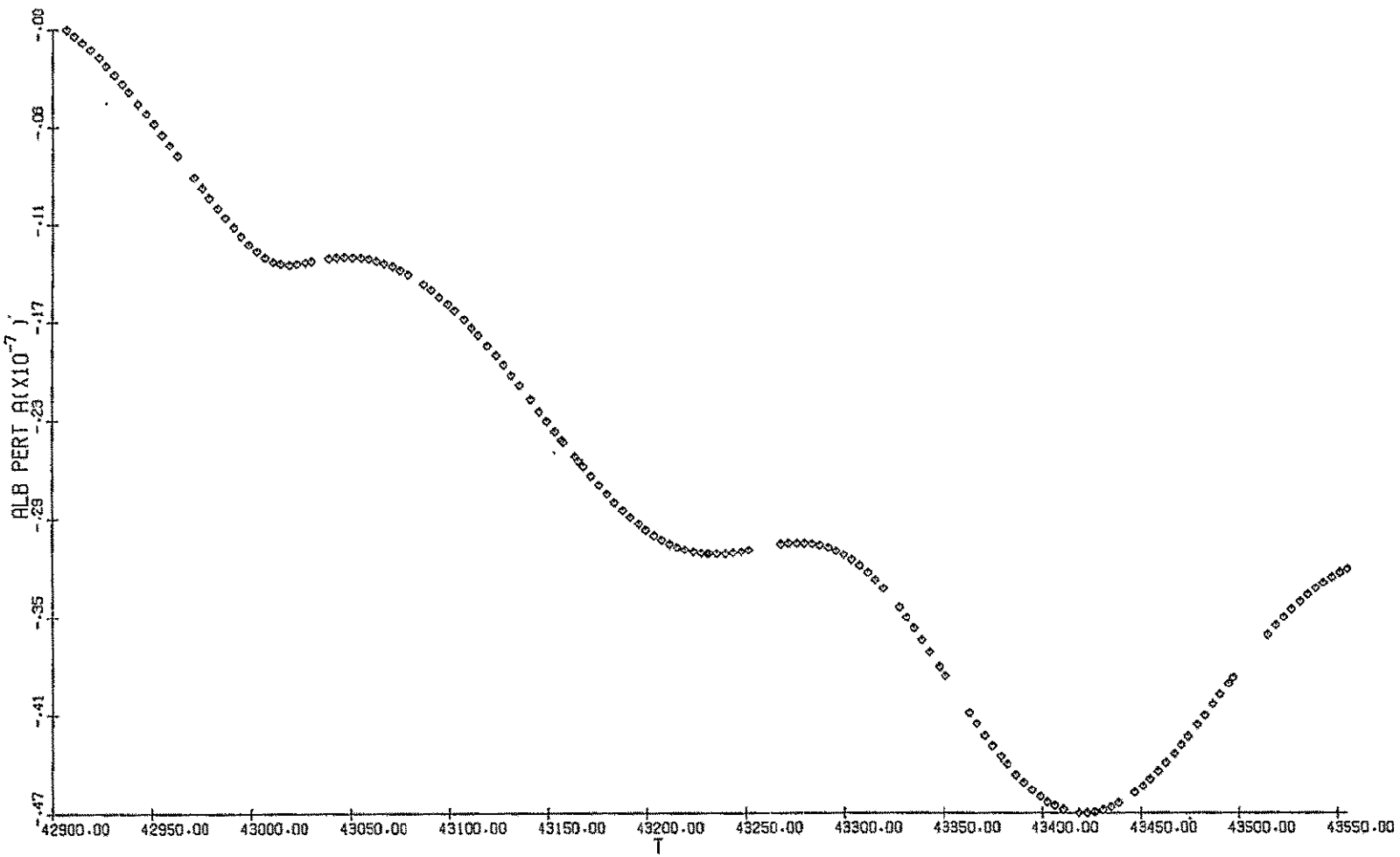

Figure 7f. Albedo radiation-pressure perturbation on the semimajor axis of Lageos.

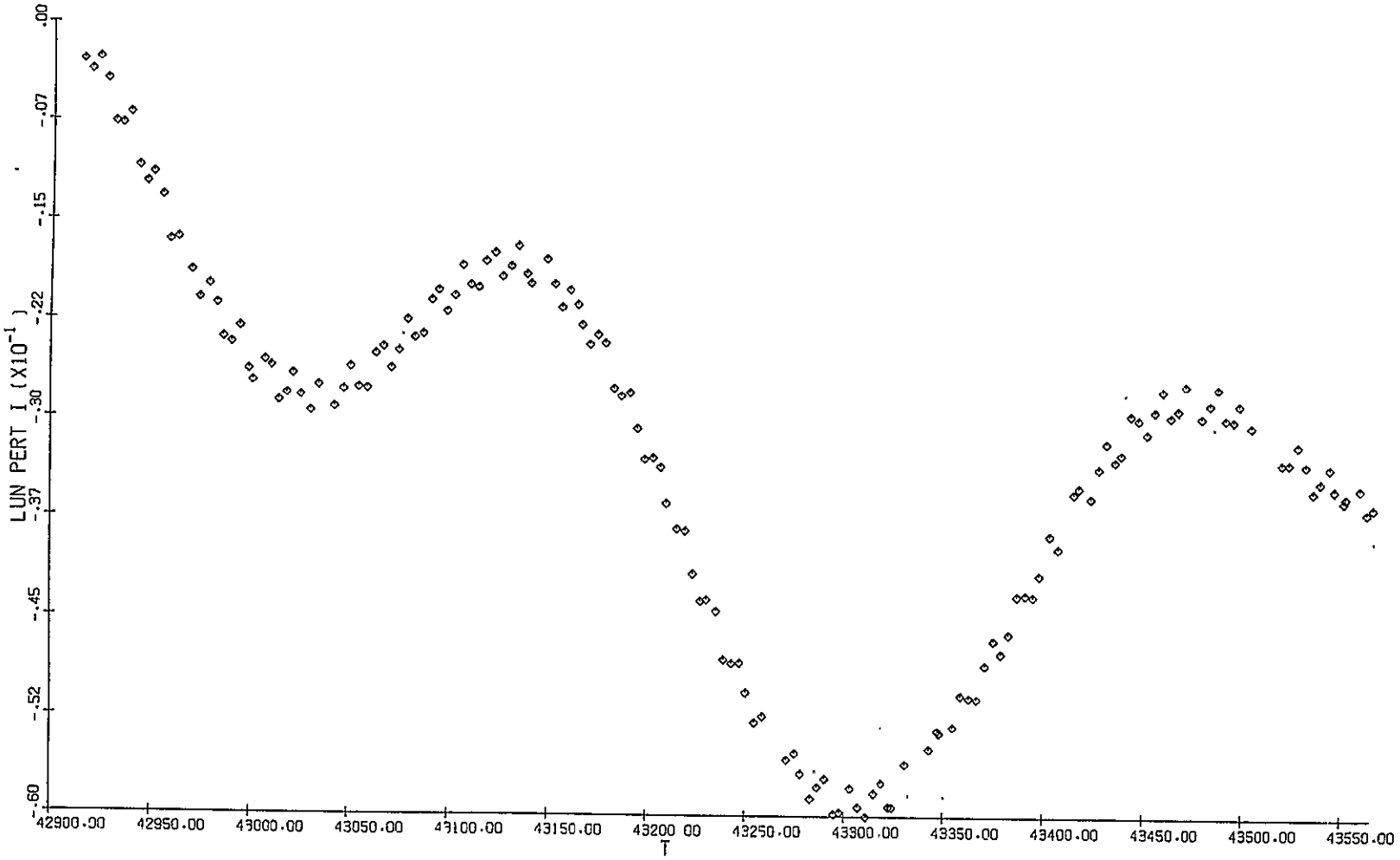

Figure 7g. Lunisolar perturbation on the inclination of Lageos.

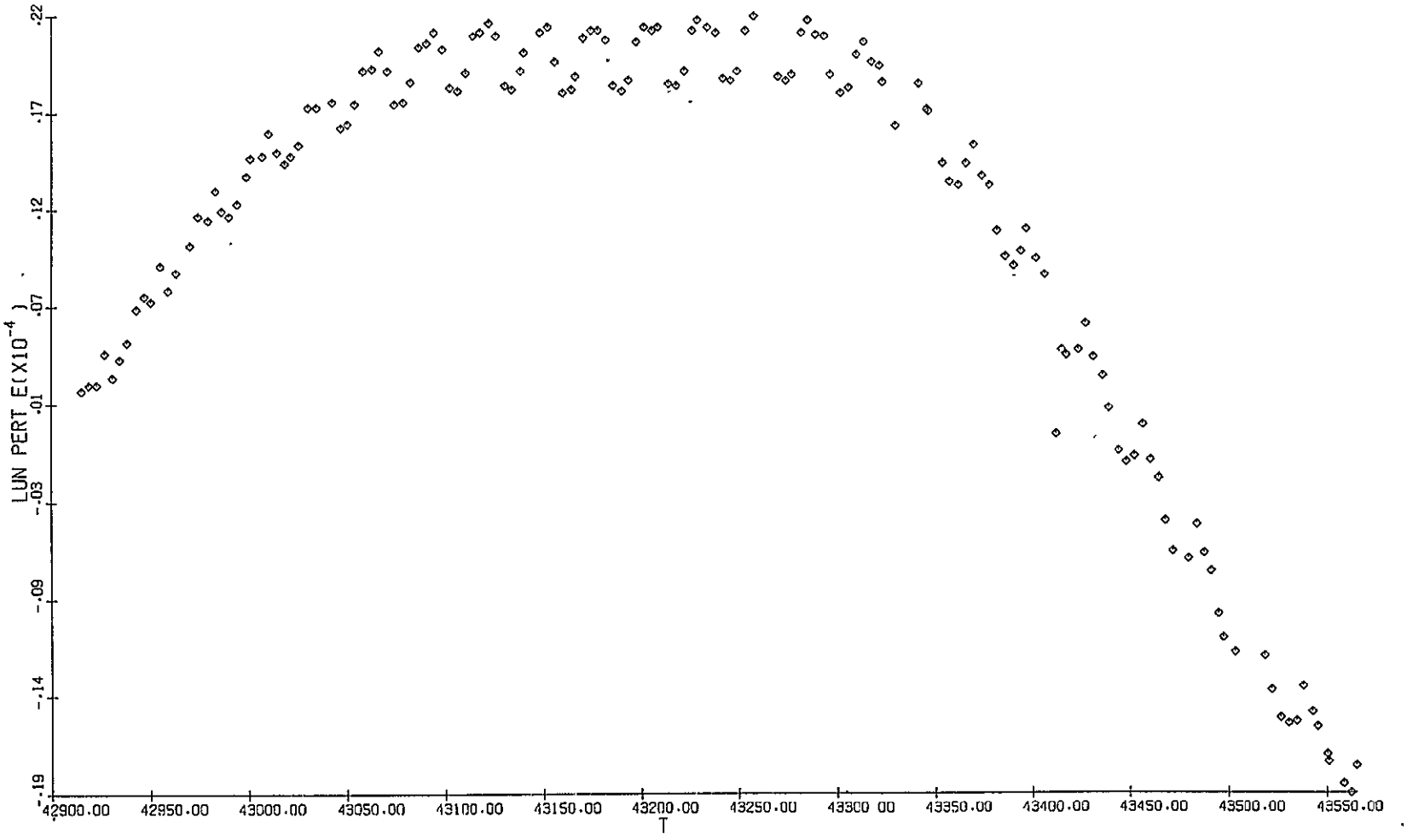

Figure 7h. Lunisolar perturbation on the eccentricity of Lageos.

7. DISCUSSION OF THE MEAN ELEMENTS

7.1 Variation in the Semimajor Axis

As pointed out in the preceding sections, Lageos was observed to have a secular decrease in its semimajor axis. Several forces have been suggested as possible causes of this anomaly, including drag, unmodeled radiation-pressure effects, albedo pressure, anisotropic radiation, interaction with the earth's magnetic field, and the Poynting-Robertson effect. Each of these is discussed in the following, where it is seen that the anomalous decrease in a remains unexplained.

It can be shown on theoretical grounds that gravitational perturbations cannot cause long-period or secular perturbations in a satellite's semimajor axis, so we are left with nongravitational effects. While it is possible that a buildup of charge and the interaction with the earth's magnetic field can create a force on a satellite, such a force must be orthogonal to the velocity vector and therefore cannot affect the energy (that is, the semimajor axis) of the satellite. The Poynting-Robertson effect can also be evaluated, and although it contributes to the change in a, the change is too small to account for the observation.

7.1.1 Neutral particle drag

The change in period of a satellite, or the corresponding change in a, has been used to infer atmospheric density. Employing an approximate expression from King-Hele (1964, p. 117), we can obtain the density ρ from the change in period dT/dt:

$$\rho = - \frac{\dot{T}}{3\pi a F (A/m) C_D} \quad , \tag{1}$$

where we take

$$a = 12 \times 10^{8} \text{ cm} \quad ,$$

$$F = 1 \quad ,$$

$$A/m = 0.00689 \text{ cm}^2 \text{ g}^{-1} \quad ,$$

$$C_D = 2.2 \quad ,$$

$$\dot{T} = \frac{\Delta T}{T} = -\frac{3}{2}\frac{\Delta a}{a} = -1.25 \times 10^{-10} \quad ,$$

$$\rho = 7.3 \times 10^{-19} \text{ g cm}^{-3}$$

From Jacchia (1971), we see that this atmospheric density would occur at an altitude of 2000 km.

The Jacchia (1971) atmospheric-density models provide a reliable description of the density to an altitude of 2000 km, and they have been used with good success for satellite analysis to a height of 3600 km (Slowey, 1974). The atmosphere above 2000 km is primarily made up of neutral hydrogen, the constituent for which the models are the least reliable, with an error as large as a factor of 3. The Jacchia model predicts a maximum density at 6000 km of $\rho_{max} = 8.9 \times 10^{-21}$ g cm^{-3}. Using the factor of 3, then, we could expect the neutral atmosphere to have a density of, at most, $\rho_{max} = 2.7 \times 10^{-20}$ g cm^{-3}. This predicts $\dot{a} = -0.037$ mm day^{-1}, which is too small by at least a factor of 27.

7.1.2 The Poynting-Robertson effect

The Poynting-Robertson (P-R) effect is viewed as an aberration in most texts on celestial mechanics. It results from the consequences of absorption and re-emission of radiation on the motion of small bodies. First considered

by Poynting (1903), the investigation was discussed in its most fundamental form by Robertson (1937), who was concerned with the lifetime of small particles in the solar system. This work has also had important consequences for comets (Wyatt and Whipple, 1950). There are some important differences in the results for small bodies orbiting a planet, as described below.

Although Robertson developed the equations of motion in the full relativistic form, we can start with his equation reduced to the Newtonian approximation. His equations are based on the assumptions that it is a spherical body, that the body absorbs all the energy falling on it from a point source of radiation, that the rotational motion of the body can be ignored, and that the transfer of energy within the body is such that it is ultimately radiated isotropically. In the equations of motion here, we retain only the first-order terms in the ratio of the velocity of the body v^α to the velocity of light c. The equations can then be written in terms of two vectors:

$$v^\alpha = \frac{dx^\alpha}{dt} \quad , \qquad n^\alpha = \frac{\ell^\alpha}{c} \quad , \tag{2}$$

in which n^α is the unit vector in the direction of the incident radiation. Thus, if v_n is the component of velocity v^α in the direction of n^α, the equations of motion become

$$m \frac{dv^\alpha}{dt} = f\left(1 - \frac{v_n}{c}\right) n^\alpha - \frac{f v^\alpha}{c} \quad , \tag{3}$$

where f is the force acting on the body. The first term on the right is the force due to direct radiation pressure in the direction of the incoming beam, decreased by the doppler factor $(1 - v_n/c)$. The second term represents the tangential drag known as the P-R effect.

The body absorbs energy at the rate cf and reradiates it such that the outgoing radiation may be thought of as carrying away electromagnetic

momentum at the rate fv^{α}/c, since it is distributed isotropically about the particle, which moves with velocity v^{α}. Through conservation of total momentum (mechanical plus electromagnetic), the body must lose momentum at the rate fv^{α}/c, which results in the force represented by the last term in equation (3).

Robertson considered the case of a body moving in the gravitational field of the sun, absorbing and readmitting the sun's radiation. In this case, n^{α} is the unit vector along the radius vector from the sun, and the energy density d falls off inversely as the square of the distance $r_{\odot}$ from the sun. If S is the solar constant ($S = 1.35 \times 10^{6}$ ergs cm^{-2} sec^{-1}), Robertson's equations would be

$$d = \frac{S}{c}\left(\frac{a_{\oplus}}{r_{\odot}}\right)^{2} \quad , \tag{4a}$$

$$f = A\,\frac{S}{c}\left(\frac{a_{\oplus}}{r_{\odot}}\right)^{2} \quad , \tag{4b}$$

where $a_{\oplus}$ is the mean distance of the earth to the sun and A is the effective cross-section area. In this case, the equations of motion become those of a resisting medium, which are discussed extensively in classical works on celestial mechanics (Plummer, 1918; Smart, 1953).

In the case of a body orbiting a planet, the force f no longer depends on the coordinates of the body, assuming that it is illuminated; rather, it becomes

$$f = A\,\frac{S}{c} \quad . \tag{5}$$

In treating direct solar radiation pressure, the usual variation of $(a_{\oplus}/r_{\odot})^{2}$ must be taken into account, although it does not change the essential properties of the motion.

Since the P-R effect is due to radiation of electromagnetic momentum, it can be written in terms of the absolute temperature of the body. If the body is in thermal equilibrium and is continuously illuminated, its temperature can be calculated by equating the incoming and radiating energy:

$$\pi a^2 S = 4\pi a^2 \sigma T^4 \quad , \tag{6}$$

where a is the radius of the body (assumed spherical) and σ is the Stefan-Boltzmann constant ($\sigma = 5.672 \times 10^{-5}$ erg cm^{-2} sec^{-1} °K^{-4}); this gives T = 278°K. Therefore, if the body temperature remains approximately constant while in a planet's shadow, the P-R effect is approximately constant. This is an essential difference from direct radiation pressure, which ceases while a body is in a planet's shadow. Furthermore, other sources of energy that increase the body's temperature (e.g., albedo or electromagnetic radiation from the planet and internal sources) will increase the P-R source. We can then write

$$f = \frac{\pi A \sigma T^4}{c} \tag{7}$$

The equations of motion for a body in orbit about a planet can readily be found to be

$$\ddot{r} - r(\dot{\theta})^2 = -\frac{\mu}{r^2} - \beta\dot{r} \quad , \tag{8a}$$

$$\frac{d}{dt}(r^2\dot{\theta}) = -\beta r^2\dot{\theta} \quad , \tag{8b}$$

where r and θ are the coordinates of the body with respect to the planet's center of mass, $\mu = GM$, and $\beta = f/mc$. In our application, β is assumed to be small, although the solution obtained below will hold for any β. Equation (8b) is integrated immediately. If we let the angular momentum $H = r^2\dot{\theta}$, equation (8b) becomes

$$\frac{d}{dt} H = -\beta H \quad , \tag{9}$$

which gives*

$$H = H_0 \varepsilon^{-\beta t} \tag{10}$$

Recall that the angular momentum can be written $H = [\mu a(1 - e^2)]^{1/2}$ for an instantaneous osculating ellipse. We can find the relation between r and θ by sustituting u = 1/r in equation (8a). A differential equation for u in terms of θ can be obtained by using

$$\frac{d}{dt} = u^2 H \frac{d}{d\theta} \tag{11}$$

The resulting equation is

$$\frac{d^2u}{d\theta^2} + u = \frac{\mu}{H^2} \tag{12}$$

If θ is assumed to change rapidly compared to H, then the solution of equation (12) can be written as

$$r = \frac{a(1 - e^2)}{1 + e \cos \theta} = \frac{\left(H_0^2/\mu\right) \varepsilon^{-2\beta t}}{1 + e \cos \theta} \tag{13}$$

To obtain the relation between θ and t, we can write equation (10),

$$r^2 \dot{\theta} = H_0 \varepsilon^{-\beta t} \tag{14}$$

*We use ε for the base of natural logarithms, not be confused with e, the eccentricity of an orbit.

Using equation (13) for r, we get

$$\frac{H_0^3 \, d\theta}{(1 + e \cos \theta)^2} = \mu^2 \varepsilon^{3\beta t} \, dt \quad , \tag{15}$$

which, if e is constant, integrates to

$$\frac{H_0^3}{1 - e^2} \left[\frac{2}{\sqrt{1 - e^2}} \tan^{-1} \left(\sqrt{\frac{1 - e^2}{1 + e}} \tan \frac{\theta}{2} \right) - \frac{e \sin \theta}{1 + e \cos \theta} \right]$$

$$= \frac{\mu^2}{3\beta} \varepsilon^{3\beta t} \quad . \tag{16}$$

From the basic relation for our ellipse, we have

$$\frac{e \sin \theta}{1 + e \cos \theta} = \frac{e \sin E}{\sqrt{1 - e^2}} \quad , \tag{17}$$

where E is the eccentric anomaly. We recognize the first term in the left bracket as E, from

$$\tan \frac{E}{2} = \sqrt{\frac{1 - e^2}{1 + e^2}} \tan \frac{\theta}{2} \quad . \tag{18}$$

Equation (16) reduces to a form of Kepler's equation:

$$\frac{H_0^3}{(1 - e^2)^{3/2}} (E - e \sin E) = \frac{\mu^2}{3\beta} \varepsilon^{3\beta t} \quad , \tag{19a}$$

$$H_0^2 = \mu a_0 \left(1 - e_0^2\right) \quad , \tag{19b}$$

$$E - e \sin E = \left(\frac{1 - e^2}{1 - e_0^2}\right)^{3/2} \frac{\mu^{1/2}}{a_0^{3/2}} \frac{\varepsilon^{3\beta t}}{3\beta} \tag{19c}$$

where the subscript 0 indicates the initial values, a_0 and e_0. From Kepler's third law, we can write this in a somewhat more familiar form:

$$E - e \sin E = \left(\frac{1 - e^2}{1 - e_0^2}\right)^{3/2} n_0 \frac{\varepsilon^{3\beta t}}{3\beta} \tag{20}$$

where the instantaneous mean motion $n \cong n_0 \varepsilon^{3\beta t}$.

Now we can calculate the change in a due to the P-R effect. For Lageos, we have

$$\begin{aligned} \beta &= \frac{A}{m} \frac{S}{c^2} \\ &= 0.00689 \times \frac{1.35 \times 10^{-6}}{(3 \times 10^{10})^2} \\ &= 1.034 \times 10^{-17} \text{ sec}^{-1} \end{aligned} \tag{21}$$

From equation (20) and Kepler's third law,

$$a = a_0 \varepsilon^{-2\beta t} \quad , \tag{22}$$

which gives

$$\frac{da}{dt} = -2a_0\epsilon^{-2\beta t}$$

$$= -0.02 \text{ mm day}^{-1} \text{ for Lageos} \quad . \tag{23}$$

This decrease is too small by a factor of 50 to explain the observed decrease in the semimajor axis of Lageos.

The above calculated rate assumes that the spacecraft temperature is in equilibrium with the solar-energy flux. However, other sources of energy could also raise the temperature. To account for the observed 1.0 mm day^{-1} decrease, therefore, the spacecraft temperature would have to be $(50)^{1/4}$ times the equilibrium temperature, i.e.,

$$278° \times (50)^{1/4} = 739°K \quad . \tag{24}$$

It seems unlikely that the spacecraft would be at such a temperature. The satellite was designed and tested to be in a narrow temperature range centered on 0°C. At the temperature predicted by equation (24), laser returns would probably not be possible owing to degradation of the optical performance.

7.1.3 Solar radiation-pressure perturbations

Although the calculations of the solar radiation-pressure perturbations and the earth's reflected radiation perturbations have been extensively checked (Aksnes, 1976; Lautman, 1977a,b), we must consider possible shortcomings in the theory. The values of the perturbations are listed in Appendix A and plotted in Figure 7a-h. The total effect to be explained, of approximately 1 mm day^{-1}, is 73 cm after 769 days. The theoretical model gives 24 cm for the direct solar radiation pressure and 14 cm for the

albedo pressure, for a total of about half the anomalous effect. To explain the variation in Lageos' semimajor axis by increasing the effective area-to-mass ratio used in the model would require multiplying A/m by a factor of 2.92, which is quite unreasonable.

In addition, we can dismiss a scale error in the radiation-pressure calculation as being the cause by examining the perturbation as a function of time. First, the character of the perturbation in the semimajor axis depends on the shadowing condition. The periods of shadowing, i.e., when part of the satellite's orbit is in the earth's shadow, can be identified by examining the perturbations in the inclination. The satellite began in a shadowing condition and soon passed into a nonshadowing condition at about MJD 42925; shadowing recommenced just after MJD 43100 and continued until approximately MJD 43210. In general, the conditions with nonshadowing have slowly changing and smaller perturbations. It can be shown that for a satellite orbiting a spherical earth, i.e., no zonal harmonics, the perturbations in the semimajor axis must average to zero over a complete orbit. This is not strictly true for a satellite with large secular perturbations. In any case, there is no discernible correlation between the occurrence of shadowing and the secular change in the semimajor axis. Furthermore, if the unmodeled perturbation in a were due either to an error in the radiation-pressure software or to the physical model, it should be correlated with the shadowing condition of the satellite, but we see from Figures 6a and 7a that there is no correlation at all.

A simple scale change in the radiation and albedo pressures would introduce large errors in the agreement of the other orbital elements. In particular, the eccentricity exhibits an unexplained change that is quite large. Increasing the perturbation amplitude in the semimajor axis to explain what is observed would cause the unexplained change in the eccentricity to increase. Therefore, the radiation-pressure perturbations do not seem to be likely sources for explaining the secular decrease in a.

C-2

Anomalous radiation-pressure accelerations in satellite orbits have been observed and studied in the past (Smith and Kissell, 1971; Slowey, 1974). In these cases, the effect was on a balloon that was deformed and therefore nonisotropic in shape; consequently, the force of radiation absorption and consequent reradiation was not along the line of sight to the sun, but along some other direction that gave rise to some rather large effects. A classical study by Shapiro (1963) found that this effect could be 30 times the size of the perturbation, assuming spherical symmetry. Lageos, however, is unlikely to have deformed significantly, although some nonisotropic reradiation due to the satellite's rotation about its spin axis might be postulated. Since the orientation of the spin axis is not known, a definitive calculation cannot be made. On the other hand, a satellite will despin through eddy-current dissipation due to interaction with the earth's magnetic field. We know that the spin rate ω as a function of time t (Nixon, 1974) can be written

$$\omega = \omega_0 \epsilon^{-t/\tau} \quad ,$$

where

$$\tau = \frac{5\pi \times 10^9 \rho}{4\beta_0^2 \alpha} \quad \text{(cgs units)}$$

and ω_0 is the initial spin rate, ρ is the material density, α is the conductivity, and β is the flux density. For an aluminum sphere the size of Lageos, the time constant is about 2.7 months and the spin rate will drop from 90 to 1 rpm in about 1 year. Therefore, if the anomalous acceleration were due to some nonisotropic reradiation, the effect should decrease to zero after about a year. But in the case of Lageos, no noticeable change has occurred in the secular decrease after more than 2 years.

Before leaving the subject of nongravitational perturbations, we should point out that most attention has been paid to Lageos' semimajor axis, because its variation remains unexplained. In the next section, we will see that unmodeled variations in the right ascension of the ascending node and in the inclination also exist; they are small but comparable in size to the direct solar radiation-pressure perturbation. Furthermore, little attention has been given to the residual variations in the argument of perigee and eccentricity, both of which have significant unmodeled changes. The very large unmodeled variation in the argument of perigee is accompanied by an even larger calculated solar radiation-pressure perturbation; in this instance, therefore, small improvements in the radiation-pressure treatment could improve that perturbation significantly. In all cases, there are dynamical relations between the perturbations that must hold, and no claim can be made to have modeled the satellite's motion with confidence until all six orbital elements are properly modeled.

7.2 Variations in the Inclination and the Right Ascension of the Ascending Node

Figures 6a-e show the observed mean elements (taken from the numerical values in Appendix A) for 769 days. For the plot of the right ascension, a secular change of $\dot{\Omega} = 0\overset{\circ}{.}34266230$ day^{-1} was removed. If we can use this value, the position of Lageos' orbit for 2 years can be calculated with an accuracy of 20 m in inclination and 90 m in the node.

The theoretical value of $\dot{\Omega}$, the rate of the node, is $\dot{\Omega} = 0\overset{\circ}{.}34261239$ day^{-1}, according to the GEM 10 geopotential coefficients and the expression of Kinoshita (1977). The difference between the theoretical value and the value we adopted is $5^\circ \times 10^{-5}$ day^{-1}, which is rather large. This fractional difference, 0.00015, will limit the accuracy with which *a priori* long-term predictions of the satellite node can be made. The difference, however, is small compared with the direct lunar and solar perturbations of $2\overset{\circ}{.}5 \times 10^{-4}$ day^{-1} and large compared with the contribution due to the permanent tidal deformation of $2^\circ \times 10^{-5}$ day^{-1}, both of which are modeled. If the

difference between the observed and the theoretical value of $\dot{\Omega}$ is ascribed to an error in J_2, then J_2 must be corrected by 10^{-7}, which is large compared to its formal uncertainty of $\pm 10^{-9}$. It is difficult to attribute this difference only to errors in the geopotential model, although they certainly make some contribution.

Most of the variation in Ω appears to be a long-period effect; it is probably due to a long-period tide, of which there are several, or to the zonal harmonics. The principal long-period zonal-harmonic perturbation, with a period of 1690 days, is very long compared with the available data span. Its amplitude is $2^\circ \times 10^{-4}$, comparable to the variation seen here. To remove this long-period effect, a cubic polynomial was fit by least squares to both the inclination and the node data. After rejecting data points with large residuals, 164 points remained. In addition, a three-point smoothing filter was used on the reduced data; the smoothed data are plotted in Figure 8a and 8b. The results of the fitting and smoothing calculation are given in Table 7.

Table 7. Summary of smoothed data.

Variance	Inclination (μdeg)	Node (μdeg)
Noise	7.24	6.22
Signal	23.50	14.03

By using the smoothed data as true, an estimate of the uncertainty of each observation was made. The noise estimated in this way was about 7 μdeg, equivalent to about 1.4 m. Since the amount of information remaining in these observations is significant, autocorrelation functions were applied to suggest the source of the information. The autocorrelation function for the node is given in Figure 9. Also, a high-pass filter with a window corresponding to periods shorter than 120 days was used; the autocorrelation function of the filtered data is shown in Figures 10a and 10b.

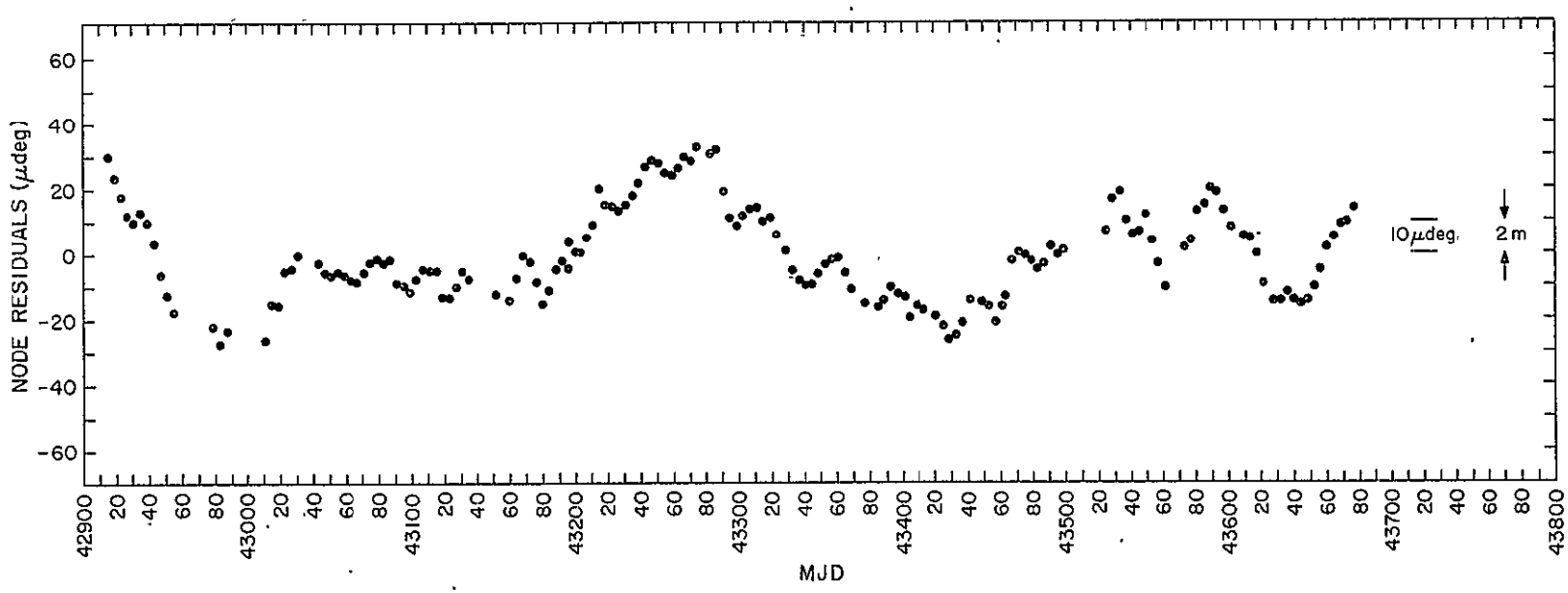

Figure 8a. Residuals of smoothed Lageos node.

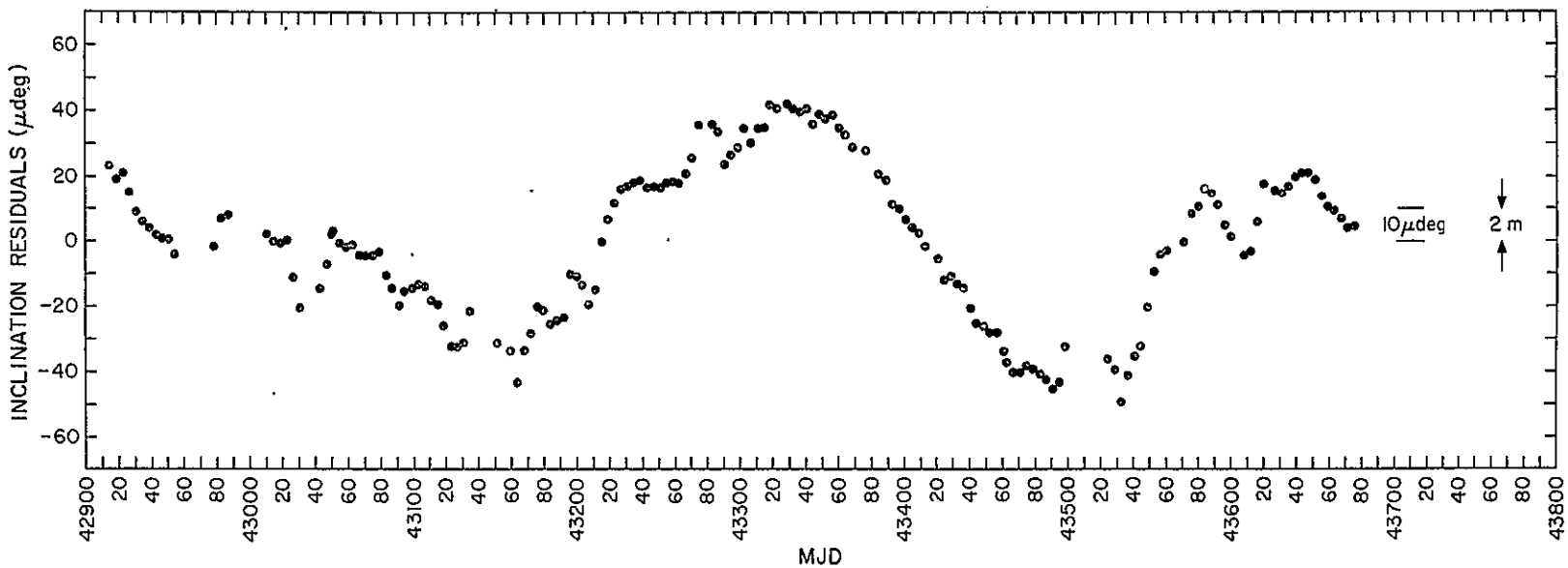

Figure 8b. Residuals of smoothed Lageos inclination.

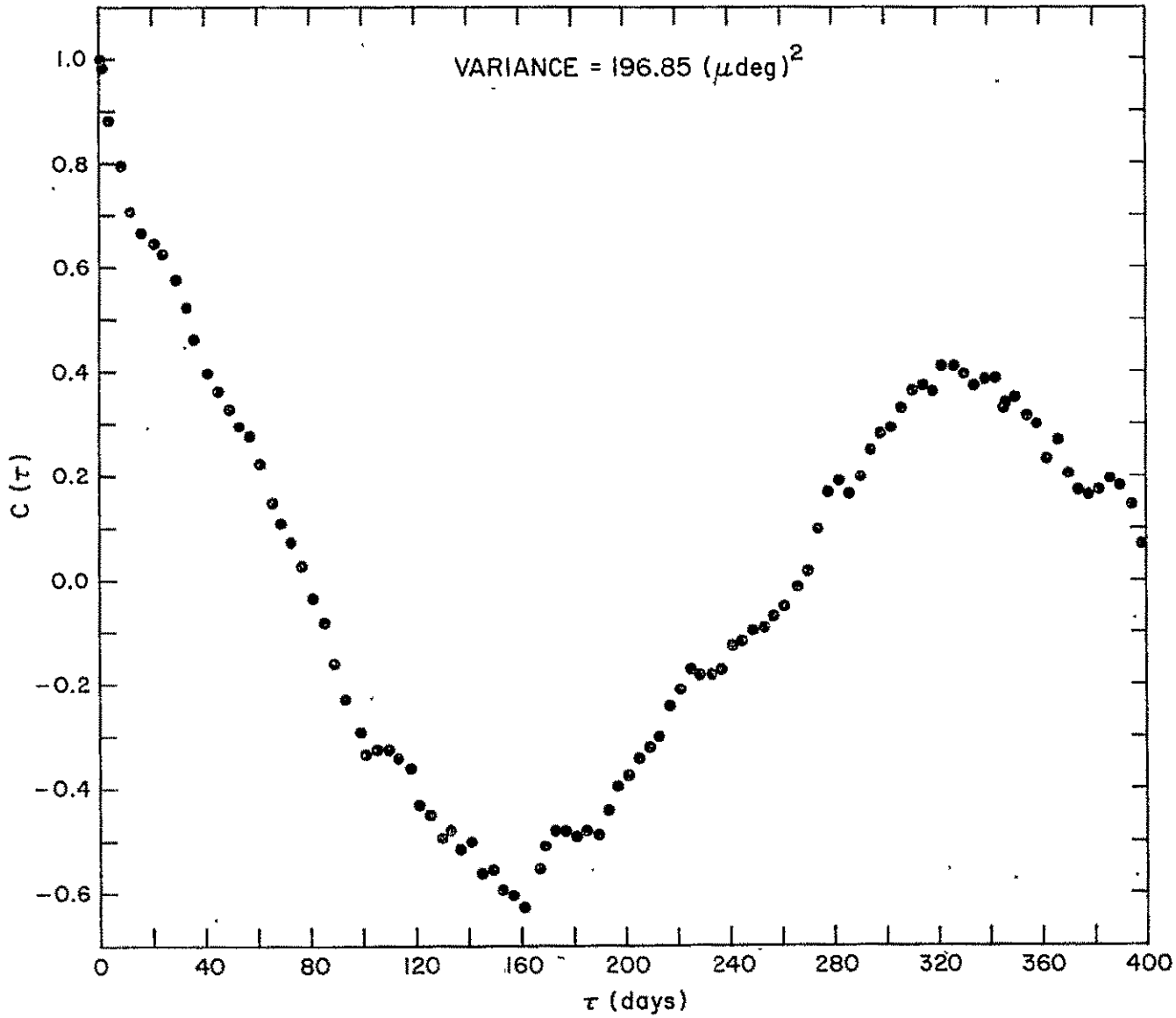

Figure 9. Autocorrelation function of smoothed Lageos node residuals.

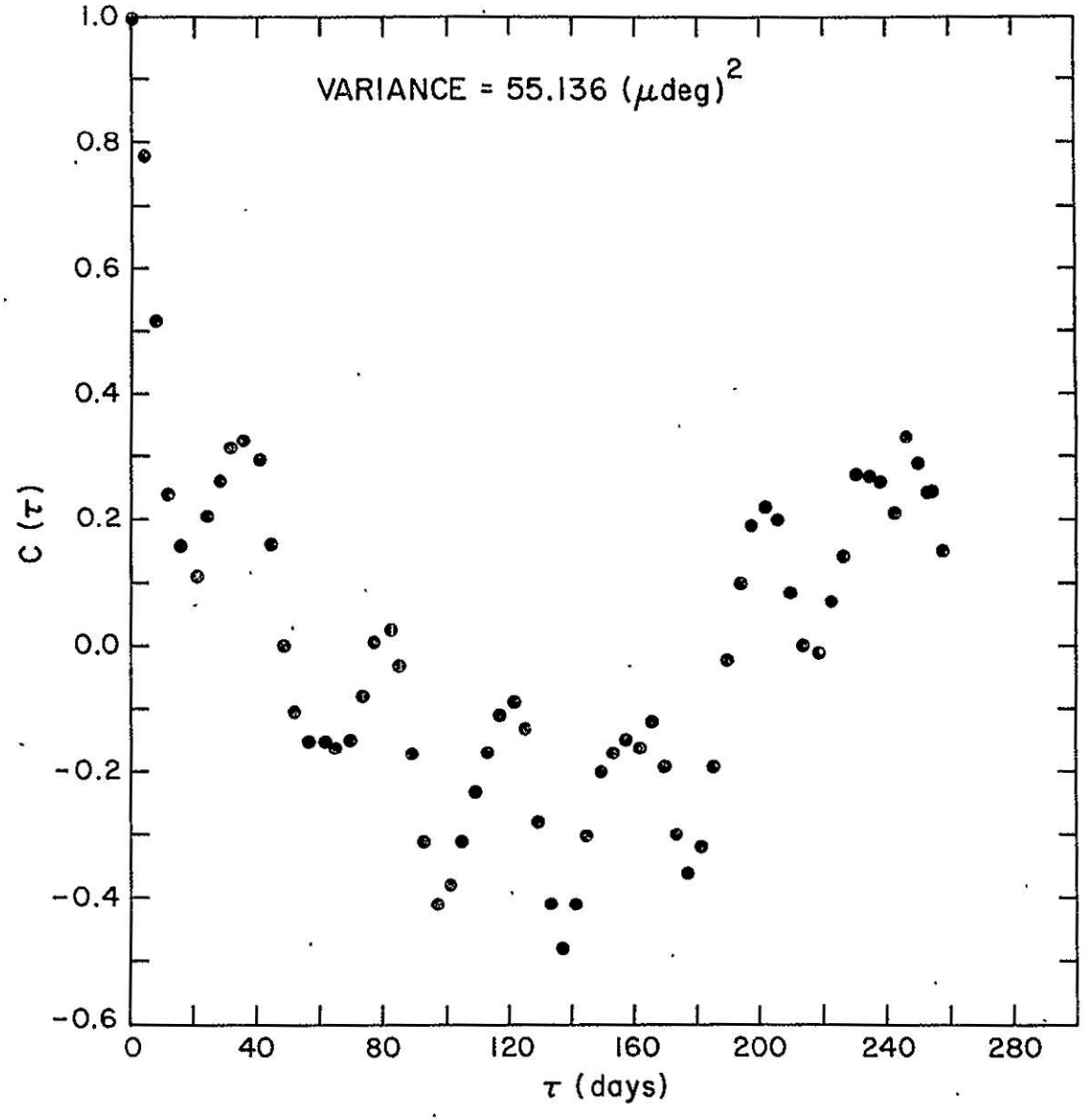

Figure 10a. Autocorrelation function of smoothed and filtered Lageos node residuals.

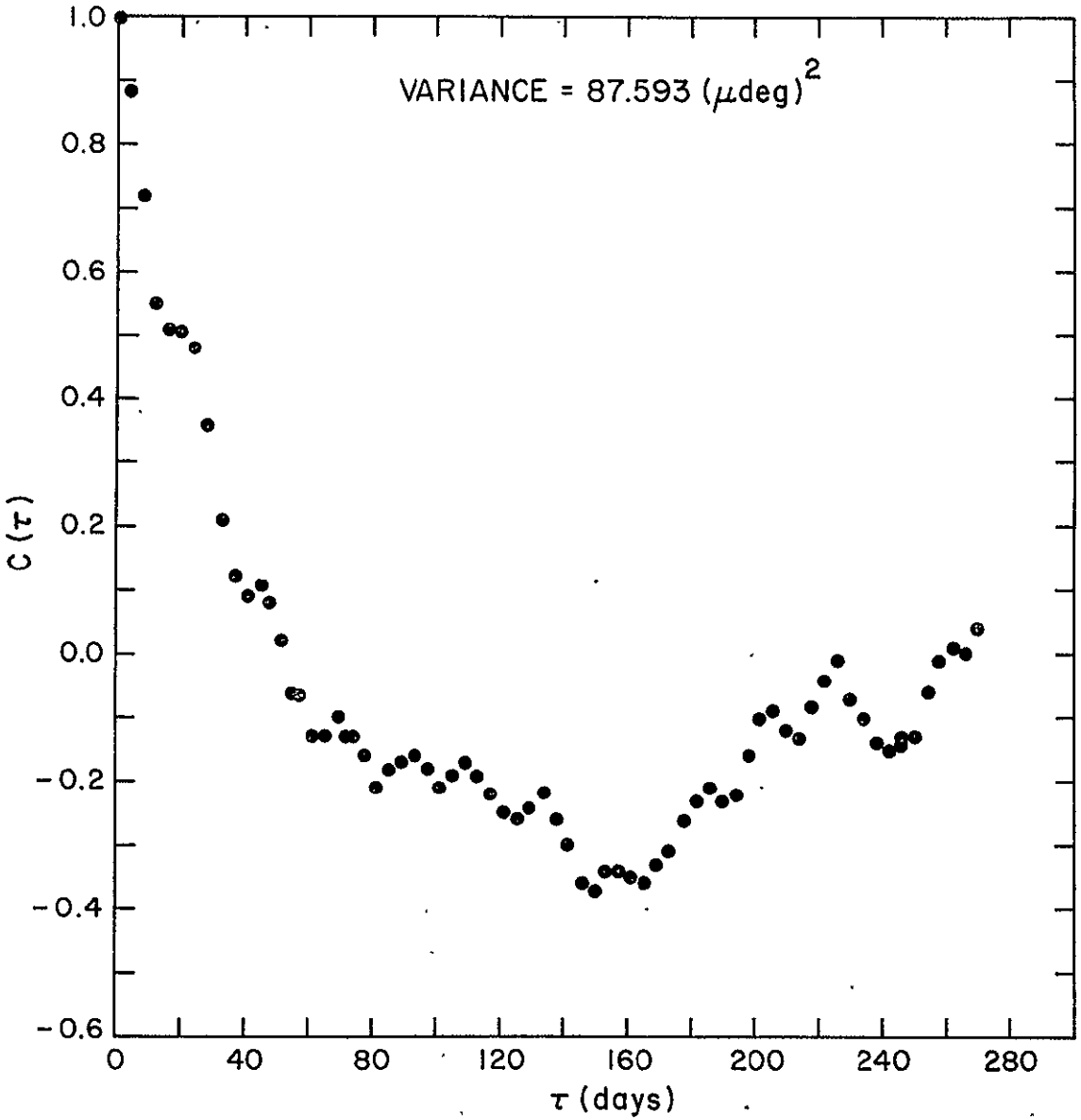

Figure 10b. Autocorrelation function of smoothed and filtered Lageos inclination residuals.

No sharp periodic signal is identified in the autocorrelation functions, although there is a suggestion of a period of approximately 28 days in the data and in both autocorrelation functions. Significant ocean-tide perturbations would be expected at that frequency, as none has been modeled in the orbit program. The zonal tide Mm is a particular condidate. There is also a hint in the filtered inclination data of information at a period of less than 20 days. In addition, a number of small but significant long-period tidal perturbations exist, which could produce the continuum of spectral energy at long periods. A selection of them is given in Table 8 to suggest where further analysis would be useful if these variations in the Lageos orbit are to be explained. Table 8 gives the amplitude of the solid-body tide as a measure of the perturbations. The body tides are, of course, already modeled. Generally, the ocean tides are less than 10% of the body tides, if an equilibrium theory for the ocean tides holds. When an ocean resonance occurs, the tides could be considerably larger.

Table 8. Sample of tidal constituents for Lageos.

Doodson	Darwin	$D_{\ell mp}$	Orbital period (days)	Perturbation amplitude of Ω (μdeg)	Perturbation amplitude of I (μdeg)
056.554	SA	0.01156	365	2.7	0
057.555	SSA	0.07281	183	8.53	0
065.455	Mm	0.08254	27.55	1.43	0
155.655	M1	-0.02964	28.30	1.35	0.36
162.556	π1	0.01028	137.71	1.68	0.61
164.554	—	-0.00147	559.91	1.37	0.35
175.455	J1	-0.02964	26.85	0.80	0.34
265.455	L2	-0.02667	28.57	0.25	0.87
272.556	T2	0.02476	158.49	1.94	4.65

7.3 Orbital Accuracy

By orbital accuracy, we mean, given 8 days of data, how accurately can the orbit be determined at some other time? In Section 7.2, we showed that Lageos' orientation in space could be known to about 0.01% of its secular rate, or to within $5° \times 10^{-5}$ day^{-1} of the secular motion of the node, from *a priori* information on such perturbing forces as the earth's gravity field and tides. However, the phase, i.e., the mean anomaly, was much worse than that, owing to the unexplained change in the satellite's semimajor axis. Further, if empirical values are adopted for the secular rates, then the uncertainties in the long-period perturbations (longer than 800 days) are about $5° \times 10^{-4}$. These very long-period perturbations are probably caused by unmodeled tides and by differences in the GEM 10 geopotential model from the true geopotential. If the long-period perturbations are somehow empirically obtained, then the remaining variations, which are probably due to unmodeled ocean tides, are about 14 μdeg in the node and 23 μdeg in inclination, or 2.8 and 4.6 m, respectively, in position. Finally, the overall accuracy of the orbital elements was estimated to be about 7 μdeg, or 1.4 m.

We need also to look at the accuracy of the short-period perturbations. In this case, the principal causes of the uncertainties are the geopotential model, the station coordinates, and, possibly at some level, the analytical theory. Unfortunately, most of the data have an accuracy of 1 to 2 m, as borne out from the formal standard error of each orbit, which was consistently 1 to 2 m, and the orbital accuracy is clearly better than this.

For a limited time, data from more accurate laser systems were available for use in the orbit computation; these are the NASA laser stations in Table 3. For the first 2 years of Lageos data, Table 9 gives the overall standard deviation σ and the number of observations n for each 8-day arc. Also listed are the σ and the number of observations from each station. The distribution of the data over these 2 years is also shown.

The data from the four SAO sites always fit to within 1 to 2 m, which is consistent with the assumed accuracy. On the other hand, the data from the NASA sites are considered to have an accuracy better than 10 cm, and the data fits are consistently 40 to 60 cm. Thus, we conclude that the accuracy of the orbital ephemeris is about 50 cm. Gaposchkin (1978) estimates the uncertainty of the analytical theory to be less than 20 cm. The most likely candidates contributing to the ephemeris error are the geopotential model and the station coordinates. At this level of accuracy, polar motion and UT1 will also contribute to the orbital error.

The nonstationarity of the remaining residuals indicates that the geophysical information is not periodic, and therefore, these residuals should be correlated with other data. The obvious data are the observed variations in UT1. However, the possibility that these variations are instrumental should also be assessed. Instrumental sources could, for example, come from the nonuniform distribution of the data in time.

Table 9. Standard deviation σ and number of observations n for 2 years of Lageos data, by station.

			Station number													
			7061		7063		7080		7082		7907		7921		7929		7943	
Epoch	σ (m)	n	σ(m)	n	σ(m)	n	σ(m)	n	σ(m)	n	σ(m)	n	σ(m)	n	σ(m)	n	σ(m)	n
42911	1.22	542			0.50	(62)					1.30	(168)	1.18	(266)	1.61	(46)		
42915	1.34	605			0.70	99					1.61	253	1.01	121	1.37	132		
42919	1.06	1368			0.65	384					1.39	279	0.98	514	1.30	191		
42923	1.03	1653			0.60	433					1.23	254	1.09	857	1.29	109		
42927	1.37	1313			0.51	104					1.44	216	1.38	752	1.47	241		
42931	1.40	1286									1.57	158	1.25	750	1.57	378		
42935	1.26	1296			1.04	152					1.74	37	1.22	730	1.38	327		
42939	1.28	1278			0.62	208					1.71	18	1.26	756	1.58	296		
42943	1.49	1170			0.28	56					1.62	112	1.56	590	1.44	412		
42947	1.62	1229									1.88	335	1.48	524	1.53	370		
42951	1.28	1480	1.61	47							1.43	527	1.12	736	1.29	170		
42955	1.19	1378	0.98	77	0.30	103					1.30	491	1.21	577	1.23	130		
42959	1.23	1001	1.39	30	0.41	103					1.51	199	1.36	313	1.05	356		
42963																		
42967	1.58	121	1.24	109							3.07	12						
42971	4.84	137	3.54	112							8.04	25						
42975																		
42979	1.31	347					0.42	3			1.64	120			1.07	224		
42983	1.48	380					0.19	3			1.39	252			1.64	125		
42987	1.34	443									1.27	419			2.16	24		
42991	1.39	346									1.36	292			1.41	54		
42995	1.46	397									1.49	308			1.27	89		
42999	1.48	495									1.39	381			1.69	114		
43003	1.29	250									1.00	137			1.54	113		

Table 9. (Cont.)

			Station number													
			7061		7063		7080		7082		7907		7921		7929		7943	
Epoch	σ (m)	n	σ(m)	n	σ(m)	n	σ(m)	n	σ(m)	n	σ(m)	n	σ(m)	n	σ(m)	n	σ(m)	n
43007	1.31	145													1.27	145		
43011	1.49	225											1.12	101	1.69	124		
43015	0.98	329					0.56	58					0.98	243	1.41	28		
43019	0.80	354	0.31	74			0.72	58					0.86	197	1.20	25		
43023	1.06	309	0.38	74									1.02	178	1.56	57		
43027	1.34	406											1.16	313	1.78	93		
43031	1.26	363											1.13	315	1.81	48		
43035	0.95	165											0.86	138	1.19	27		
43039	1.74	247					0.54	2			1.61	26	1.67	192	2.10	27		
43043	1.67	353					1.26	20			2.18	26	1.79	240	0.95	16	0.69	51
43047	1.50	699					0.66	18	0.36	4	1.13	42	1.56	298	1.53	177	1.51	160
43051	1.36	1044							1.06	118	1.24	107	1.36	337	1.25	342	1.84	140
43055	1.35	900							0.77	114	1.36	165	1.50	281	1.18	224	1.61	116
43059	1.43	1025									1.09	312	1.51	534	1.39	43	1.75	136
43063	1.18	1109					0.77	39	0.84	64	0.91	367	1.35	489	1.22	99	1.44	51
43067	1.32	1005					0.43	39	1.22	104	1.15	400	1.62	302	1.33	100	1.21	60
43071	1.24	951	0.63	12			1.16	52	1.36	64	1.12	480	1.52	186	1.10	62	1.23	95
43075	1.17	1211	0.99	120			1.03	84	0.65	24	1.01	525	1.62	181	1.37	179	0.90	98
43079	1.30	1721	0.72	322			0.57	47			1.22	503	1.48	467	1.41	262	1.38	120
43083	1.34	1888	0.68	461			0.87	44			1.37	301	1.55	602	1.47	299	1.60	181
43087	1.34	2077	0.82	600			0.67	53	1.65	2	1.25	348	1.61	512	1.61	323	1.49	239
43091	1.23	1948	0.79	575			0.90	35	0.87	203	1.34	471	1.55	384	1.48	165	1.57	115
43095	1.24	1646	0.72	363			1.22	45	0.89	418	1.34	444	1.43	260	1.73	47	2.57	69
43099	1.24	2202	1.03	803			0.81	46	1.30	395	1.43	426	1.32	259	1.17	104	1.48	169
43103	1.30	2198	1.07	890			1.49	48	0.93	177	1.45	342	1.43	530	1.88	117	1.44	94
43107	1.09	1329	0.61	228			0.58	36			1.17	349	1.16	589	1.20	127		

Table 9. (Cont.)

			Station number							
			7061	7063	7080	7082	7907	7921	7929	7943
Epoch	σ (m)	n	σ(m) n	σ(m) n	σ(m) n	σ(m) n	σ(m) n	σ(m) n	σ(m) n	σ(m) n
43111	1.49	1448					1.40 532	1.59 524	1.37 155	1.30 237
43115	1.26	1635	1.00 382				1.22 400	1.60 293	1.28 196	1.21 364
43119	1.64	1384	1.44 581				1.50 196	1.69 202	1.39 147	2.15 258
43123	1.64	1613	2.29 239				1.24 275	1.32 660	1.59 205	2.01 234
43127	1.56	1453	0.70 98				1.41 322	1.58 578	1.16 203	2.11 252
43131	1.38	1067	1.80 45				1.45 231	1.35 230	1.23 197	1.33 364
43135	1.47	878					1.19 172	1.52 279	1.31 144	1.61 283
43139	0.90	293	0.54 97					1.02 120		0.99 76
43143										
43148	1.86	578					1.96 104	2.34 84		1.60 390
43152	1.60	701					1.02 71	1.85 232		1.50 398
43156	2.33	488						2.11 316		2.51 172
43160	1.60	673					1.49 220	1.50 292	2.26 11	1.81 150
43164	1.32	865					1.40 379	1.30 120	1.29 22	1.20 344
43168	1.17	795					1.33 291		1.17 89	1.03 415
43172	1.24	775					1.49 175	1.01 84	1.45 78	1.08 438
43176	1.28	730					1.36 186	1.32 224	1.36 29	1.16 291
43180	1.77	941					1.63 295	1.60 452	1.39 78	2.64 116
43184	2.12	1215					2.51 151	1.83 607	1.59 72	2.41 385
43188	1.69	1143						1.63 580	1.63 48	1.74 515
43192	1.70	892						1.50 549	2.34 55	1.77 288
43196	1.07	562						1.03 407	0.99 31	1.14 124
43200	1.69	573					1.29 11	1.27 332	2.73 33	1.59 197
43203	1.29	712					1.32 13	1.18 404	1.62 33	1.34 262
43207	0.95	611						0.95 510	0.92 33	0.93 68
43211	1.51	748						1.40 530	1.68 10	1.67 208

Table 9. (Cont.)

Epoch	σ (m)	n	Station number													
			7061		7063		7080		7082		7907		7921		7929		7943	
			σ(m)	n	σ(m)	n	σ(m)	n	σ(m)	n	σ(m)	n	σ(m)	n	σ(m)	n	σ(m)	n
43215	2.02	1073											1.56	499	2.13	10	2.34	564
43219	1.81	1023											1.43	384	2.39	40	1.96	599
43223	1.43	960											1.04	397	1.95	169	1.49	394
43227	1.47	741											1.14	273	1.54	192	1.65	276
43231	1.51	764									1.22	97	1.01	149	1.53	62	1.66	456
43235	1.60	1153									1.69	158	1.41	184	2.16	71	1.55	740
43239	1.41	1207									0.98	116	1.36	304	1.33	72	1.49	715
43243	1.59	1299									1.52	98	1.30	350			1.66	851
43247	1.75	1279									1.75	214	1.36	233	2.76	5	1.83	827
43251	1.34	1239									1.31	373	1.10	175	2.22	5	1.39	686
43255	1.40	1440									1.39	561	1.34	113			1.41	766
43259	1.54	1279									1.51	516	1.48	73			1.56	690
43263	1.40	1315									1.28	484	1.52	61			1.45	770
43267	1.49	1433									1.45	633	1.51	72			1.50	728
43271	1.34	1354									1.32	628	1.48	85	1.99	33	1.29	608
43275	1.31	868									1.23	413	0.87	36	1.40	85	1.33	334
43279	1.10	260									0.92	94			1.14	145	1.21	21
43283	1.91	447													1.29	259	1.04	188
43287	2.33	697											1.59	73	1.86	207	2.60	417
43291	3.43	518											1.41	73	2.13	40	3.69	405
43295	1.11	409									1.09	149					1.10	260
43299	1.49	782									1.50	554					1.37	228
43303	1.81	1447									1.71	829	0.89	46	3.01	46	1.87	526
43307	1.93	1750									2.05	775	1.22	46	2.02	129	1.78	800

Table 9. (Cont.)

			Station number													
			7061		7063		7080		7082		7907		7921		7929		7943	
Epoch	σ (m)	n	σ(m)	n	σ(m)	n	σ(m)	n	σ(m)	n	σ(m)	n	σ(m)	n	σ(m)	n	σ(m)	n
43311	1.57	1339									1.35	725			1.87	133	1.77	481
43315	1.56	1288									1.40	864			2.25	111	1.64	313
43319	1.52	1907									1.39	1042	1.22	85	1.85	203	1.64	577
43323	1.42	1126									1.27	571	1.14	85	1.63	129	1.33	341
43327																		
43329	1.51	1663									1.45	893			0.93	18	1.57	752
43333	1.36	1566									1.39	637			1.10	48	1.33	881
43337	1.35	1576									1.41	628			1.26	112	1.30	836
43341	1.39	1779									1.42	690			1.39	120	1.35	969
43345	1.61	1778									1.64	554			1.58	133	1.55	1091
43349	1.53	1008									1.59	423			1.69	75	1.43	510
43353	1.56	1310									1.50	509			1.34	33	1.51	768
43357	1.52	1792									1.56	726			1.40	183	1.51	883
43361	1.50	1613									1.70	667			1.32	214	1.33	732
43365	1.54	1740									1.80	578			1.32	182	1.38	980
43369	1.55	1482									1.90	382			1.08	172	1.45	928
43373	1.45	1397									1.82	91	1.72	49	1.31	162	1.42	1095
43377	1.43	1474											1.73	136	1.22	106	1.41	1232
43381	1.61	1239									1.41	215	1.70	216	1.00	27	1.62	781
43385	1.53	965									1.16	524	1.73	225	1.12	27	2.11	189
43389	1.27	733									1.13	359	1.42	95	1.28	124	1.41	155
43393	1.38	845									1.40	351	1.31	161	1.02	124	1.47	209
43397	1.56	601									1.61	332	1.36	216			1.38	53
43401	1.43	513									1.24	279	1.54	234				
43405	1.45	1201									1.43	579	1.33	382			1.62	240
43409	1.47	1306									1.56	523	1.40	272			1.38	511

Table 9. (Cont.)

			Station number											
			7061		7063		7080		7082		7907		7921		7929		7943	
Epoch	σ (m)	n	σ(m)	n	σ(m)	n	σ(m)	n	σ(m)	n	σ(m)	n	σ(m)	n	σ(m)	n	σ(m)	n
43413	1.33	872									1.38	466	1.26	108	2.02	27	1.15	271
43417																		
43421	1.37	1452									1.50	335	1.22	263	1.46	35	1.35	819
43425	1.29	1260									1.52	406	1.27	53	1.21	19	1.15	782
43429	1.47	1231									1.69	176	1.47	331	1.62	62	1.36	662
43433	1.93	1296									1.95	75	1.55	597	1.48	62	2.27	562
43437	1.71	1023									1.90	170	1.38	377	1.62	81	1.90	395
43441	1.64	1256									1.52	395	1.51	327	1.82	147	1.77	386
43445	1.58	1365									1.64	638	1.39	406	1.74	112	1.59	209
43449	1.52	1250									1.51	424	1.47	464	1.61	142	1.57	220
43453	1.55	1144									1.76	180	1.42	325	1.62	244	1.45	395
43457	1.47	902									1.75	144	1.39	275	1.47	201	1.38	282
43461	1.80	603									1.97	50	1.45	226	2.16	89	1.74	238
43463	1.72	1080									2.26	161	1.50	477	1.58	75	1.73	367
43467	1.97	1392									1.70	312	1.64	539	2.44	79	2.35	462
43471	1.54	1364									1.68	392	1.35	596	1.75	44	1.62	332
43475	1.41	1285									1.33	480	1.28	648			1.97	157
43479	1.33	1414									1.26	622	1.24	627			1.77	165
43483	1.52	1568									1.47	433	1.26	750			1.95	385
43487	1.67	1261									1.55	241	1.45	576			1.95	444
43491	1.31	1091									1.33	295	1.21	598			1.51	198
43495	1.42	1004									1.47	306	1.26	547			1.79	151
43499	1.21	447									1.34	151	1.03	175			1.21	121
43503																		
43507																		

Table 9. (Cont.)

			Station number													
			7061		7063		7080		7082		7907		7921		7929		7943	
Epoch	σ (m)	n	σ(m)	n	σ(m)	n	σ(m)	n	σ(m)	n	σ(m)	n	σ(m)	n	σ(m)	n	σ(m)	n
43511																		
43513	5.67	821											5.69	647	12.11	174		
43517	3.59	844											2.88	705	6.26	139		
43521	6.64	802											4.70	481	12.75	59	5.73	262
43525	2.91	748											2.94	290	5.17	196	2.39	262
43529	0.91	870											1.46	98	1.06	772		
43533	1.02	1733											1.16	644	1.04	913	0.81	176
43537	1.07	1374											1.15	684	1.28	394	0.98	296
43541	1.06	1286											1.14	950	1.42	216	0.88	120
43545	1.15	1863											1.21	1372	1.20	115	0.99	376
43549	1.19	1291									1.11	10	1.20	830			0.97	451
43553	1.01	647									1.17	10	1.05	455	1.74	107	1.20	75
43557	1.15	1117											1.12	978	2.56	99	1.82	40
43561	1.52	2447											1.58	2184	1.58	197	2.24	66
43565	1.21	1835											1.28	1610	1.76	197	1.24	28
43569	1.44	793											1.31	648	1.53	27	1.82	118
43573	1.27	1171									1.53	132	1.50	858	1.73	102	1.04	79
43577	1.03	1260									1.36	404	1.38	569	1.46	287		
43581	1.09	1705									1.41	287	1.34	1077	1.38	234	1.12	107
43585	1.20	1525									1.93	15	1.35	1381	1.87	22	1.32	107
43589	1.04	801											1.33	801				
43593	1.09	713											1.39	630			1.37	83
43597	1.09	900									1.62	239	1.29	578			1.51	83
43601	1.37	2293									1.72	834	1.52	1019			1.43	440
43605	1.49	2276									1.73	593	1.97	796			1.16	887

Table 9.. (Cont.)

			Station number													
			7061		7063		7080		7082		7907		7921		7929		7943	
Epoch	σ (m)	n	σ(m)	n	σ(m)	n	σ(m)	n	σ(m)	n	σ(m)	n	σ(m)	n	σ(m)	n	σ(m)	n
43609	1.33	1956									1.61	404	2.19	582			1.23	970
43613	1.37	2762									1.82	550	1.80	1190			1.37	1022
43617	1.54	2584									1.89	482	1.84	1553			1.75	549
43621	1.63	2447									1.72	861	2.00	984			1.79	602
43624	1.13	955									1.20	171	1.25	606			1.00	178
43628	1.22	1502									1.39	287	1.35	601			1.23	614
43632	1.38	2050									2.08	664	1.45	456			1.38	930
43636	1.41	3021									1.82	1105	1.48	1160			1.50	756
43640	1.48	4348									1.55	1257	1.97	1632			1.38	1459
43644	1.51	3763									1.49	772	1.91	1523			1.45	1468
43648	1.31	2278									1.34	792	1.50	1213			1.83	273
43652	1.15	2372									1.33	1120	1.46	744			1.18	508
43656	1.13	2144									1.43	685	1.62	954			1.11	505
43660	1.09	2075									1.39	380	1.39	1695				
43664	1.05	2929									1.32	832	1.13	2097				
43668	1.08	4052									1.40	1329	1.16	2355			1.26	368
43672	1.19	3479									1.56	1145	1.46	1677			1.22	657
43676	1.28	2053									1.55	1004	1.55	761			1.68	288
43680	1.16	1669									1.42	744	1.35	256			1.27	669
43684	1.16	2335									1.18	968	1.58	698			1.25	669
43688	6.93	2264									7.00	1289	5.18	648			10.83	327

8. CONCLUSIONS

1. The Lageos satellite has an extraordinarily stable orbit, and the objectives for its use can certainly be met.

2. Analysis of 1-m data has contributed significantly to the study of Lageos and will do so for some time.

3. The present orbital accuracies are as follows:

- $5° \times 10^{-4}$ day^{-1} for secular effects.
- 500 μdeg for periods longer than 800 days.
- 25 μdeg for periods between 8 and 500 days.
- 1.5 m for periods between 1 and 8 days.
- 50 cm for periods less than 1 day.

Most of, but not all, these variations are probably due to unmodeled ocean tides and body tides.

4. The unmodeled acceleration remains unexplained. It is unlikely to be the result of neutral atmospheric drag, magnetospheric effects, the Poynting-Robertson effect, or anomalous radiation-pressure effects; it cannot be caused by gravitational effects.

5. Improvements in the orbital accuracy will come from the following sources:

- Improved tide models.
- Improved gravity-field models.
- Improved station coordinates.
- Improved data accuracy and distribution.
- Refined models of nongravitational forces.

9. ACKNOWLEDGMENTS

Special thanks go to Dr. David Smith, Goddard Space Flight Center, for providing the station coordinates derived by GSFC in advance of publication. This analysis was significantly aided by the Experimental Geophysics Department of SAO, who provided most of the data utilized and assisted in assessing the data quality. Finally, the analysis could not have been completed without the computer time provided by the Air Force Geophysics Laboratory, Bedford, Massachusetts, and by the Smithsonian Astrophysical Observatory.

10. REFERENCES

Aksnes, K., 1976. Short-period and long-period perturbations of a spherical satellite due to direct solar radiation. Celest. Mech., vol. 13, pp. 89-104.

Arnold, D. A., 1978. Optical and infrared transfer function of the Lageos retroreflector array. Final Rep., NASA Grant 09-015-002, Smithsonian Astrophys. Obs., May, 191 pp.

Deprit, A., and Zahar, R., 1966. Numerical integration of an orbit and its concomitant variations by recurrent power series. Zeit. Angew. Math. Phys., vol. 17, pp. 426-430.

Doodson, A. T., 1921. The harmonic development of the tide-generating potential. Proc. Roy. Soc. A, vol. 100, pp. 305-329.

Fitzmaurice, M. W., Minott, P. O., Abshire, J. B., and Rowe, H. E., 1977. Prelaunch testing of the Laser Geodynamic Satellite (Lageos). NASA/GSFC Tech. Paper 1062, October, 96 pp.

Gaposchkin, E. M., editor, 1973a. 1973 Smithsonian Standard Earth (III). Smithsonian Astrophys. Obs. Spec. Rep. No. 353, 388 pp.

Gaposchkin, E. M., 1973b. Satellite dynamics. In 1973 Smithsonian Standard Earth (III), ed. by E. M. Gaposchkin, Smithsonian Astrophys. Obs. Spec. Rep. No. 353, pp. 85-192.

Gaposchkin, E. M., 1974. Earth's gravity field to the eighteenth degree and geocentric coordinates for 104 stations from satellite and terrestrial data. Journ. Geophys. Res., vol. 79, pp. 5377-5411.

Gaposchkin, E. M., 1978. Recent advances in analytical satellite theory. Presented at the 9th GEOP Conference, Columbus, Ohio, October; proceedings in press.

Hori, G., 1966. Theory of general perturbations with unspecified canonical variables. Publ. Astron. Soc. Japan, vol. 18, pp. 286-296.

Jacchia, L. G., 1971. Revised static models of the thermosphere and exosphere with empirical temperature profiles. Smithsonian Astrophys. Obs. Spec. Rep. No. 332, 113 pp.

Kaula, W. M., 1966. Theory of Satellite Geodesy. Blaisdell Publ. Co., Waltham, Mass., 124 pp.

Kaula, W. M., chairman, 1970. The Terrestrial Environment: Solid-Earth and Ocean Physics. Report of a Study at Williamstown, Mass. NASA CR-1579, 152 pp.

King-Hele, D., 1964. Theory of Satellite Orbits in an Atmosphere. Butterworths, London, 164 pp.

Kinoshita, H., 1977. Third-order solution of an artificial satellite theory. Smithsonian Astrophys. Obs. Spec. Rep. No. 379, 104 pp.

Kozai, Y., 1961. Effects of solar radiation pressure on the motion of an artificial satellite. Smithsonian Astrophys. Obs. Spec. Rep. No. 56, pp. 25-33.

Kozai, Y., 1973. A new method to compute lunisolar perturbations in satellite motion. Smithsonian Astrophys. Obs. Spec. Rep. No. 349, 27 pp.

Kozai, Y., and Kinoshita, H., 1973. Effects of motion of the equatorial plane on the orbital elements of an earth satellite. Celest. Mech., vol. 7, pp. 356-366.

Lautman, D. A., 1977a. Perturbations of a close-earth satellite due to sunlight diffusely reflected from the earth. Celest. Mech., vol. 15, pp. 387-420.

Lautman, D. A., 1977b. Perturbations of a close-earth satellite due to sunlight reflected from the earth. II. Variable albedo. Celest. Mech., vol. 16, pp. 3-25.

Lerch, F. J., Klosko, S. M., and Laubscher, R. E., 1977. Gravity model improvement using GEOS-3 (GEM 9 & 10). Presented at the Spring Meeting of the American Geophysical Union, Washington, D.C., May.

Marini, J. W., and Murray, C. W., Jr., 1973. Correction of laser range tracking data for atmospheric refraction at elevations above 10 degrees. NASA/GSFC Document X-591-73-351, November.

Melchior, P., publisher, 1975. Comptes Rendus de la XVIe Assemblée Générale de l'U.G.G.I. Intl. Union Geodesy and Geophysics Publ. Office, Paris.

National Aeronautics and Space Administration, 1975. LAGEOS Phase B technical report. NASA/MSFC Tech. Memo. NASA TM-X-64915, February, 118 pp.

Nixon, D. D., 1974. Spin stabilization of Lageos. Internal Memo, NASA/MSFC, May 16, 3 pp.

Plummer, H. C., 1918. An Introductory Treatise on Dynamical Astronomy. Republ., Dover Publ., Inc., New York, 1960, 343 pp.

Poynting, J. H., 1903. Radiation in the solar system: Its effect on temperature and pressure on small bodies. Phil. Trans. Roy. Soc. A, vol. 202, p. 525.

Rabe, E., 1961. Determination and survey of periodic Trojan orbits in the restricted problem of three bodies. Astron. Journ., vol. 66, pp. 500-513.

Robertson, H. P., 1937. Dynamical effects of radiation in the solar system. Mon. Not. Roy. Astron. Soc., vol. 97, pp. 423-438.

Shapiro, I. I., 1963. Effects of sunlight pressure on air density determinations involving cylindrical satellites. Journ. Geophys. Res., vol. 68, pp. 5349-5354.

Slowey, J., 1974. Radiation-pressure and air-drag effects on the orbit of the balloon satellite 1963 30D. Smithsonian Astrophys. Obs. Spec. Rep. No. 356, 94 pp.

Smart, W. M., 1953. Celestial Mechanics. Longmans, Green, and Co., London, 381 pp.

Smith, D. E., and Kissell, K. E., 1971. Anomalous accelerations of the PAGEOS spacecraft. NASA/GSFC Document X-553-71-338, August, 6 pp.

United States Naval Observatory, 1954. Improved Lunar Ephemeris, 1952-1959. Nautical Almanac Office, Washington, D.C., 422 pp.

Weiffenbach, G. C., and Hoffman, T. E., 1970. A passive stable satellite for earth-physics applications (Cannonball, a satellite for accurate laser ranging). Smithsonian Astrophys. Obs. Spec. Rep. No. 329, 50 pp.

Wyatt, S. P., Jr., and Whipple, F. L., 1950. The Poynting-Robertson effect on meteor orbits. Astrophys. Journ., vol. 111, pp. 134-141.

APPENDIX B

ANALYSIS OF SEASAT DATA

Quarterly Report No. 1 and 2

For the period 24 October 1978 through 24 April 1979

Contract No. SR 34080

Principal Investigator
Dr. E. M. Gaposchkin

Prepared for

Massachusetts Institute of Technology
Cambridge, Massachusetts 02139

Prepared by

Smithsonian Institution
Astrophysical Observatory
Cambridge, Massachusetts 02138

The Smithsonian Astrophysical Observatory
and the Harvard College Observatory
are members of the
Center for Astrophysics

TABLE OF CONTENTS

		Page
1	INTRODUCTION	1
2	OBJECTIVES	2
3	ANALYSIS	3
4	SOFTWARE DEVELOPMENT	6
5	DATA PROCESSED	8
	5.1 Geoids	8
	5.2 Altimetry	8
6	PLANS	25
7	REFERENCES AND BIBLIOGRAPHY	26
8	COST SUMMARY	28
	APPENDIX A: Significant Wave-Height Correction Tables	A-1

ANALYSIS OF SEASAT DATA

Quarterly Report No. 1

1. INTRODUCTION

This quarterly report is intended to cover the work done since the beginning of the contract (24 October 1978) through 24 April 1979. Because of the late start of the effort, this report covers the initial 6-month period. Until now, the tasks have been discussed informally as the work proceeded, and no formal work plan was established. The plans for the next quarter are given in Section 6.

2. OBJECTIVES

The Smithsonian Astrophysical Observatory (SAO) is supporting the Massachusetts Institute of Technology (MIT) in executing the National Oceanic and Atmospheric Administration/National Aeronautics and Space Administration (NOAA/NASA) Seasat Contract "Oceanographic Studies Using Seasat A Altimetric Data," NOAA Contract MO-A01-78-00-4327, MIT OSP 87314. The broad objective of this effort is to combine Seasat 1 altimeter data with gravity data and ocean-density data to determine the general circulation of the ocean, with particular attention on the western North Atlantic. It is anticipated that by the end of the first year, quantitative understanding will have been achieved as to the limitations of the altimeter, geodetic, and hydrographic data, and preliminary circulation models will have been made.

During this first investigative phase of the work, SAO has concentrated on processing the Seasat altimeter data and testing a number of recent geoid models. The results of these computations have been provided to MIT, and preliminary assessments of the altimeter data and the present geoids have been made. Some attention has also been given to instrumental and tidal contributions to the altimeter signal.

3. ANALYSIS

During the first phase of the work, attention has been given to the problem of interpolating the geoid along the altimeter track and smoothing the sea-surface topography signal to obtain the slope of the sea-surface topography and the surface velocity of the ocean, assuming that geostrophy holds. The necessity for interpolation and smoothing comes about in two ways. First, the geoid is generally specified at grid points, while altimeter observations are made at arbitrary points; some method must be selected to estimate the geoid between the grid points appropriately. Second, the given geoid values and the altimeter data are not known without error, and the scheme chosen to estimate the geoid and the sea-surface topography should take this into account.

Two approaches to the smoothing and interpolation problem seem appropriate. The first is an extension of the Wiener-Kolmogorov filtering theory known as collocation. Collocation employs statistical information about the signal to be estimated and the error signal in terms of their covariance functions and assumes that there is no cross correlation between the signal and the error. In the case of the geoid error and the sea-surface topography, it is doubtful that they are uncorrelated.

However, the collocation approach will generate an estimate of the signal that is an analytical function; i.e., it has an infinite number of derivatives and is therefore suitable for describing functions related to solutions of Laplace's equation, which are harmonic. Collocation analysis, however, has a practical limit, in that it involves inverting an $n \times n$ matrix for each interpolation point, where n is the total number of data points. This method has been used extensively (Gaposchkin, 1973, 1979) and will probably be the basis of improving our estimate of the geoid itself.

A second approach starts with the notion of using piecewise continuous polynomials to improve smoothness locally, with a least-squares estimate of the parameters. The general theory is known as B-spline theory and has reached a high degree of sophistication. Spline theory places no a priori constraint on the signal to be modeled. In general, it can allow an arbitrary number of discontinuities in a function that otherwise has an arbitrary (finite) number of derivatives. It has been generalized to estimations, in a least-squares sense, of both one-dimensional and two-dimensional functions. An added benefit for analysis of sea-surface topography is that any derivative can be calculated from the B-spline representation with essentially no further work. Several general articles on modern spline theory are given in Section 7. From the point of view of this project, spline fits are powerful for the following reasons. We are required to make no a priori assumptions about the properties of the signal to be estimated other than its continuity, and the numerical procedure provides a weighted least-squares estimate of the signal and thus can be made general and efficient.

Therefore, after a survey of the existing spline-fitting algorithms, three programs have been written, as described in Section 4. In summary, two of the programs do two-dimensional least-squares spline estimates of the geoid along an altimeter track. The basic difference between them is the coordinate system employed. The first uses the system of latitude and longitude in which the geoid data are given. A bicubic spline fit is made to all the data within the rectangle containing the altimeter track. Seasat 1 obliquely intersects the coordinate axes. This program has the advantage that by placing the points matching the piecewise continuous polynomials (knots) at the observed geoid points, the calculation is reduced to interpolation. However, it is not computer efficient in that many geoid values must be used that are not geographically near the track, leading to an unnecessary burden in computing with no essential improvement in the estimate. The second version approximately uses the altimeter subsatellite track as the x axis in the coordinate system. Only points near the track need be used; "near" is defined by an input parameter, currently taken to be within 1° of the track. The disadvantage

is that the knots can no longer be made to correspond to the data points, and thus this program does not reduce to interpolation in the limit. Tests using these two programs in least-square estimates give very similar results.

The third program using B-spline fitting comprises an input geoid, altimeter data, and ephemeris data and uses the spline to estimate the sea-surface topography and its derivative, which is converted to a surface velocity.

4. SOFTWARE DEVELOPMENT

The programing effort has been done in two phases. The first phase was done quickly to provide a first set of data to MIT for preliminary evaluations. The second phase was aimed at providing a more efficient unified system that will allow expansion and modification as future needs become clear. Figure 1 schematically shows the form of the data files, the processing programs, and the data flow. The heart of the system is an Altimeter Data Base (ADB), which exists in a direct-access randomly accessible disk file. The coded files will eventually be deleted or used only as temporary intermediate storage. Further streamlining of the data-processing system will be done as needed.

Highlights of the system follow:

1) Any number of direct-access files can be added. Currently, there are three geoids and 21 altimeter tracks.

2) Results of the computations are saved in the ADB without previous information being destroyed (within limits, of course). Therefore, several models can be computed for later comparison.

3) The plotting program can display any linear combination of data in the ADB. Results of this program are given in Section 5.

All blocks shown in Figure 1 are working and have given reasonable results. In particular, the Mofjeld (1975) tide model was tested, with results identical to the test cases provided by MIT. These tides are significantly different from those provided by the Jet Propulsion Laboratory (JPL) (the Estes, 1977, model). However, the contribution of the tide to the surface-velocity calculation was negligible, and no further tests were conducted.

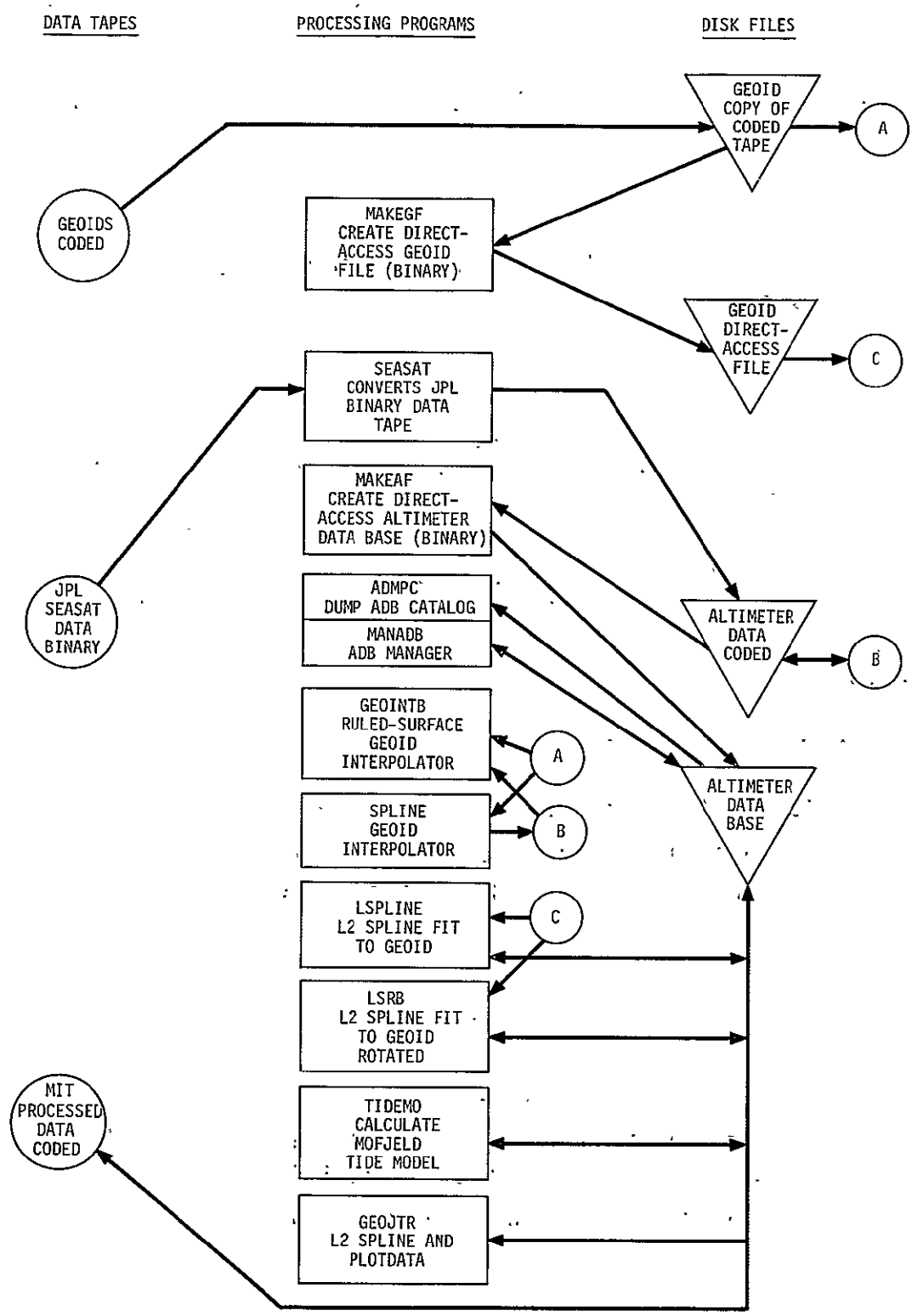

Figure 1. Seasat data-processing system.

5. DATA PROCESSED

5.1 Geoids

Four geoids are now available in the data-processing system. They are listed in Table 1.

Table 1. Geoids available.

Geoid	Resolution	Geographical coverage	Source
GEM 10B	0	Global	GSFC
Geos, surface	15'	$15°.75 \leq \phi \leq 45°.25$ $279° \leq \lambda \leq 304°.25$	Marsh et al. (1978)
Gravimetric	1°	Global	GSFC
Gravimetric	5'	$16° \leq \phi \leq 39°$ $278° \leq \lambda \leq 300°$	Marsh and Chang (1978)

In addition, we have received the geoid derived by Mader (1979). The four geoids have been calculated along the altimeter tracks of available Seasat data by using a variety of methods, and the results have been provided to MIT.

5.2 Altimetry

We currently have 21 tracks of Seasat altimeter data in the ADB. These tracks are summarized in Table 2, which is a listing of the ADB catalog. Of these 21 tracks, four are not in the western North Atlantic and therefore not of immediate interest. Note that two tracks have inadvertently been inserted twice.

Table 2. Contents of ADB.

THERE ARE 23 TRACKS OF ALTIMETER DATA					FIRST POINT		LAST POINT			CATALOG
FILE NAME	SATELLITE	MJD	REVOLUTION	POINTS	ϕ (deg)	λ (deg)	ϕ (deg)	λ (deg)		ORDINAL
A189.SFA	7806401	43699	189	571	10.6293	302.4470	43.3386	285.7094	0	1
FIRST TRACK IN CALIBRATION AREA										
A198.SFA	7806401	43699	198	566	51.0358	300.8903	18.1063	280.8912	0	2
SECOND TRACK IN CALIBRATION AREA										
A285.SFA	7806401	43703	235	300	44.8217	298.4536	28.6828	288.6732	0	3
CAL.AREA, WEST OF BERMUDA										
A277.SFA	7806401	43703	277	600	6.9099	306.8318	39.8302	290.9781	0	4
NEAR OVER-FLIGHT										
A242.SFA	7806401	43702	242	2800	44.7669	296.9725	28.8938	287.3388	0	5
CAL. AREA										
A443.SFA	7806401	43717	443	200	45.6701	296.0392	25.3833	283.9987	0	6
NUMEROUS DATA OUTAGES; BLUNDER POINTS										
A486.SFA	7806401	43720	486	400	45.9857	297.7314	23.1987	284.4230	0	7
CAL. AREA										
A521.SFA	7806401	43722	521	6100	5.6434	307.1570	39.2109	291.1925	0	8
OVERFLIGHT OF BERMUDA										
A486.SFA	7806401	43720	486	400	45.9857	297.7314	23.1987	284.4230	0	9
CAL. AREA										
A529.SFA	7806401	43723	529	400	46.0348	299.2147	24.1921	286.3291	0	10
CAL. AREA										
A564.SFA	7806401	43725	564	600	5.5939	308.6215	38.5586	293.0484	0	11
CAL. AREA										
A521.SFA	7806401	43722	521	6100	5.6434	307.1570	39.2109	291.1925	0	12
OVERFLIGHT OF BERMUDA										
A572.SFA	7806401	43726	572	245	43.9295	299.0579	30.7498	291.0007	0	13
CAL. AREA										
A1287.DAT	780640	14377	60128	196	18.8524	234.1143	41.9342	143.9002	0	14
KUROSHIO CURRENT; FIRST 5 PTS. HAVE NO H*										
A234.SFA	7806401	43702	234	6100	7.0312	305.3433	40.5588	289.0621	0	15
NEAR-FLIGHT OVER BERMUDA										
A1289.SFA	7806401	43776	1289	4700	46.9692	304.8829	21.3058	289.9247	0	16
BERMUDA OVERFLIGHT										
A1295.SFA	7806401	43776	1295	900	49.2436	156.1348	0.1030	130.4600	0	17
PACIFIC OCEAN										
A1296.SFA	7806401	43776	1296	300	10.8618	293.4967	29.3012	285.2385	0	18
SOME DATA OUTAGES										
A1373.SFA	7806401	43782	1373	700	2.3611	162.9555	41.0809	144.4739	0	19
KUROSHIO CURRENT										
A1375.SFA	7806401	43782	1375	4800	46.9655	304.8765	20.9809	289.7750	0	20
BERMUDA OVER-FLIGHT										
A1381.SFA	7806401	43782	1381	900	49.2815	156.1662	0.1441	130.4727	0	21
PACIFIC OCEAN										
A1382.SFA	7806401	43782	1382	300	10.9855	293.4474	28.8666	285.4540	0	22
CAL. AREA										
A478.SFA	7806401	43719	478	600	5.8228	305.6407	38.7772	290.0207	0	23
NEAR OVER-FLIGHT										

To illustrate the present capability, several plots are given. The track on revolution 189 is selected because 1) it crosses the Puerto Rico Trench, which has a significant geoid undulation, and 2) it crosses the Gulf Stream to the north. The geometry of the pass is given in Figure 2, where the boundaries of the 5' × 5' gravimetric geoid to be used are shown. The geoid is evaluated along the subsatellite track in four ways. First, ruled-surface interpolation is used; second, the spline fit is used as an interpolation; third, the spline fit is used with a spacing of 0°.30; and finally, the spline fit is made by using data within 1° of the track and a knot spacing of 0°.30. The results of the least-squares fit are summarized in Table 3.

Table 3. Spline fit to geoid.

Knot spacing	Geoid data (number of points)	rms (m)	Comment
0°.0833	5371	0.000	System of ϕ, λ
0°.30	5371	0.252	System of ϕ, λ
0°.30	8336	0.119	Calculated along track

The geoids are plotted in Figures 3 through 5. Owing to the large amount of computer time needed for the spline fit in the ϕ, λ coordinate system, a shorter section of track along the northern side of the Puerto Rico Trench is calculated. Also shown in Figures 6 through 8 are the surface velocity in knots calculated from the gradient of the sea-surface topography. The sea-surface topography is obtained from other information given by the Seasat project — that is, the computed satellite altitude (from Goddard Space Flight Center), the observed altitude, the ocean tides (Estes, 1977), the atmospheric-pressure correction (Fleet Numerical Weather Center), and the correction for significant wave height. The significant wave-height correction tables obtained from Wallops Island Flight Center are provided in Appendix A. Figures 9, 10, and 11 show the difference in geoid height between the least-squares fit along track and the other three geoid estimates. Figures 12, 13, and 14 show the surface velocity implied by this difference. This would correspond to the error in the velocity due to the error in geoid height, assuming the least-squares spline fit along the subsatellite track to be the true geoid.

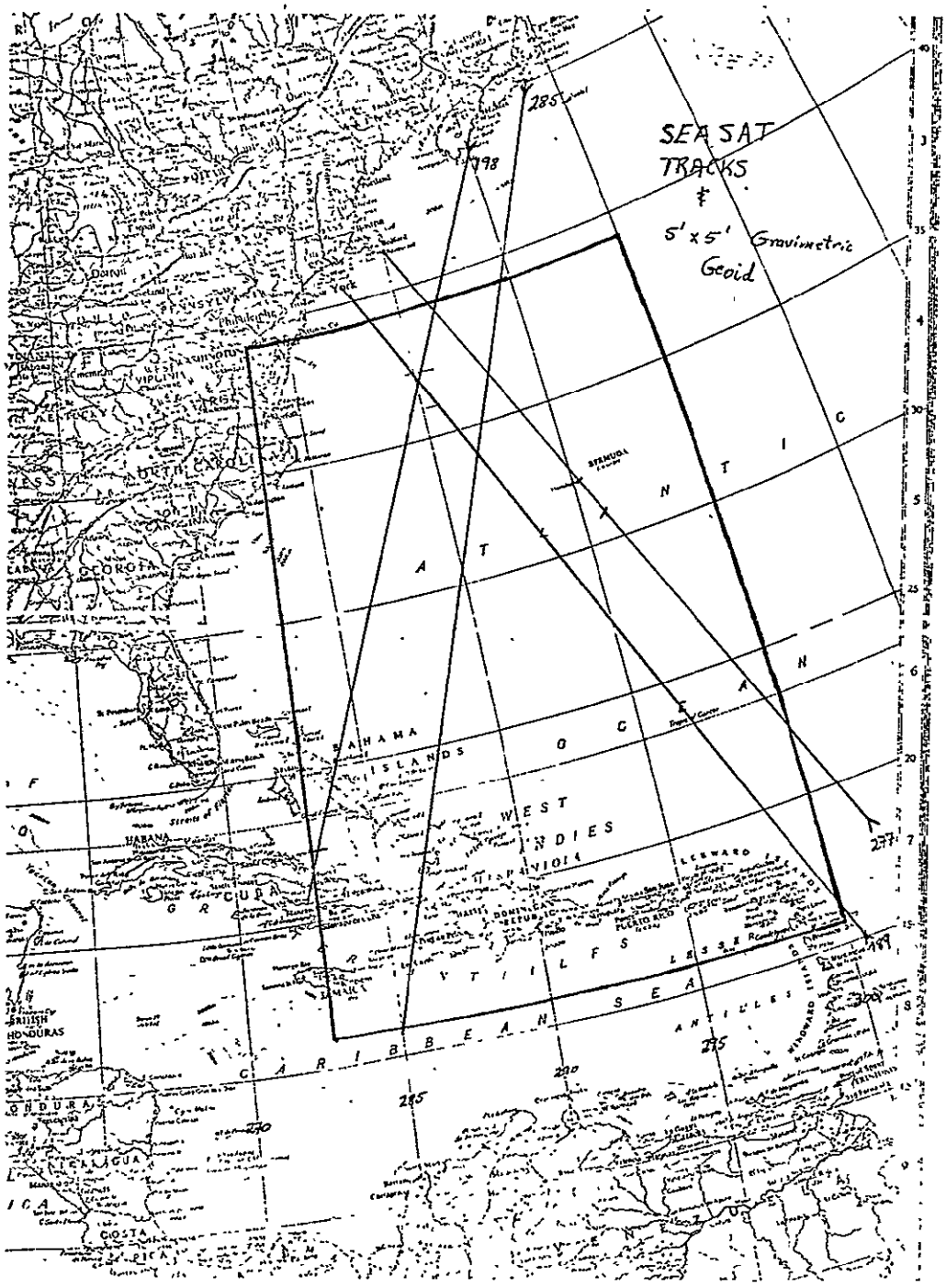

Figure 2. Seasat tracks and 5' × 5' gravimetric geoid.

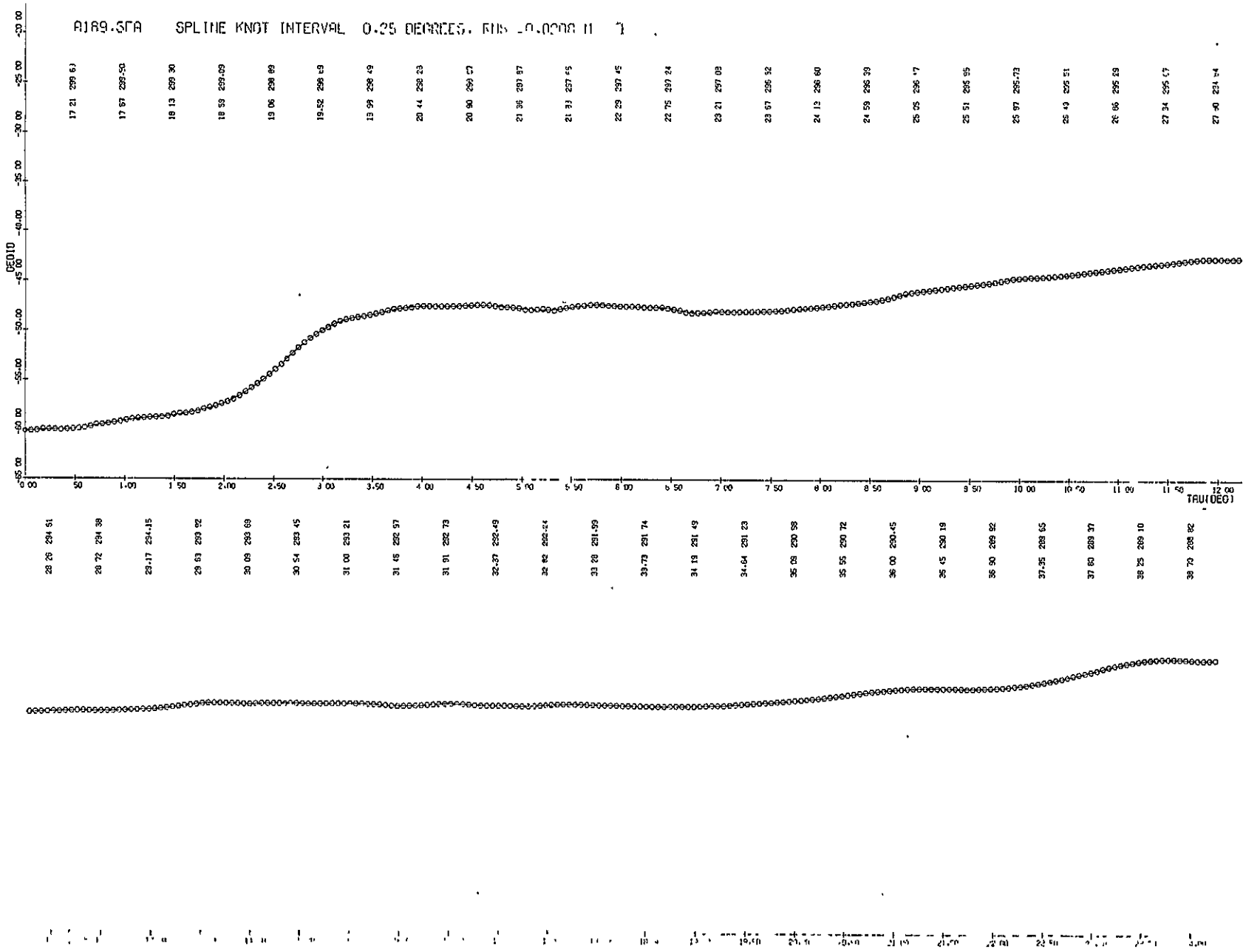

Figure 3. Geoid height (meters) calculated using ruled-surface interpolation to 5' × 5' gravimetric geoid.

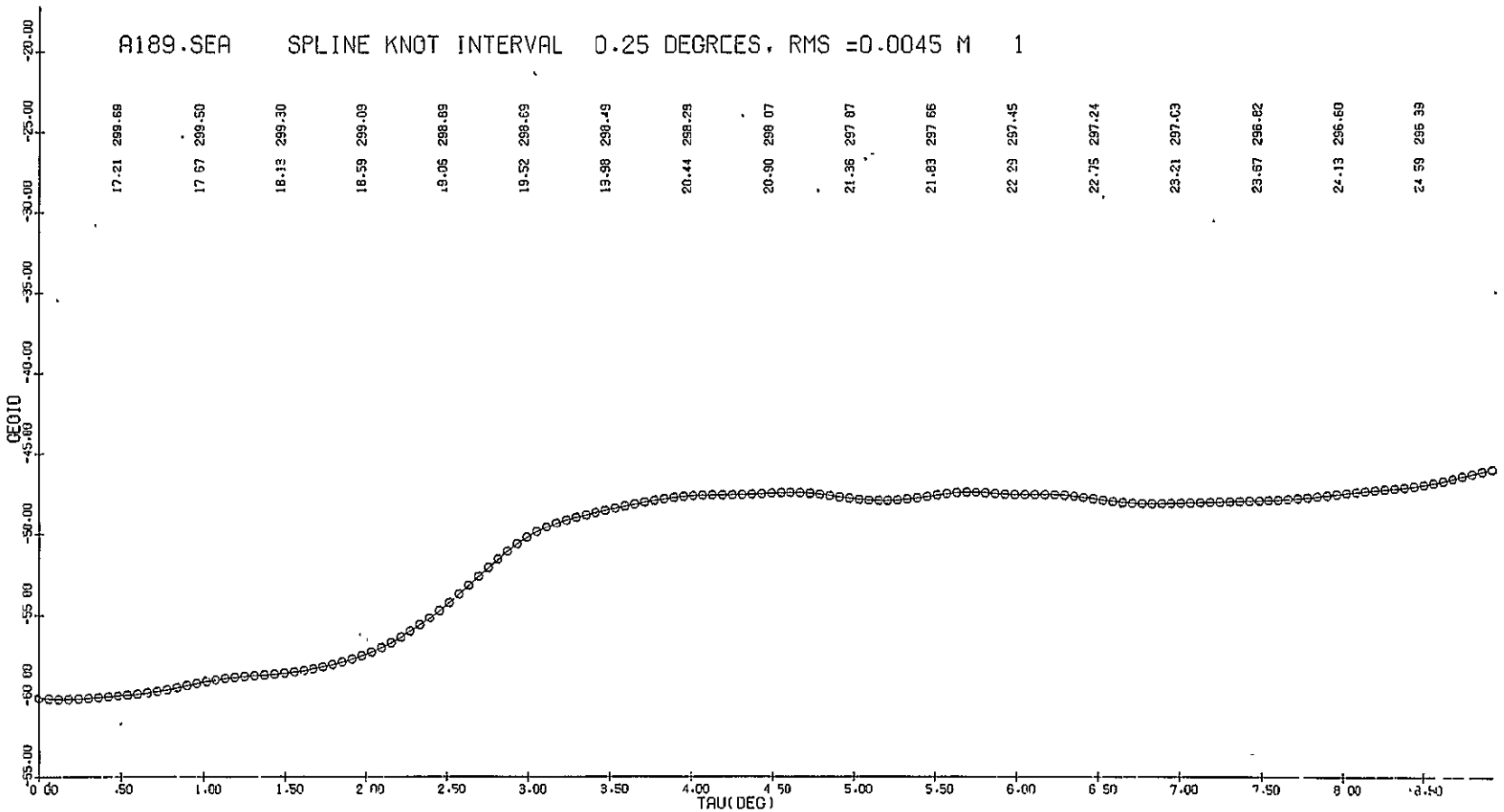

Figure 4. Geoid height (meters) calculated using least-squares spline fit in system of latitude and longitude on 5' × 5' gravimetric geoid.

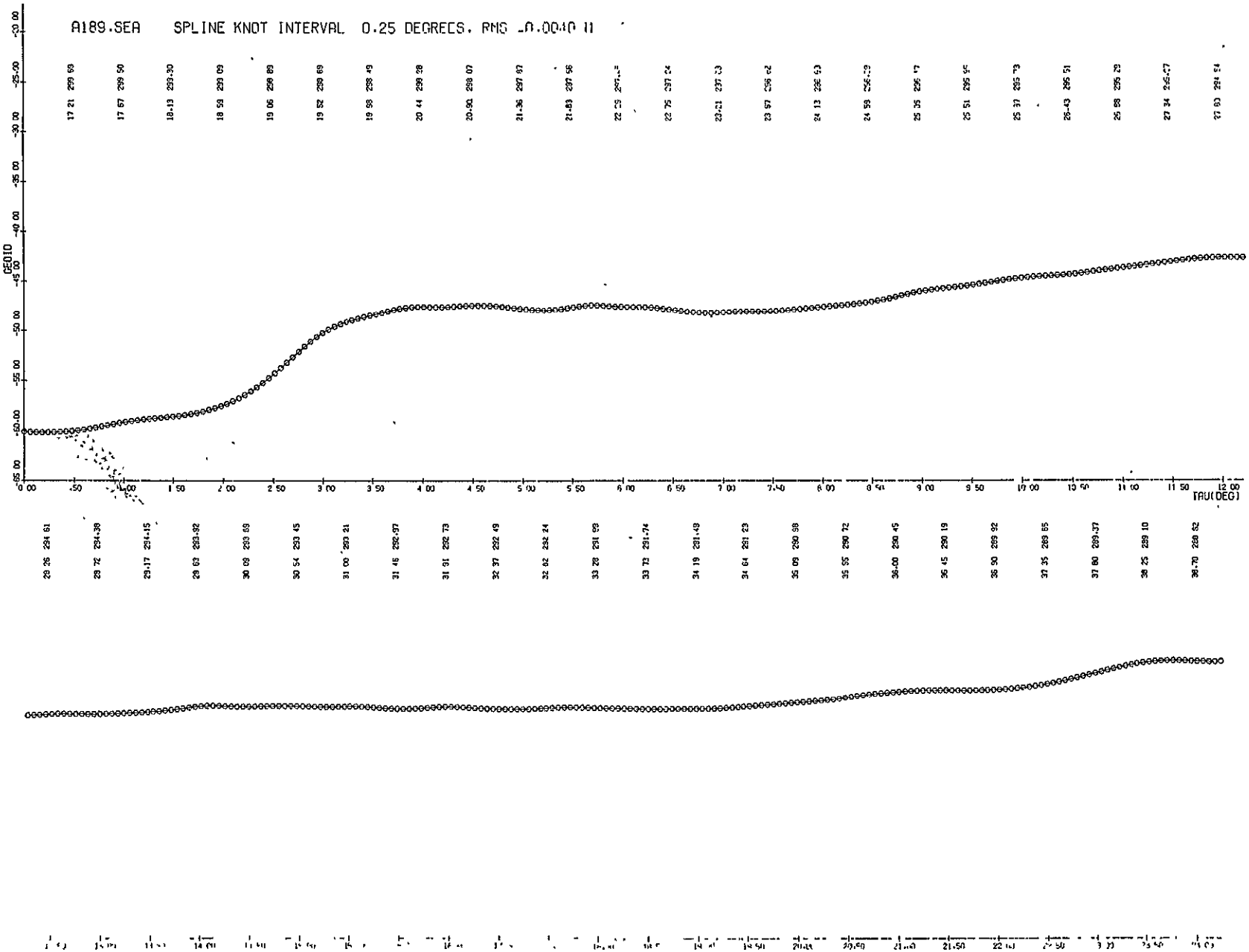

Figure 5. Geoid height (meters) calculated using least-squares spline fit in system of altimeter track on 5' × 5' gravimetric geoid.

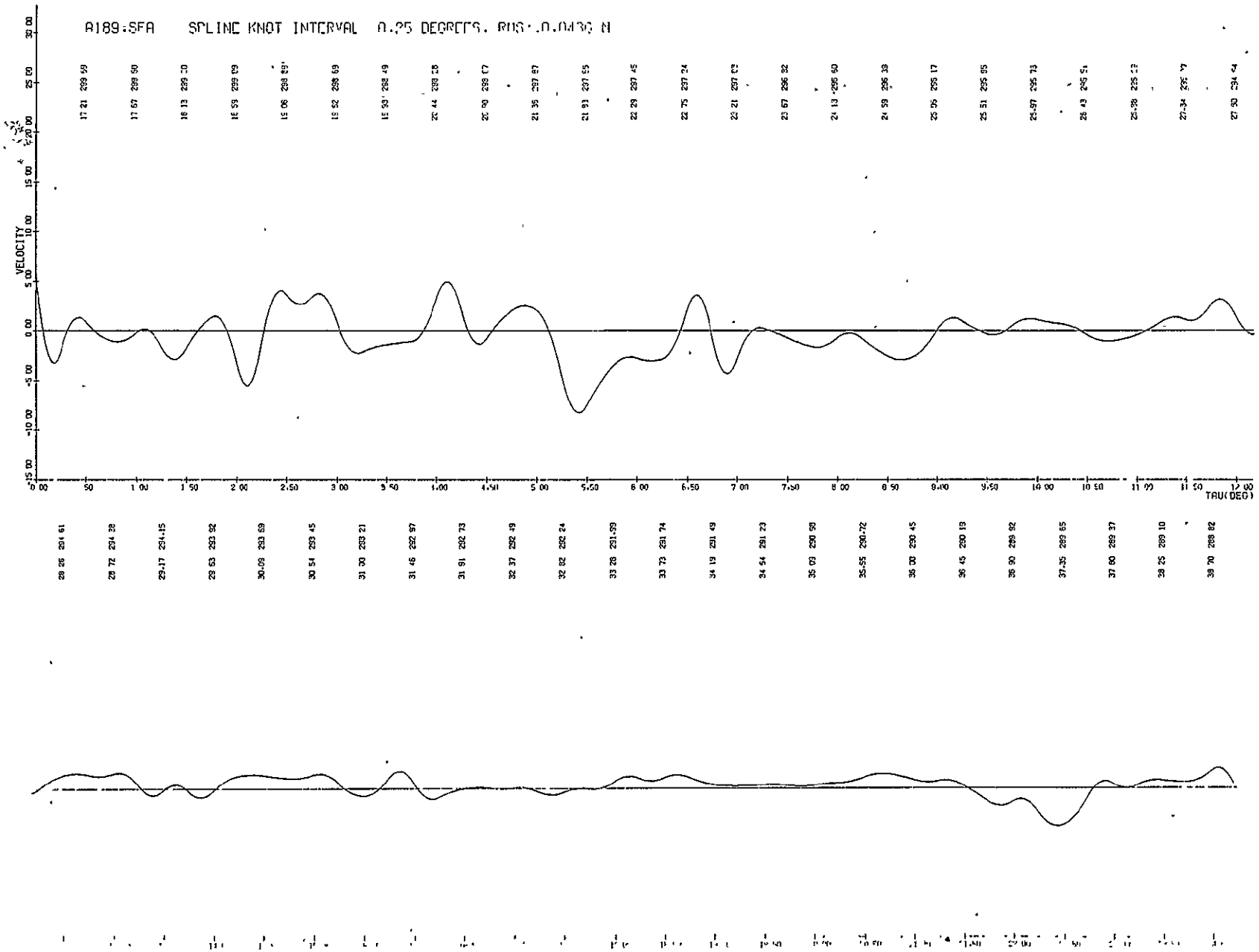

Figure 6. Surface velocity (knots) calculated using geoid derived from ruled-surface interpolation on 5' × 5' gravimetric geoid.

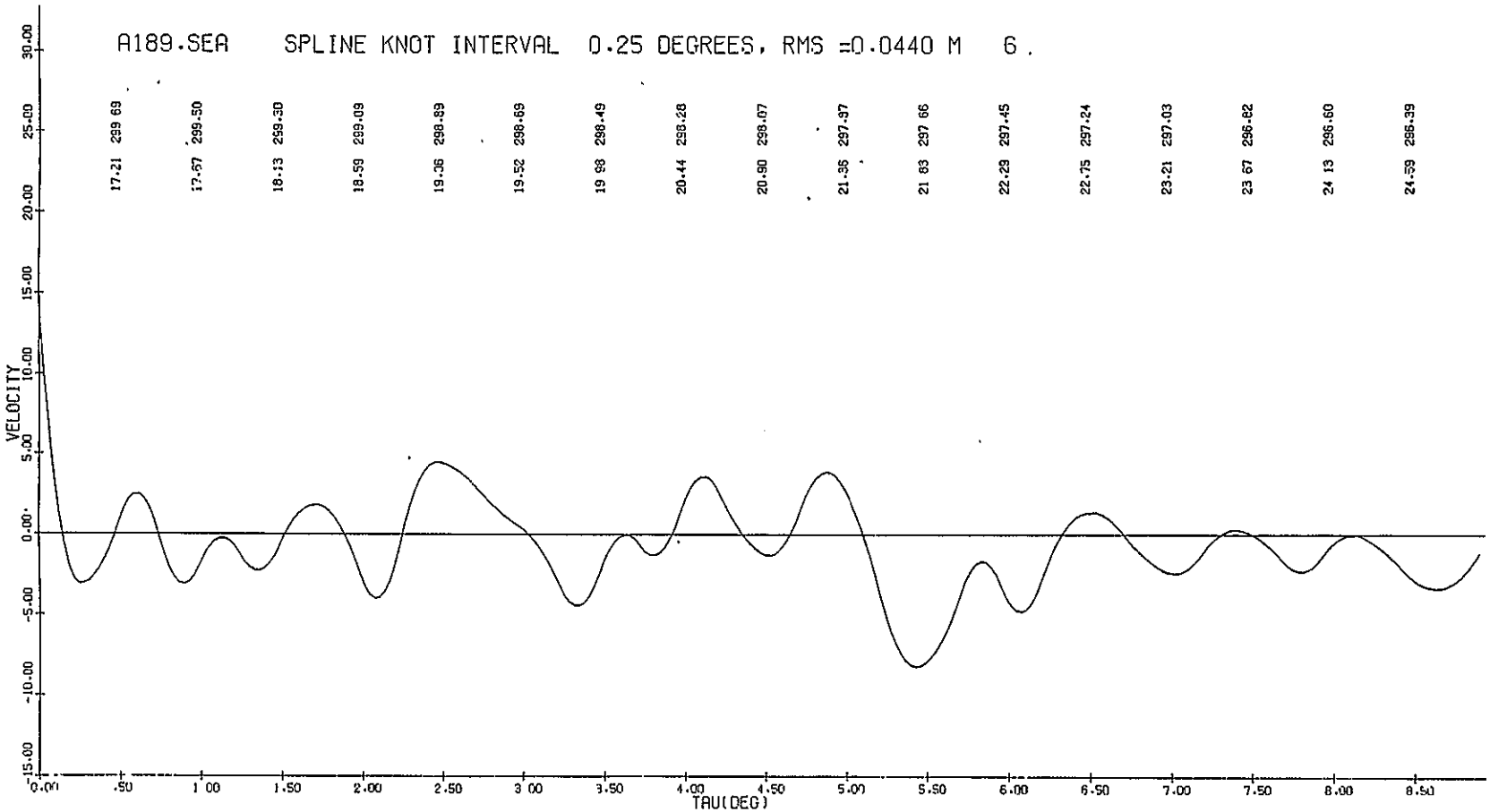

Figure 7. Surface velocity (knots) calculated using least-squares spline fit in system of latitude and longitude on 5' × 5' gravimetric geoid.

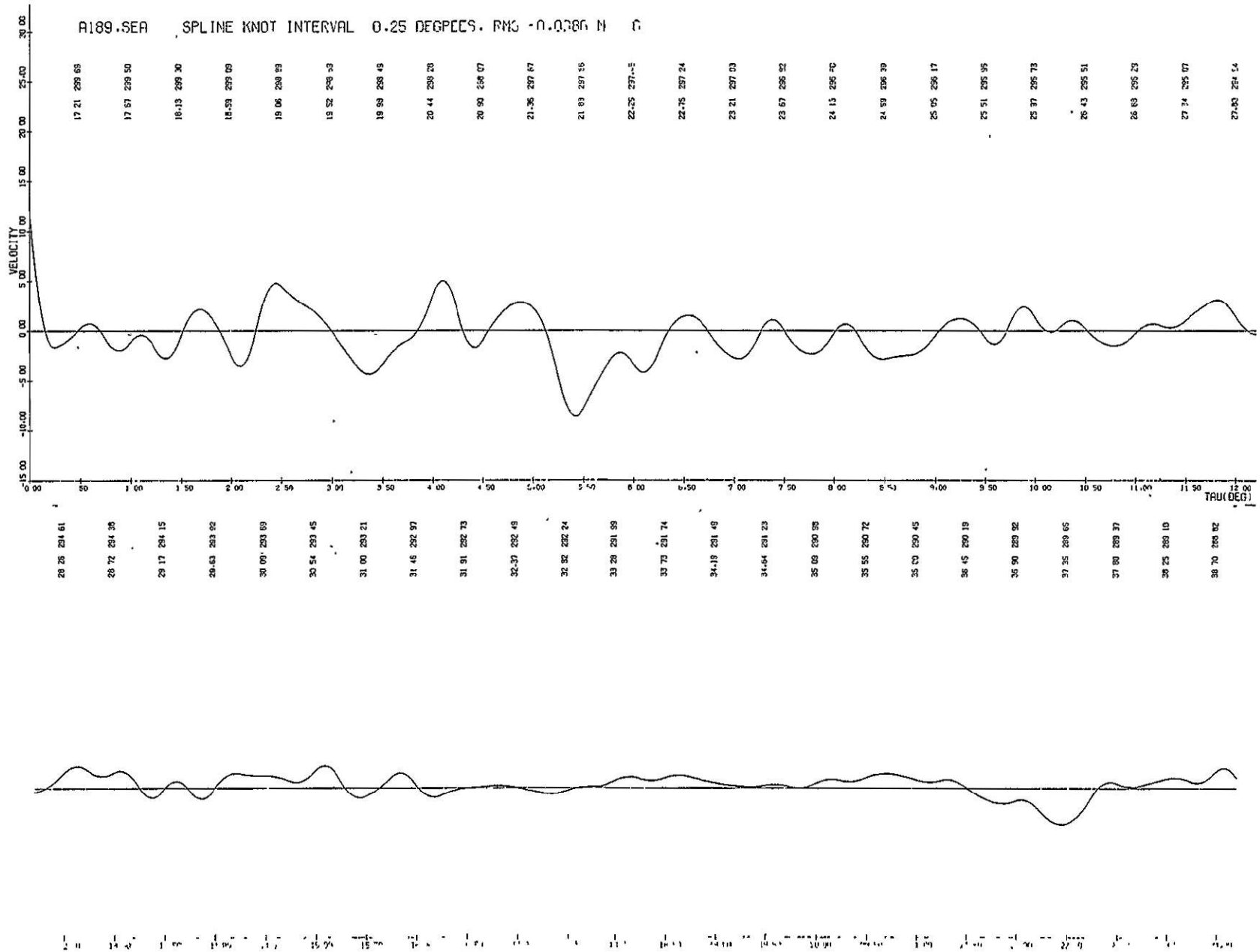

Figure 8. Surface velocity (knots) calculated using least-squares spline fit in system of altimeter track on 5' × 5' gravimetric geoid.

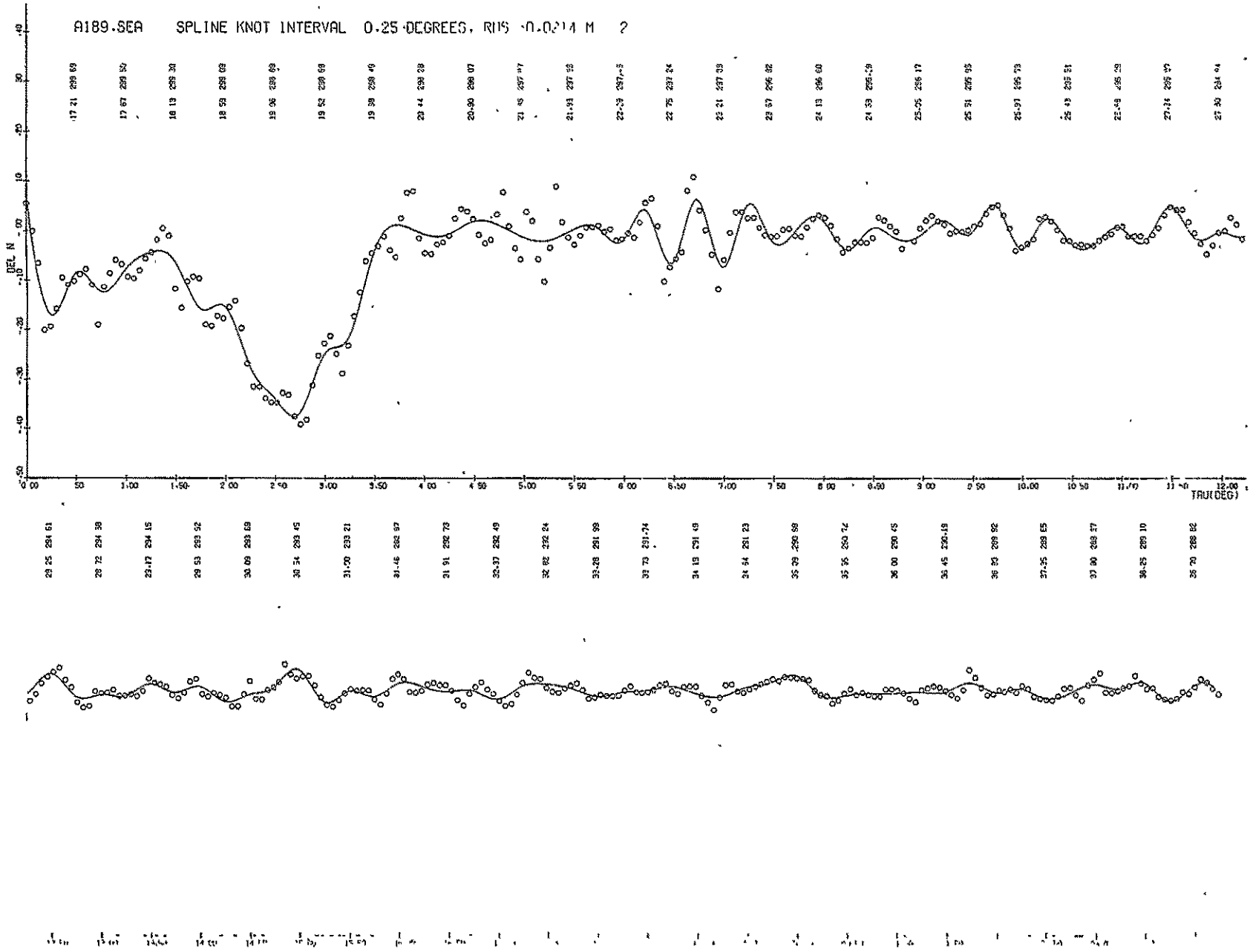

Figure 9. Difference in geoid of ruled-surface interpolation and least-squares spline fit (meters).

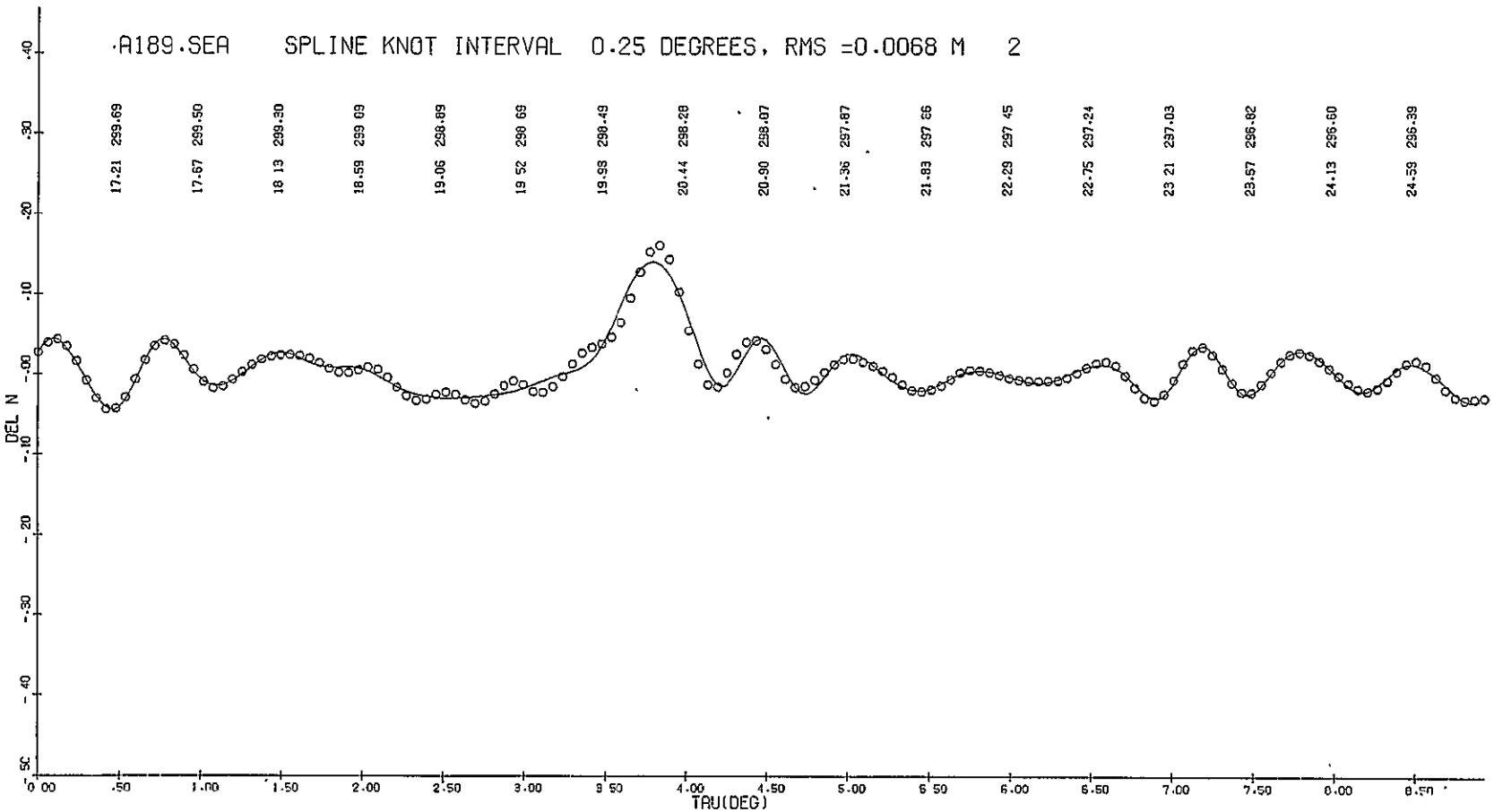

Figure 10. Difference in geoid of least-squares spline fit in system of latitude and longitude and least-squares spline fit in system of altimeter track (meters).

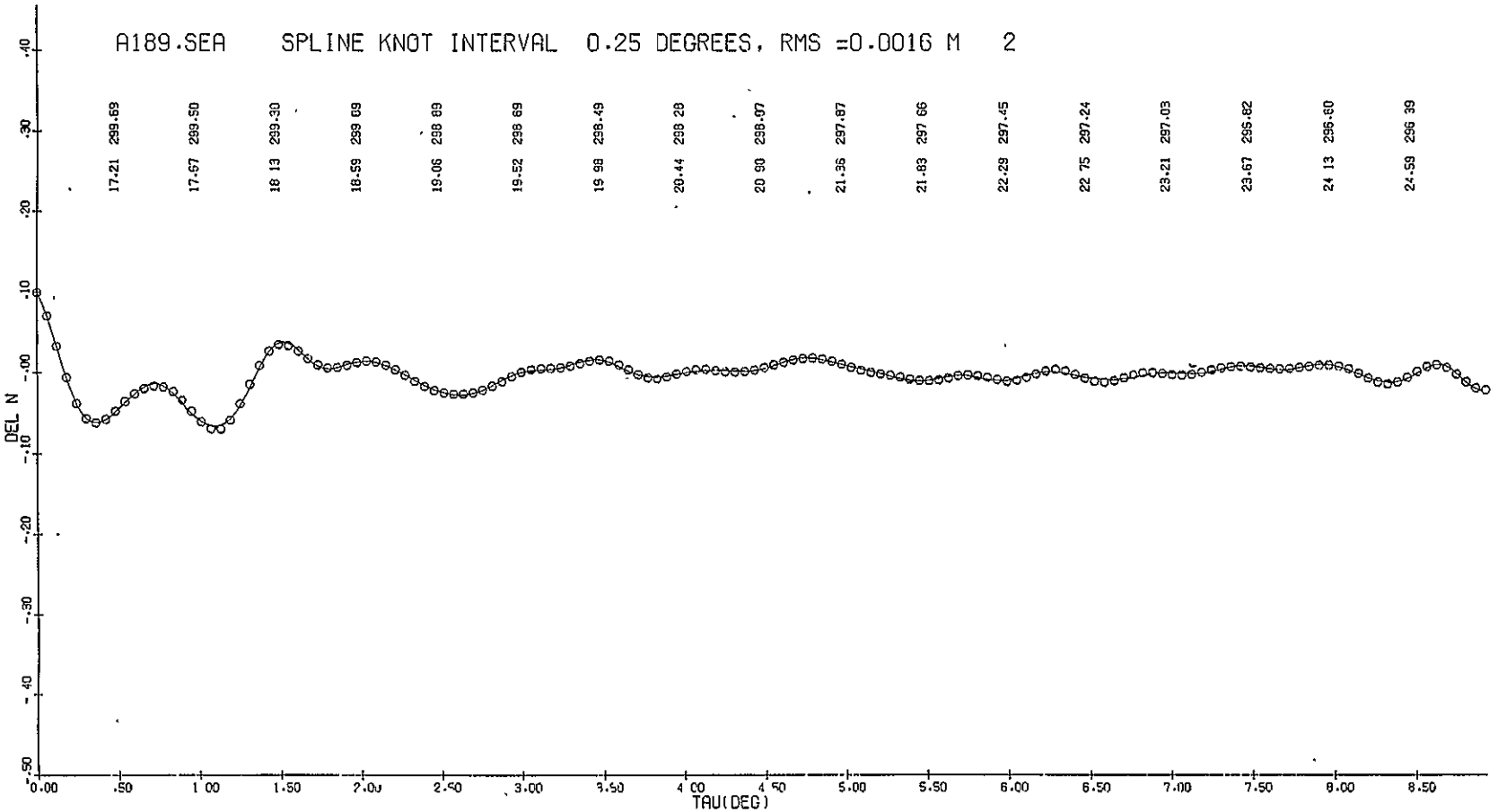

Figure 11. Difference in geoid height (meters) of least-squares spline fit with 2° swath width and 4° swath width.

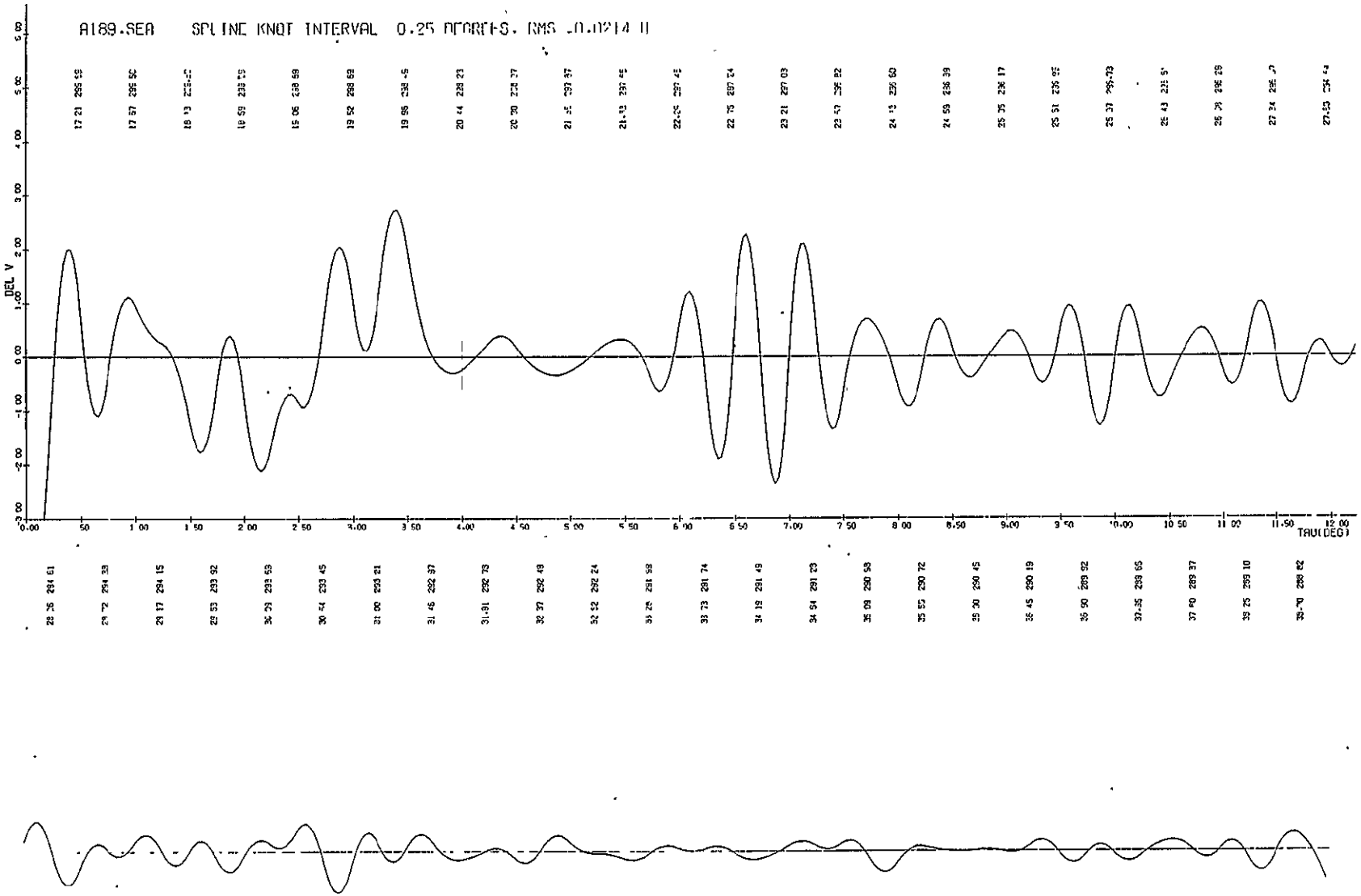

Figure 12. Difference in velocity (knots) between ruled-surface interpolation and least-squares spline fit.

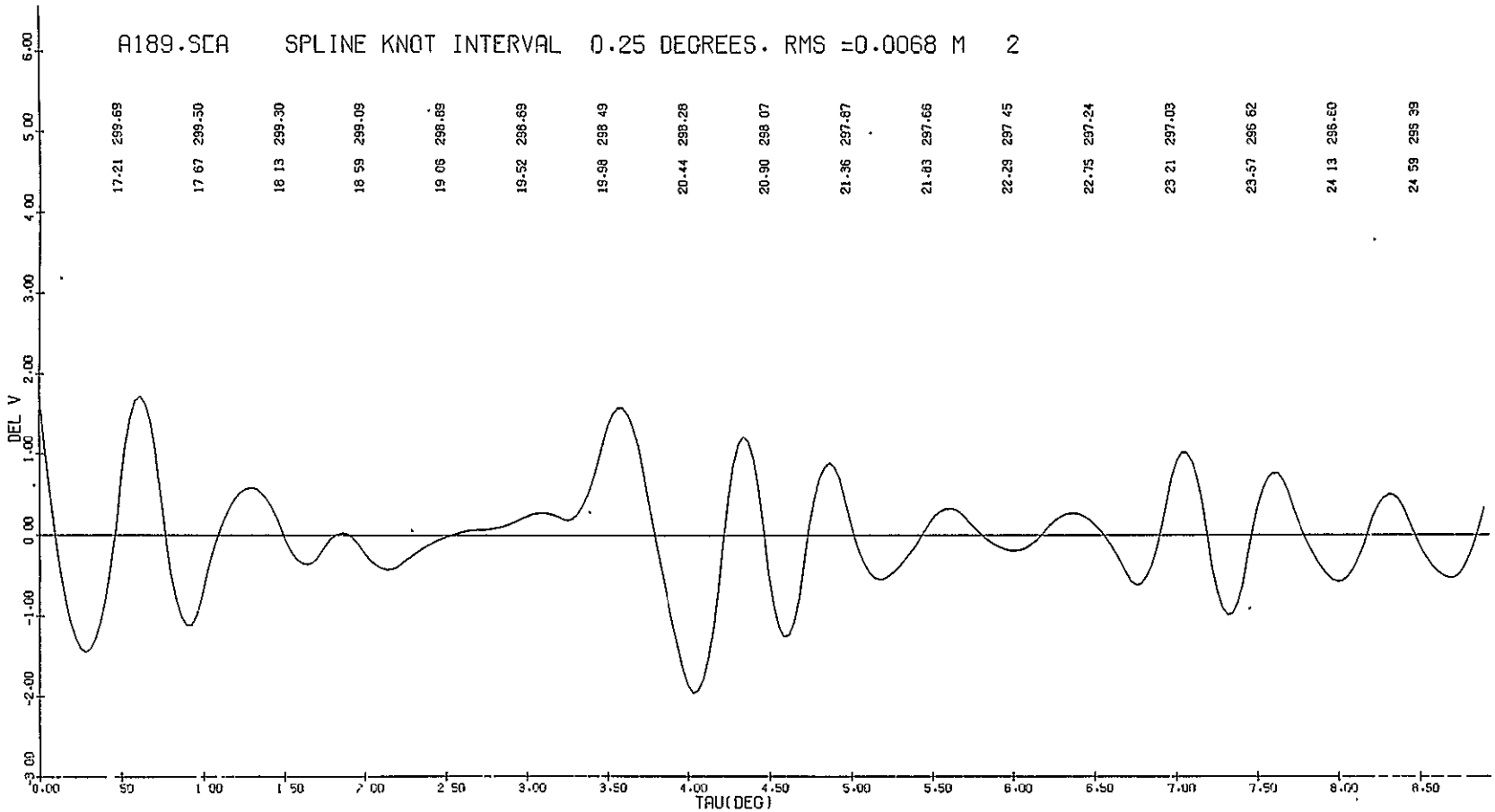

Figure 13. Difference in velocity of least-squares fit in system of latitude and longitude and least-squares spline fit in system of altimeter track (knots).

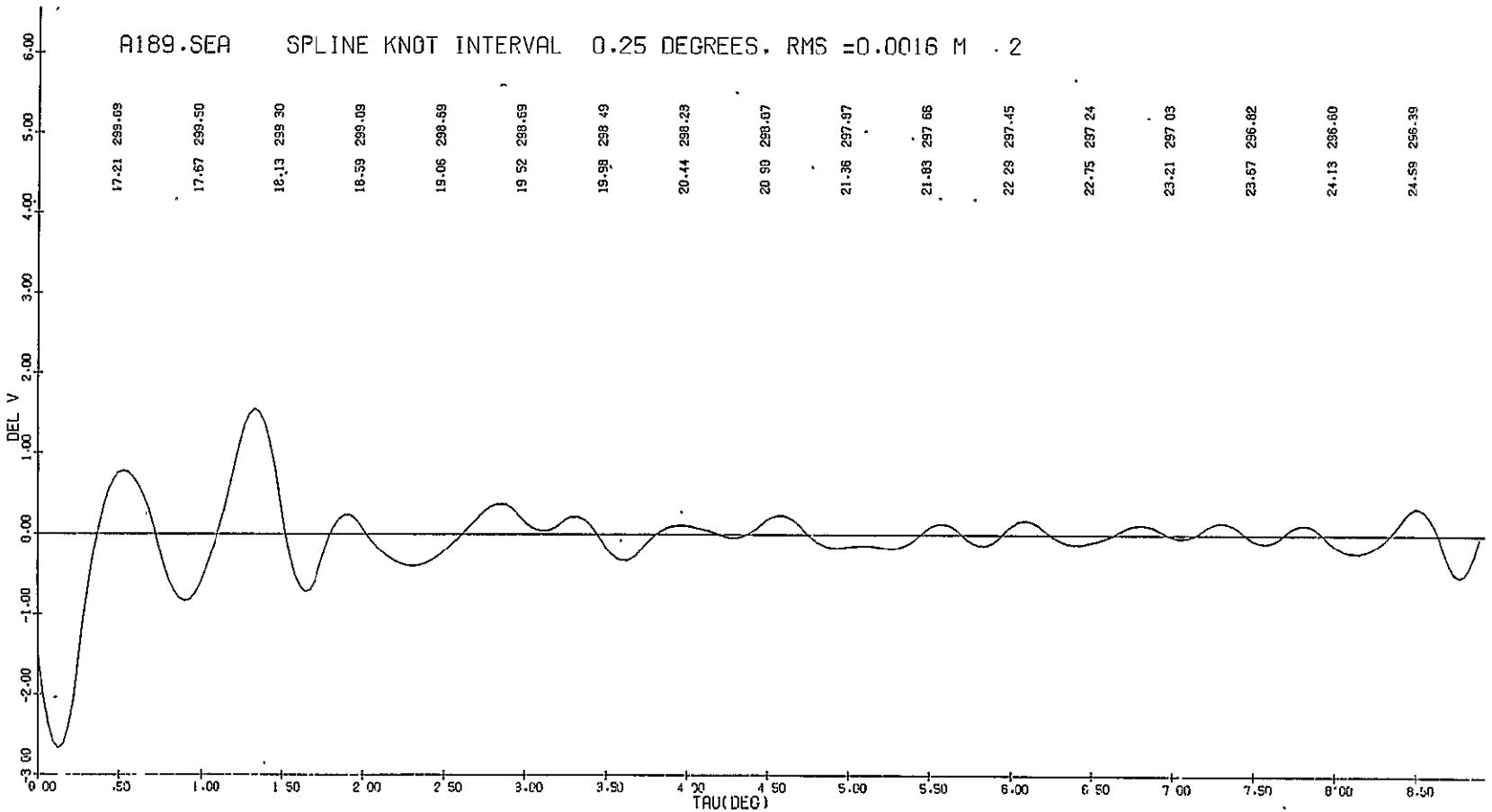

Figure 14. Difference in velocity (knots) of least-squares spline fit with 2° swath width and 4° swath width.

The differences between the various interpolants for the geoid are generally less than 20 cm, with root-mean-square (rms) differences of 1 to 60 mm. This, of course, is not true for the ruled surface, which has much larger differences. Although 20 cm is better than or comparable to the accuracy of the geoid data themselves, this difference implies differences in the surface velocity of more than 2 knots in some places. This difference is purely mathematical, being the result of employing a number of computation algorithms with different sets of data. Such large differences must be viewed with concern, though, as they can introduce errors in the derived ocean currents comparable to the signal sought. It must be concluded that, even with rather sophisticated least-squares interpolation, further analysis is necessary to ensure that the maximum information content can be extracted from the available geoid data. While it would be preferable to separate the testing of the geoid model from considerations of the believability of the ocean signal, this last consideration may be necessary in order to make a sensible choice between the alternative interpolants.

6. PLANS

1) The gravimetric geoid (Mader, 1979) will be incorporated in the processing system and selected profiles will be calculated.

2) The global tidal model by Schwiderski (1978) will be implemented. We currently have the data and programs for a CDC 6000 computer. More complete tests of this model and of Mojfeld's (1975) will be conducted.

3) The data given at 10 sec^{-1} will be averaged to obtain points at 1 sec^{-1}.

4) When the next release of Seasat data arrives, expected soon, it will be processed and inserted into the ADB.

5) A survey will be made, and processed gravity data collected, to begin an improvement of the gravimetric geoid in the western North Atlantic.

6) Analysis of interpolation methods will continue.

7. REFERENCES AND BIBLIOGRAPHY

Cox, M. G., 1972. The numerical evaluation of B-splines. Journ. Inst. Math. Appl., vol. 10, pp. 134-149.

de Boor, C., 1972. On calculating with B-splines. Journ. Approx. Theory, vol. 6, pp. 50-62.

de Boor, C., 1978. Splines as linear combinations of B-splines. A survey. In Approximation Theory II, ed. by G. G. Lorentz, C. K. Chui, and L. L. Schumaker, Academic Press, New York, pp. 1-47.

de Boor, C., 1978. A Practical Guide to Splines. Vol. 27, Applied Mathematical Sciences, Springer-Verlag, New York, 392 pp.

Estes, R. H., 1977. A computer software system for the generation of global ocean tides including self-gravitation and crustal loading effects. NASA X-920-77-82, Goddard Space Flight Center, Greenbelt, Maryland, 59 pp.

Gaposchkin, E. M., editor, 1973. 1973 Smithsonian Standard Earth (III). Smithsonian Astrophys. Obs. Spec. Rep. No. 353, 388 pp.

Gaposchkin, E. M., 1979. Estimation of 550-km × 550-km mean gravity anomalies and mean geoid heights. Smithsonian Astrophys. Obs. Spec. Rep. No. 384, 67 pp.

Gentleman, W. M., 1973. Least squares computations by Givens transformations without square roots. Journ. Inst. Math. Appl., vol. 12, pp. 329-336.

Hayes, J. G., 1970. Curve fitting by polynomials in one variable. In Numerical Approximation to Functions and Data, ed. by J. G. Hayes, Athlone Press, London.

Hayes, J. G., 1974. Numerical methods for curve and surface fitting. Bull. Inst. Math. Appl., vol. 10, pp. 144-152.

Hayes, J. G., and Halliday, J., 1974. The least-squares fitting of cubic spline surfaces to general data sets. Journ. Inst. Math. Appl., vol. 14, pp. 89-103.

Mader, G. L., 1979. A revised 5' gravimetric geoid and associated errors for the North Atlantic calibration error. NASA Contractor Report 156851, Wallops Flight Center, Wallops Island, Virginia, 32 pp.

Marsh, J. G., and Chang, E. S., 1978. 5' detailed gravimetric geoid in the Northwestern Atlantic Ocean. Marine Geod., vol. 1, no. 3, pp. 253-261.

Marsh, J. G., et al., 1978. Estimation of mean sea surfaces in the North Atlantic, the Pacific, and the Indian Ocean using Geos 3 altimeter data. Presented at the Second International Symposium on the Uses of Artificial Satellites for Geodesy and Geodynamics, Lagonissi, Greece, May.

Mofjeld, H. O., 1975. Empirical model for tides in the western North Atlantic Ocean. NOAA Technical Report ERL 340-AOML 19, U.S. Dept. of Commerce Environmental Research Laboratories, Boulder, Colorado, 24 pp.

Schumaker, L. L., 1978. Fitting surfaces to scattered data. In Approximation Theory II, ed. by G. G. Lorentz, C. K. Chui, and L. L. Schumaker, Academic Press, New York, pp. 203-268.

Schwiderski, E. W., 1978. Ocean tide model including M_2 tidal charts. NAVSWS/DK-K05, Naval Surface Weapons Laboratory, Dahlgren, Virginia, 53 pp.

8. COST SUMMARY

Financial Status Report
April 24, 1979

Of the total amount of $65,000 authorized for the 17-month (extended) period for this research, approximately $16,825 has been spent as of 24 April 1979; $48,175 is required to complete. No funding problems are anticipated.

Expended to April 24, 1979 (approx.)	$ 16,825.
Cost to Complete (through March 30, 1980)	48,175.
TOTAL	$ 65,000.
Variance	0

APPENDIX A

SIGNIFICANT WAVE-HEIGHT CORRECTION TABLES

TABLE FOR S-6 AND S-16

MODEL H 1/3	ATTITUDE	COMPUTED H 1/3	DELTA H 1/3(M)	HEIGHT ERROR(CM)
0.0	0.00	0.5600	-0.5600	-4.3482
0.0	0.05	0.5600	-0.5600	-4.3257
0.0	0.10	0.5600	-0.5600	-4.2291
0.0	0.15	0.5600	-0.5600	-4.0573
0.0	0.20	0.5600	-0.5600	-3.8484
0.0	0.25	0.5600	-0.5600	-3.5723
0.0	0.30	0.6400	-0.6400	-3.2414
0.0	0.35	0.6400	-0.6400	-2.8469
0.0	0.40	0.6400	-0.6400	-2.4050
0.0	0.45	0.7200	-0.7200	-1.8975
0.0	0.50	0.7200	-0.7200	-1.3442
0.0	0.55	0.7200	-0.7200	-0.7640
0.0	0.60	0.8000	-0.8000	-0.2015
0.0	0.65	0.8000	-0.8000	0.4839
0.0	0.70	0.8800	-0.8800	1.2001
0.0	0.75	0.8800	-0.8800	1.9596
0.5	0.00	0.7200	-0.2200	-3.8870
0.5	0.05	0.7200	-0.2200	-3.8619
0.5	0.10	0.7200	-0.2200	-3.7583
0.5	0.15	0.7200	-0.2200	-3.6091
0.5	0.20	0.7200	-0.2200	-3.3955
0.5	0.25	0.7200	-0.2200	-3.1230
0.5	0.30	0.8000	-0.3000	-2.7789
0.5	0.35	0.8000	-0.3000	-2.4089
0.5	0.40	0.8000	-0.3000	-1.9626
0.5	0.45	0.8800	-0.3800	-1.4650
0.5	0.50	0.8800	-0.3800	-0.9602
0.5	0.55	0.8800	-0.3800	-0.3345
0.5	0.60	1.0000	-0.5000	0.2580
0.5	0.65	1.0000	-0.5000	0.8996

MODEL H 1/3	ATTITUDE	COMPUTED H 1/3	DELTA H 1/3(M)	HEIGHT ERROR(CM)
0.5	0.70	1.0800	-0.5800	1.6157
0.5	0.75	1.0800	-0.5800	2.2968
1.0	0.00	1.0800	-0.0800	-3.0110
1.0	0.05	1.0800	-0.0800	-2.9815
1.0	0.10	1.0800	-0.0800	-2.8858
1.0	0.15	1.1600	-0.1600	-2.7377
1.0	0.20	1.1600	-0.1600	-2.5262
1.0	0.25	1.1600	-0.1600	-2.2630
1.0	0.30	1.1600	-0.1600	-1.9493
1.0	0.35	1.1600	-0.1600	-1.5500
1.0	0.40	1.1600	-0.1600	-1.1571
1.0	0.45	1.2400	-0.2400	-0.6866
1.0	0.50	1.2400	-0.2400	-0.1758
1.0	0.55	1.2400	-0.2400	0.3942
1.0	0.60	1.4000	-0.4000	0.9851
1.0	0.65	1.5600	-0.5600	1.6196
1.0	0.70	1.5600	-0.5600	2.2879
1.0	0.75	1.6400	-0.6400	3.0066
1.5	0.00	1.5600	-0.0600	-2.2821
1.5	0.05	1.5600	-0.0600	-2.2478
1.5	0.10	1.5600	-0.0600	-2.1755
1.5	0.15	1.5600	-0.0600	-2.0311
1.5	0.20	1.5600	-0.0600	-1.8306
1.5	0.25	1.6400	-0.1400	-1.5582
1.5	0.30	1.6400	-0.1400	-1.2556
1.5	0.35	1.6400	-0.1400	-0.9079
1.5	0.40	1.7200	-0.2200	-0.4936
1.5	0.45	1.7200	-0.2200	-0.0464
1.5	0.50	1.7200	-0.2200	0.4756
1.5	0.55	1.8800	-0.3800	1.0145
1.5	0.60	1.8800	-0.3800	1.5914
1.5	0.65	1.9600	-0.4600	2.2020

MODEL H 1/3	ATTITUDE	COMPUTED H 1/3	DELTA H 1/3(m)	HEIGHT ERROR(cm)
1.5	0.70	1.9600	-0.4600	2.8647
1.5	0.75	2.1200	-0.6200	3.5307
2.0	0.00	1.9600	0.0400	-1.7439
2.0	0.05	1.9600	0.0400	-1.7308
2.0	0.10	1.9600	0.0400	-1.6497
2.0	0.15	2.1200	-0.1200	-1.5145
2.0	0.20	2.1200	-0.1200	-1.3067
2.0	0.25	2.1200	-0.1200	-1.0587
2.0	0.30	2.1200	-0.1200	-0.7523
2.0	0.35	2.1200	-0.1200	-0.3983
2.0	0.40	2.2800	-0.2800	-0.0052
2.0	0.45	2.2800	-0.2800	0.4524
2.0	0.50	2.2800	-0.2800	0.9333
2.0	0.55	2.4400	-0.4400	1.4412
2.0	0.60	2.4400	-0.4400	2.0021
2.0	0.65	2.4400	-0.4400	2.6201
2.0	0.70	2.6000	-0.6000	3.2482
2.0	0.75	2.6000	-0.6000	3.9421
2.5	0.00	2.6000	-0.1000	-1.3542
2.5	0.05	2.6000	-0.1000	-1.3159
2.5	0.10	2.6000	-0.1000	-1.2514
2.5	0.15	2.6000	-0.1000	-1.1167
2.5	0.20	2.6000	-0.1000	-0.9411
2.5	0.25	2.6000	-0.1000	-0.6896
2.5	0.30	2.6000	-0.1000	-0.3997
2.5	0.35	2.7200	-0.2200	-0.0499
2.5	0.40	2.7200	-0.2200	0.3392
2.5	0.45	2.7200	-0.2200	0.7798
2.5	0.50	2.7200	-0.2200	1.2580
2.5	0.55	2.8800	-0.3800	1.7409
2.5	0.60	3.2000	-0.7000	4.8041
2.5	0.65	3.2000	-0.7000	5.9568

MODEL H 1/3	ATTITUDE	COMPUTED H 1/3	DELTA H 1/3(m)	HEIGHT ERROR(cm)
2.5	0.70	3.3600	-0.8600	7.2316
2.5	0.75	3.3600	-0.8600	8.4799
3.0	0.00	2.9600	0.0400	-1.9720
3.0	0.05	2.9600	0.0400	-1.9262
3.0	0.10	2.9600	0.0400	-1.7523
3.0	0.15	2.9600	0.0400	-1.4968
3.0	0.20	2.9600	0.0400	-1.1431
3.0	0.25	2.9600	0.0400	-0.6640
3.0	0.30	3.2000	-0.2000	-0.0971
3.0	0.35	3.2000	-0.2000	0.5809
3.0	0.40	3.2000	-0.2000	1.3385
3.0	0.45	3.3600	-0.3600	2.1958
3.0	0.50	3.3600	-0.3600	3.1064
3.0	0.55	3.3600	-0.3600	4.0996
3.0	0.60	3.6000	-0.6000	5.1634
3.0	0.65	3.6000	-0.6000	6.2922
3.0	0.70	3.8400	-0.8400	7.4899
3.0	0.75	3.8400	-0.8400	8.7828
3.5	0.00	3.3600	0.1400	-1.5284
3.5	0.05	3.3600	0.1400	-1.4712
3.5	0.10	3.6000	-0.1000	-1.3240
3.5	0.15	3.6000	-0.1000	-1.0560
3.5	0.20	3.6000	-0.1000	-0.6879
3.5	0.25	3.6000	-0.1000	-0.2498
3.5	0.30	3.6000	-0.1000	0.3191
3.5	0.35	3.6000	-0.1000	0.9681
3.5	0.40	3.8400	-0.3400	1.7122
3.5	0.45	3.8400	-0.3400	2.5396
3.5	0.50	3.8400	-0.3400	3.4437
3.5	0.55	4.0800	-0.5800	4.3967
3.5	0.60	4.0800	-0.5800	5.5002
3.5	0.65	4.2800	-0.7800	6.5990

MODEL H 1/3	ATTITUDE	COMPUTED H 1/3	DELTA H 1/3(m)	HEIGHT ERROR(cm)
3.5	0.70	4.2800	-0.7800	7.7791
3.5	0.75	4.5200	-1.0200	9.0420
4.0	0.00	4.0800	-0.0800	-1.1589
4.0	0.05	4.0800	-0.0800	-1.0984
4.0	0.10	4.0800	-0.0800	-0.9660
4.0	0.15	4.0800	-0.0800	-0.7105
4.0	0.20	4.0800	-0.0800	-0.3528
4.0	0.25	4.0800	-0.0800	0.1240
4.0	0.30	4.0800	-0.0800	0.6631
4.0	0.35	4.2800	-0.2800	1.2979
4.0	0.40	4.2800	-0.2800	2.0233
4.0	0.45	4.2800	-0.2800	2.8437
4.0	0.50	4.5200	-0.5200	3.7100
4.0	0.55	4.5200	-0.5200	4.6731
4.0	0.60	4.5200	-0.5200	5.7409
4.0	0.65	4.7600	-0.7600	6.8206
4.0	0.70	4.7600	-0.7600	7.9690
4.0	0.75	4.7600	-0.7600	9.1665
5.0	0.00	5.0800	-0.0800	-0.5632
5.0	0.05	5.0800	-0.0800	-0.5199
5.0	0.10	5.0800	-0.0800	-0.3671
5.0	0.15	5.0800	-0.0800	-0.1091
5.0	0.20	5.0800	-0.0800	0.2253
5.0	0.25	5.0800	-0.0800	0.6768
5.0	0.30	5.0800	-0.0800	1.2020
5.0	0.35	5.0800	-0.0800	1.8183
5.0	0.40	5.4000	-0.4000	2.5150
5.0	0.45	5.4000	-0.4000	3.2833
5.0	0.50	5.4000	-0.4000	4.1398
5.0	0.55	5.4000	-0.4000	5.0721
5.0	0.60	5.8000	-0.8000	6.0317
5.0	0.65	6.2400	-1.2400	14.4410

MODEL H 1/3	ATTITUDE	COMPUTED H 1/3	DELTA H 1/3(m)	HEIGHT ERROR(cm)
5.0	0.70	6.2400	-1.2400	16.6187
5.0	0.75	6.2400	-1.2400	18.9288
6.0	0.00	5.8800	0.1200	0.1431
6.0	0.05	5.8800	0.1200	0.2024
6.0	0.10	5.8800	0.1200	0.5175
6.0	0.15	5.8800	0.1200	0.9710
6.0	0.20	5.8800	0.1200	1.6142
6.0	0.25	6.2400	-0.2400	2.4548
6.0	0.30	6.2400	-0.2400	3.4522
6.0	0.35	6.2400	-0.2400	4.6746
6.0	0.40	6.2400	-0.2400	5.9978
6.0	0.45	6.6400	-0.6400	7.4882
6.0	0.50	6.6400	-0.6400	9.1149
6.0	0.55	6.6400	-0.6400	10.8566
6.0	0.60	7.0400	-1.0400	12.7305
6.0	0.65	7.0400	-1.0400	14.7628
6.0	0.70	7.0400	-1.0400	16.9986
6.0	0.75	7.5200	-1.5200	19.1255
7.0	0.00	7.0400	-0.0400	0.8781
7.0	0.05	7.0400	-0.0400	0.9719
7.0	0.10	7.0400	-0.0400	1.2641
7.0	0.15	7.0400	-0.0400	1.7288
7.0	0.20	7.0400	-0.0400	2.3630
7.0	0.25	7.0400	-0.0400	3.1425
7.0	0.30	7.0400	-0.0400	4.1256
7.0	0.35	7.5200	-0.5200	5.2788
7.0	0.40	7.5200	-0.5200	6.5545
7.0	0.45	7.5200	-0.5200	8.0016
7.0	0.50	7.5200	-0.5200	9.5849
7.0	0.55	8.0000	-1.0000	11.2889
7.0	0.60	8.0000	-1.0000	13.1401
7.0	0.65	8.0000	-1.0000	15.0380

MODEL H 1/3	ATTITUDE	COMPUTED H 1/3	DELTA H 1/3(m)	HEIGHT ERROR(cm)
7.0	0.70	8.4400	-1.4400	17.1138
7.0	0.75	8.4400	-1.4400	19.3270
8.0	0.00	8.0000	0.0000	1.6142
8.0	0.05	8.0000	0.0000	1.6874
8.0	0.10	8.0000	0.0000	1.9469
8.0	0.15	8.0000	0.0000	2.3821
8.0	0.20	8.0000	0.0000	2.9941
8.0	0.25	8.0000	0.0000	3.7483
8.0	0.30	8.4400	-0.4400	4.6693
8.0	0.35	8.4400	-0.4400	5.7789
8.0	0.40	8.4400	-0.4400	7.0359
8.0	0.45	8.4400	-0.4400	8.4460
8.0	0.50	8.4400	-0.4400	9.9413
8.0	0.55	9.0000	-1.0000	11.6331
8.0	0.60	9.0000	-1.0000	13.4679
8.0	0.65	9.0000	-1.0000	15.3315
8.0	0.70	9.6000	-1.6000	17.2952
8.0	0.75	9.6000	-1.6000	19.4367
9.0	0.00	9.0000	0.0000	2.2185
9.0	0.05	9.0000	0.0000	2.3040
9.0	0.10	9.0000	0.0000	2.5997
9.0	0.15	9.0000	0.0000	2.9870
9.0	0.20	9.0000	0.0000	3.6260
9.0	0.25	9.0000	0.0000	4.2989
9.0	0.30	9.0000	0.0000	5.2292
9.0	0.35	9.6000	-0.6000	6.2930
9.0	0.40	9.6000	-0.6000	7.4970
9.0	0.45	9.6000	-0.6000	8.8164
9.0	0.50	9.6000	-0.6000	10.3106
9.0	0.55	9.6000	-0.6000	11.8956
9.0	0.60	10.2400	-1.2400	13.6436
9.0	0.65	10.2400	-1.2400	15.4348

MODEL H 1/3	ATTITUDE	COMPUTED H 1/3	DELTA H 1/3(m)	HEIGHT ERROR(cm)
9.0	0.70	10.2400	-1.2400	17.3997
9.0	0.75	10.2400	-1.2400	19.3888
10.0	0.00	10.2400	-0.2400	2.8024
10.0	0.05	10.2400	-0.2400	2.9143
10.0	0.10	10.2400	-0.2400	3.1466
10.0	0.15	10.2400	-0.2400	3.5703
10.0	0.20	10.2400	-0.2400	4.1039
10.0	0.25	10.2400	-0.2400	4.8374
10.0	0.30	10.2400	-0.2400	5.7200
10.0	0.35	10.2400	-0.2400	6.7445
10.0	0.40	10.2400	-0.2400	7.8815
10.0	0.45	10.9200	-0.9200	9.1872
10.0	0.50	10.9200	-0.9200	10.6035
10.0	0.55	10.9200	-0.9200	12.1788
10.0	0.60	10.9200	-0.9200	13.8646
10.0	0.65	10.9200	-0.9200	15.5768
10.0	0.70	11.8000	-1.8000	17.4595
10.0	0.75	11.8800	-1.8800	38.9028
12.0	0.00	11.8800	0.1200	8.4778
12.0	0.05	11.8800	0.1200	8.6203
12.0	0.10	11.8800	0.1200	9.0576
12.0	0.15	11.8800	0.1200	9.8127
12.0	0.20	11.8800	0.1200	10.8352
12.0	0.25	11.8800	0.1200	12.1025
12.0	0.30	12.8800	-0.8800	13.7000
12.0	0.35	12.8800	-0.8800	15.6103
12.0	0.40	12.8800	-0.8800	17.6369
12.0	0.45	12.8800	-0.8800	20.0358
12.0	0.50	12.8800	-0.8800	22.5956
12.0	0.55	12.8800	-0.8800	25.4512
12.0	0.60	14.0800	-2.0800	28.4172
12.0	0.65	14.0800	-2.0800	31.7042

MODEL H 1/3	ATTITUDE	COMPUTED H 1/3	DELTA H 1/3(m)	HEIGHT ERROR(cm)
12.0	0.70	14.0800	-2.0800	35.2027
12.0	0.75	14.0800	-2.0800	38.5862
14.0	0.00	14.0800	-0.0800	10.2419
14.0	0.05	14.0800	-0.0800	10.3604
14.0	0.10	14.0800	-0.0800	10.7338
14.0	0.15	14.0800	-0.0800	11.4282
14.0	0.20	14.0800	-0.0800	12.4300
14.0	0.25	14.0800	-0.0800	13.6089
14.0	0.30	14.0800	-0.0800	15.1004
14.0	0.35	14.0800	-0.0800	16.8498
14.0	0.40	15.3200	-1.3200	18.8299
14.0	0.45	15.3200	-1.3200	21.0183
14.0	0.50	15.3200	-1.3200	23.4588
14.0	0.55	15.3200	-1.3200	26.1454
14.0	0.60	15.3200	-1.3200	28.9358
14.0	0.65	15.3200	-1.3200	31.9751
14.0	0.70	16.8000	-2.8000	35.1257
14.0	0.75	16.8000	-2.8000	38.4696
16.0	0.00	16.8000	-0.8000	11.8033
16.0	0.05	16.8000	-0.8000	11.9506
16.0	0.10	16.8000	-0.8000	12.3665
16.0	0.15	16.8000	-0.8000	12.9629
16.0	0.20	16.8000	-0.8000	13.8816
16.0	0.25	16.8000	-0.8000	15.0529
16.0	0.30	16.8000	-0.8000	16.4093
16.0	0.35	16.8000	-0.8000	18.0414
16.0	0.40	16.8000	-0.8000	19.9188
16.0	0.45	16.8000	-0.8000	21.9261
16.0	0.50	16.8000	-0.8000	24.2005
16.0	0.55	18.5200	-2.5200	26.6802
16.0	0.60	18.5200	-2.5200	29.4255
16.0	0.65	18.5200	-2.5200	32.1849

MODEL H 1/3	ATTITUDE	COMPUTED H 1/3	DELTA H 1/3(m)	HEIGHT ERROR(cm)
16.0	0.70	18.5200	-2.5200	35.1155
16.0	0.75	18.5200	-2.5200	38.2683
18.0	0.00	18.5200	-0.5200	13.2392
18.0	0.05	18.5200	-0.5200	13.3590
18.0	0.10	18.5200	-0.5200	13.7061
18.0	0.15	18.5200	-0.5200	14.3751
18.0	0.20	18.5200	-0.5200	15.2108
18.0	0.25	18.5200	-0.5200	16.2860
18.0	0.30	18.5200	-0.5200	17.5537
18.0	0.35	18.5200	-0.5200	19.1076
18.0	0.40	18.5200	-0.5200	20.7651
18.0	0.45	18.5200	-0.5200	22.7485
18.0	0.50	19.9200	-1.9200	24.8284
18.0	0.55	19.9200	-1.9200	27.1917
18.0	0.60	19.9200	-1.9200	29.6509
18.0	0.65	19.9200	-1.9200	32.3337
18.0	0.70	19.9200	-1.9200	35.1468
18.0	0.75	19.9200	-1.9200	38.0823
20.0	0.00	19.9200	0.0800	14.5670
20.0	0.05	19.9200	0.0800	14.7157
20.0	0.10	19.9200	0.0800	14.9900
20.0	0.15	19.9200	0.0800	15.5566
20.0	0.20	19.9200	0.0800	16.3189
20.0	0.25	19.9200	0.0800	17.3570
20.0	0.30	19.9200	0.0800	18.5586
20.0	0.35	19.9200	0.0800	19.9515
20.0	0.40	19.9200	0.0800	21.6119
20.0	0.45	19.9200	0.0800	23.4347
20.0	0.50	20.0000	0.0000	25.4114
20.0	0.55	20.0000	0.0000	27.5828
20.0	0.60	20.0000	0.0000	29.9415
20.0	0.65	20.0000	0.0000	32.4844

MODEL H 1/3	ATTITUDE	COMPUTED H 1/3	DELTA H 1/3(m)	HEIGHT ERROR(cm)
20.0	0.70	20.0000	0.0000	35.0410
20.0	0.75	20.0000	0.0000	37.8138